Methodologies for Capture Zone Delineation for the Waterloo Moraine Well Fields

by

Dawood Shahid Muhammad

A thesis
presented to the University of Waterloo
in fulfillment of the
thesis requirement for the degree of
Master of Science
in
Earth Sciences

Waterloo, Ontario, Canada, 2000

© D.S. Muhammad, 2000

I hereby declare that I am the sole author of this thesis. This is a true copy of the thesis, including any required final revisions, as accepted by my examiners.

I understand that my thesis may be made electronically available to the public.

D.S. Muhammad

Acknowledgements

I would like to thank my supervisor Dr. E.O. Frind for giving me the opportunity to work on this challenging project. His support and insightful comments were invaluable. I would like to thank my committee, Dr. David Rudolph for his interest in this study and Dr. E.D. Sudicky for his continual technical guidance for using the transport code (LTG). I am also grateful to Jos Beckers, John Molson, Rob McLaren, Anthony Radcliffe, and other colleagues at the University of Waterloo for their assistance and suggestions. Special thanks to Michelle L. Bester for critically reading the original draft of this thesis.

I would also like to thank the hydrogeologists of the Water Services Division of the Regional Municipality of Waterloo, Eric Hodgins, Jim Robinson, and Tammy Middleton, for their support and useful suggestions during the discussions. Craig Johnston of Stantec Consulting Ltd. and Paul Martin of Waterloo Hydrogeologic Inc., provided invaluable assistance with information on well field pumping history and water quality data. Without their help, my thesis would not have been as complete or as accurate.

Finally, I would like to thank my wife, Huma and kids, Usman, Umair and Anis for all their encouragement, love and support.

Abstract

The Region of Waterloo relies mainly (75 %) on local groundwater resources for its drinking water supply. The water demand is increasing with the growth of the population and there is a need to enhance the present water supplies. The Regional Municipality of Waterloo (RMOW), which is the governing body in charge of providing the drinking water supply, is conducting an extensive program to protect the groundwater resources of the Waterloo Moraine aquifer. The focus of that work is defining the wellhead protection areas of the existing production wells as well as the investigation of potential further water supply. The main goal of the work presented here is to delineate the capture zones for the major well fields of the Region. To achieve that goal, the flow for the expected pumping conditions is simulated using a fully 3D finite element model (WATFLOW) which has been proven to be highly flexible to represent the natural boundaries and the highly irregular stratigraphy by previous researchers and scholars. The modified version of this model which includes a pseudo-unsaturated module is used for the solution of flow equation.

For the delineation of capture zones, a new particle tracking code (WATRAC) as well as two advective-dispersive transport models are used by using a probabilistic approach presented by *Neupauer and Wilson* [1999]. For the probabilistic approach (Wilson's method), two transport models, a conventional time-marching code (WTC) and a time-continuous code (LTG) are used and their results are compared. The LTG is computationally more efficient than the WTC, but it gives oscillatory results close to the steady state condition. A combined used of LTG and WTC is therefore recommended to obtain the steady state capture zones. The 0.25 probability contour agrees very well with the particle tracks, except for somewhat greater transverse spreading due to the dispersion which is not considered by the particle tracking algorithm. Both methods, backward particle tracking and probabilistic advective-dispersive modelling are clearly more informative and give better insight when considered together than each by itself.

Contents

List of Figures

List of Tables

Chapter 1

Introduction

Groundwater is a precious natural resource which can be threatened by contamination and over-usage. As a community depending mostly on groundwater, the Regional Municipality of Waterloo (Ontario) is developing a strategy for the protection of this resource to guarantee a safe drinking water supply for present and future generations. The Region covers an area of approximately 1360 km^2 including the cities of Cambridge, Kitchener, and Waterloo, as well as rural areas comprising the Townships of Woolwich, Wilmot, Wellesley, and North Dumfries (Figure 1.1). There are 126 pumping wells, grouped into about 50 well fields providing approximately 75% of the water supply needs of over 400,000 residents and associated industries. In addition, some private wells are also present in the area. The dramatic growth of the Region in recent decades has provided a motivation for obtaining, as a basis for sustainable utilization, a sound understanding of this vital resource, its capacity and its susceptibility to contamination [*Martin and Frind,* 1998].

The Waterloo Moraine has been studied for several years by consultants, starting with International Water Supply (IWS) in the 1940's, and the University of Waterloo beginning in the early 1970's. Numerous undergraduate and graduate studies have been carried out relating to different aspects of the Quaternary deposits or the groundwater supply system.

A detailed regional-scale flow model of the northern part of the Moraine, the Laurel Creek watershed, was developed by *Martin* [1994]. All available data at that time was incorporated into a detailed hydrostratigraphic interpretation for the analysis of the regional groundwater flow system through three-dimensional modelling. A 3D representation was found to be required in order to capture the characteristics of the complex flow system. *Martin* [1995] further developed this model to cover the entire Waterloo Moraine.

Callow [1996] studied options to optimize production in the Greenbrook, Strange Street, and Mannheim well fields using a 3D model of a portion of the Waterloo Moraine with both MODFLOW [*Waterloo Hydrogeologic, Inc.* 1996] and WATFLOW [*Molson, et al.,* 1992]. Extraction rates were optimized for the existing well fields and potential new well sites were located on the basis of modelling results. It was concluded that the finite difference code, MODFLOW, is not suitable for detailed modelling of this kind of heterogeneous systems. The impact of discretization was assessed and the need for a fine mesh around pumping wells where large hydraulic gradients exist was recognized.

Beckers [1998] developed an automated calibration technique for the free-surface finite element code WATFLOW. Modifications were made in WATFLOW to include the unsaturated zone through an ad-hoc scaling of the hydraulic conductivities above the water table with a fairly coarse mesh discretization [*Beckers,* 1998]. This type of pseudo-unsaturated model takes the ground surface as the upper boundary and hydrogeologically significant layers which may be present above the water table can be included. Flow in the unsaturated zone was modelled by means of an empirical scaling of the hydraulic conductivities above the water table. When combined with a coarse mesh discretization suitable for watershed-scale modelling, this approach has the potential of bridging the scale-gap with surface water models [*Beckers,* 1998]. This model was coupled with a high-conductivity recharge spreading layer (RSL) over the top of the model domain to approximate the rainfall-runoff process. This modified version of WATFLOW is used in the present study to obtain the head distributions and velocity fields for use in the transport models.

At present, The Regional Municipality of Waterloo (RMOW) is conducting a comprehensive program to inventory the groundwater resource with special emphasis to delineate wellhead protection areas. A crucial aspect of this program is the delineation of capture zones for the Region's municipal wells. Capture zones are defined as the portion of the flow system that contributes groundwater to the well field [*Anderson and Woessner,* 1992].

Conventionally, the particle tracking technique is used to create capture zones and to define isochrones of arrival time. A preliminary first effort to delineate capture zones for the Region's well fields was made by the *Waterloo Hydrogeologic, Inc.,* [1995] using a 2D particle tracking technique. In this approach, particles are placed at the well face and traced under the reversed velocity field. The capture zone can then be defined by drawing an envelope around the particle paths. This results in a deterministic zonation of the surface area into zones of either capture or no capture. Using particle tracking technique, 3D capture zones were developed by *Waterloo Hydrogeologic, Inc.,* [1998, 1999].

Alternatively, a probabilistic approach to capture zone delineation can be developed by solving the advective-dispersive transport equation backward-in-time [*Liu and Wilson*, 1996; *Neupauer and Wilson*, 1999]. In this approach, a hypothetical tracer is introduced at the well face at a relative concentration of one and allowed to migrate due to advection and dispersion through the aquifer under the reversed velocity field. Two types of probability maps can be obtained using this backward-in-time method. The first is referred to as a travel-time-probability map and it describes the length of time required for water to flow from some prescribed location in the aquifer to the pumping well. It can be used to describe a well protection area, or be convoluted with estimated pollutant spatial concentrations to predict arriving pollutant concentrations [*Liu and Wilson*, 1996]. The second type of map is referred to as a location probability map, and it defines the origin of water produced at the pumping well at some time t later. It is useful in identifying possible sources of past pollution and for designing a monitoring system. This type of map has also been produced by a backward-in-time random walk approach [*Linderfelt et*

al., 1989; *Uffink*, 1989; *Wilson and Linderfelt*, 1991; *Bagtzoglou et al.,* 1992; *Chin and Chittaluru*, 1994]. Critical areas that could be missed in particle tracks are ensured coverage as the transport equation is solved everywhere in the domain by using this technique.

Martin and Frind [1998] developed a methodology to inventory the groundwater resource of the Waterloo Moraine multi-aquifer system, to characterize its susceptibility to contamination and to create the basis for optimal management and protection strategies. A particle tracking routine WTC-TRAC (developed by *Martin,* 1996) was used to generate estimates of the steady state surface capture zones for all well fields in the Moraine area. It was concluded that aquitard windows have a controlling influence on the capture zone delineation.

Conventional (time-marching) transport techniques need a fine mesh and relatively short time steps to satisfy the Peclet and Courant criteria. To satisfy the Peclet criterion, the grid must be refined especially around the wells where steep concentration gradients are present, and this could be extremely computationally burdensome for a large-scale multi-aquifer system. The Courant criterion controls the time discretization of the advective-dispersive transport equation. Violation of these criteria may produce numerical dispersion and significantly affect the accuracy of the model results.

A time-continuous transport method, the Laplace Transform Galerkin (LTG) technique is capable of yielding a highly accurate solution even when a relatively coarse finite element mesh is employed [*Sudicky,* 1989]. The Courant constraint imposed by conventional time-stepping schemes is not necessary in this technique.

Sudicky [1989] developed the Laplace Transform Galerkin technique and applied it to the problem of solute transport in porous media. After subdivision of the problem domain into finite elements by the Galerkin procedure, this method uses a Laplace transformation to eliminate the temporal derivatives appearing in the space-discretized set of ordinary differential equations. In the first version of the LTG code, numerical inversion of the Laplace transformed nodal concentration

in Laplace p space was performed using the *Crump* [1976] algorithm. *Sudicky* [1989] demonstrated by examples that this technique is capable of providing highly accurate solutions for grid Peclet numbers in excess of 30. In the latest version of the code, a new inversion technique developed by *De Hoog* [1982], which is greatly superior to *Crump's* scheme for reducing oscillations of the inverse in the neighborhood of a discontinuity (i.e., sharp front) and is in general more efficient [*Sudicky*, 1989] was used.

Sudicky [1990] presented LTG technique for the numerical solution of solute transport problems in multi-dimensional double-porosity media. The utility of the model was demonstrated by applying it to the problem of solute transport in a sandy-type aquifer having a random, spatially-correlated hydraulic conductivity field and comprised of slightly porous grains that admit intergranular diffusion but do not conduct fluid.

Sudicky et al., [1992] extended the Laplace Transform Galerkin method for application to discretely fractured media with emphasis on large-scale modelling capabilities. Traditional modelling approaches have limited ability to simulate contaminant migration in large-scale porous formations containing a complex network of discrete fractures. In addition to time-related complexities, these methods also require a fine spatial discretization to represent sharp concentration gradients at the interface between fractures and the matrix. The LTG technique avoids time stepping and permits the use of a relatively coarse grid without compromising accuracy.

Bester [1999] compared ten transport solution techniques at increasingly coarser grid spacing with the goal of finding the most efficient model that was able to accurately simulate the transport processes. Particularly, the time-continuous Laplace Transform Galerkin method was compared to time-stepping methods to observe solution behavior at high grid Peclet numbers. That research showed that the LTG method exhibits significantly less numerical error than the time-stepping methods with coarse grid resolution even at Peclet numbers in excess of 64.

While advective particle tracking techniques are definitely simple and efficient, the probability plume produced by the solution of advective-dispersive transport equation using Wilson's technique is considered more realistic [*GLL et al.,* 1998]. The dispersive term in this case represents the uncertainty due to heterogeneity which is known to exist in the Waterloo Moraine multi-aquifer system, but cannot be incorporated explicitly because of inadequate data and unrealistic computational requirements. It also eliminates the need to draw an envelope curve around the bundle of particle tracks.

1.1 Purpose of Study

This study focuses on the 3D capture zone delineation for all the major well fields of the Waterloo Moraine area using particle tracking and Wilson's method, with emphasis on the Greenbrook well field. RMOW is interested in determining the 2-year, 10-year, and steady state capture zones.

For particle tracks, a new code (WATRAC) developed by *Frind* [2000, in preparation] is used. The technical details of this new code are being presented in a forthcoming research paper [Pers. communication with E.O. Frind]. For Wilson's approach, WTC and LTG (advective-dispersive transport models) are applied in this study.

The main objectives of the study are:

1. Comparison of capture zones produced by LTG with other techniques (i.e., particle tracking and time-marching transport method) using different mesh refinements. The Greenbrook well field is used for this purpose, but the methodology is applicable to any 3D geometrical system.

2. Determination of steady state capture zone for Greenbrook well field by:

   - Time-marching transport model (WTC) starting from time zero.

- Time-marching transport model (WTC) using the results from LTG as an initial condition.

3. Identification of most efficient and accurate approach for the delineation of capture zones in complex 3D systems. The Greenbrook well field is selected for this purpose. Velocity fields generated by WATFLOW [*Beckers et al.*, 2000] are used to delineate 2-year, 10-year, and steady state capture zones.

4. Evaluation of the possible sources of contamination observed at the Greenbrook well field.

1.2 Assumptions and Limitations

The conditions assumed in this study are:

i. Steady state flow condition,

ii. Density-independent flow and transport condition,

iii. Contaminant is conservative,

iv. Non-fractured porous media,

v. Incompressible fluid, and

vi. Simplified unsaturated (pseudo-unsaturated) zone representation.

1.3 Site Description

The proposed study area (Figure 1.1), which is approximately 740 km^2, encompasses the Waterloo Moraine and surrounding areas. The area includes the cities of Waterloo and Kitchener as well as portions of neighboring townships. The area is drained by the Grand River and its tributaries, the Nith and Conestogo Rivers. The

topography is a characteristic of a moraine environment with an undulating surface and isolated swampy areas and ponds where the watertable intersects the ground surface. The geology of the Moraine is a Quaternary kame and kettle complex formed by interlobate glacial activity during the late Wisconsin age. The glacial overburden consists of a variety of materials including clay, interbedded tills, fine sand, sandy gravel and coarse gravel, and ranges in thickness from 30 m to more than 100 m. A detailed description of the glacial geology is given by *Chapman and Putnam* [1984], and *Karrow* [1993]. The climate is semi-humid with an average minimum and maximum temperatures of 2.7^o C and 12^o C, respectively. The precipitation ranges from 780 to 1000 mm in the form of rain and water-equivalent snow [*Karrow*, 1987].

1.4 Hydrogeology of the Study Area

The hydrogeology of the study area is complex due to the glacial origins of the aquifers in the Region. Local relief form broad till plains drained by the Grand River to the prominent Waterloo Sandhills in the central western portion. Topographic elevation ranges from 400 mASL in the west to 317 mASL approaching the Grand River.

Glaciation of the Waterloo Region in the late Wisconsinan period (23,000 - 10,000 years ago) was responsible for both the shape of the bedrock topography and the structure of the overlying Quaternary sediments. This era of glaciation featured three main periods: the Missouri, Port Bruce and Port Huron stadials, separated by the Erie and Mackinaw intervals [*Karrow,* 1987, 1993]. Ice lobes originating from the basins of Lake Huron, Erie and Ontario and from the Georgian Bay basin met during these stadials in the Waterloo Region [*Karrow,* 1987]. The Quaternary features and structure of the Region originated during the advancements, stationary phases and retreats of these ice lobes. The complex glacial geology has significantly influenced the development of the groundwater resources in the Region

and is fundamental to the understanding of the regional hydrogeology.

The stratigraphy is very complex with a heterogeneous distribution of hydraulic conductivity. Despite this heterogeneity, three relatively continuous till units, the Port Stanley/ Tavistock, Maryhill, and Catfish Creek tills have been identified throughout the Moraine [*Karrow,* 1993]. The youngest of these, the Port Stanley/Tavistock till, is found near the surface overlying large portions of the upper aquifer. The next youngest, the Maryhill till, is a clay-rich, low permeability unit lying beneath the upper aquifer. In many areas, this unit acts as an infiltration and contamination barrier for the underlying aquifers, however, windows of high-conductivity material have been observed or inferred in recent studies [*Martin and Frind*, 1998]. The Catfish Creek till, lying below the Maryhill till, is a dense, stony silt till containing portions that act as an aquifer [*Karrow*, 1993, *Petrie,* 1985]. Because of this variability, it has appeared to be discontinuous at a local scale. A fourth discontinuous till unit, named the Pre-Catfish Creek till, is found locally overlying the bedrock. The hydrostratigraphic relationships are shown schematically in Figure 1.2. Glaciofluvial sand and gravel deposits located between the major till units form the major aquifers in the system. The upper aquifer, thought to be reworked Maryhill till, is the most extensive and regionally continuous unit. It is also the most productive source of water. The two lower aquifers, which are often found as pockets of discontinuous sand and gravel, are productive locally. Important contributions to the understanding of Moraine hydrostatigraphy were made by *Rudolph* [1985], *Farvolden et al.,* [1987], *Rudolph and Farvolden* [1989], *Woeller and Farvolden* [1989], *Paloschi* [1993] and *Terraqua* [1995].

Over the last about 30 years, the conceptual model of the aquifer system of the Region has undergone various refinements with the addition of new data. The first conceptual model was prepared by *Dixon* [1963] and was later adopted by *Woeller* [1982] for the study of the Greenbrook well field. It was also used by *Rudolph* [1985], *Martin* [1994], and *Terraqua* [1995] in their Waterloo Moraine Study. These previous studies determined a multi-aquifer system represented by a series of four aquifers and four aquitards as shown in Figure 1.3. Due to the complex nature of

the Moraine, local areas within the study area may deviate from this conceptual model.

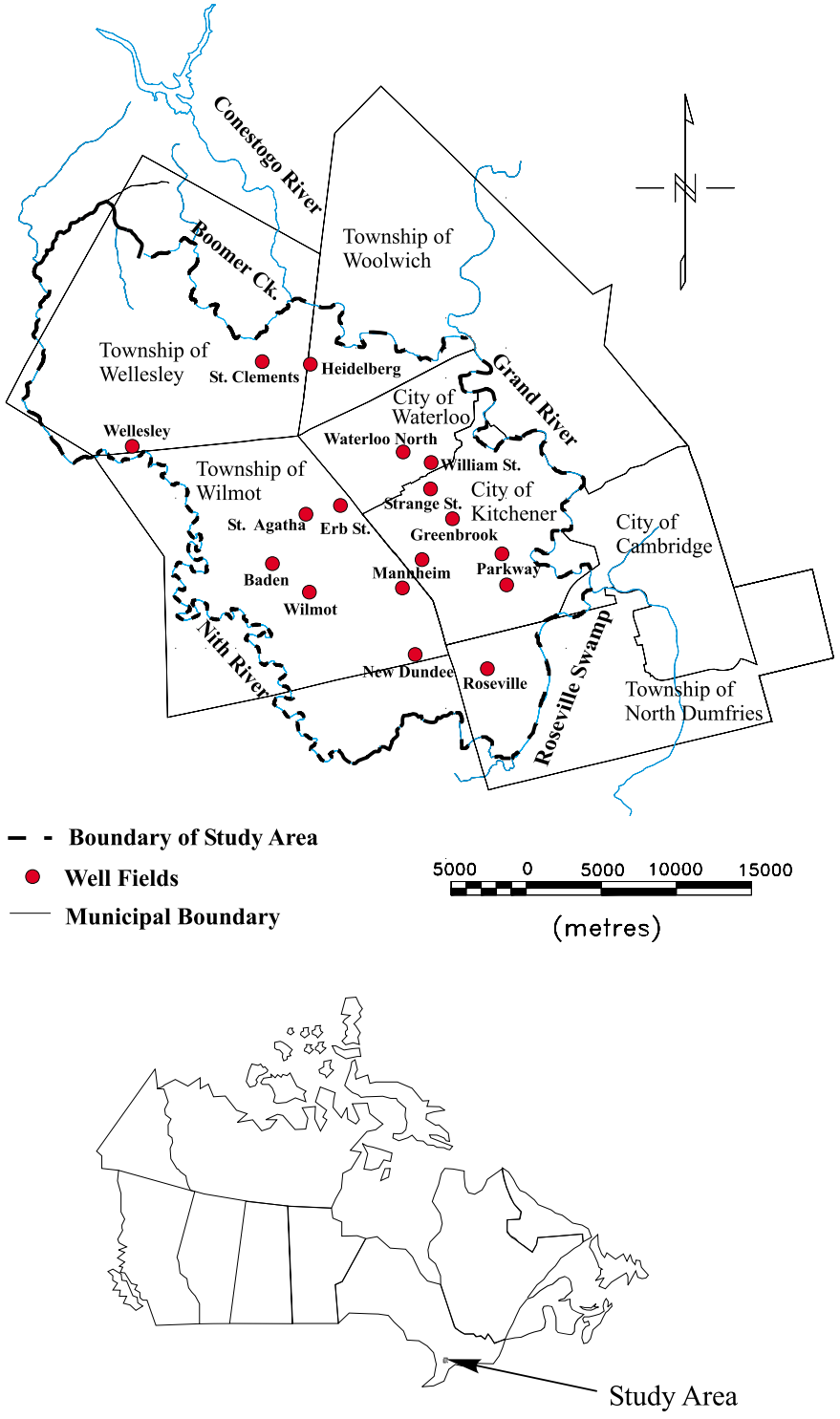

Figure 1.1: Location of study area.

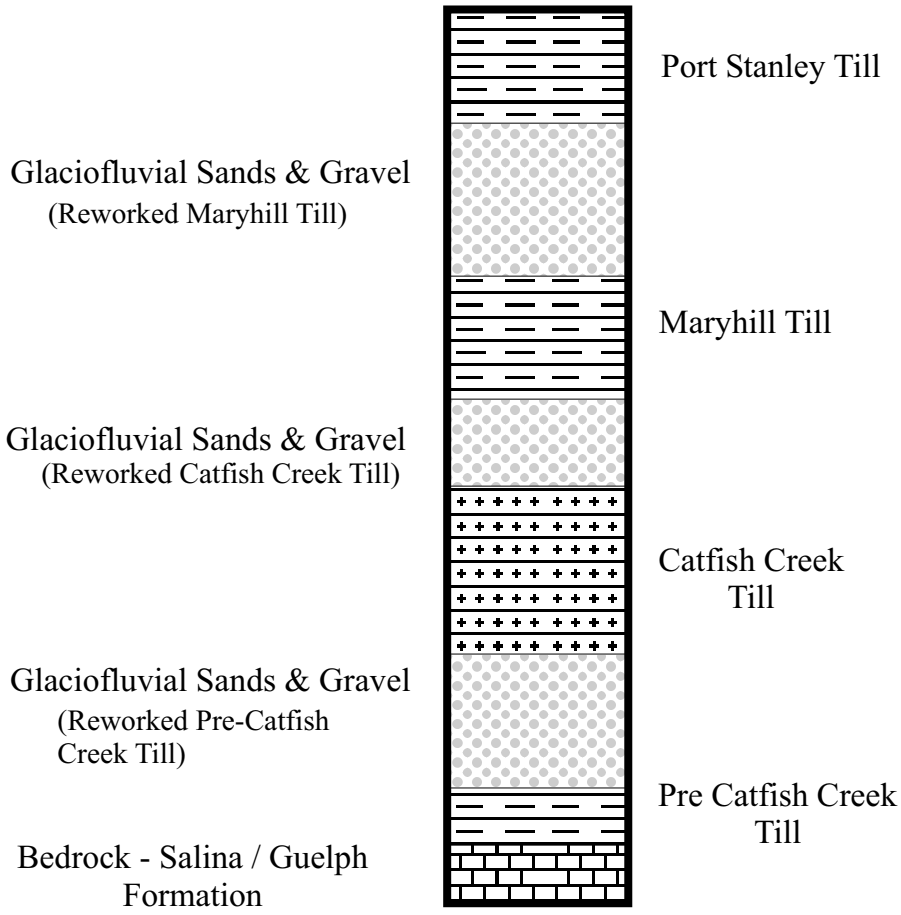

Figure 1.2: Vertical profile of general geology (adapted from Callow, 1996).

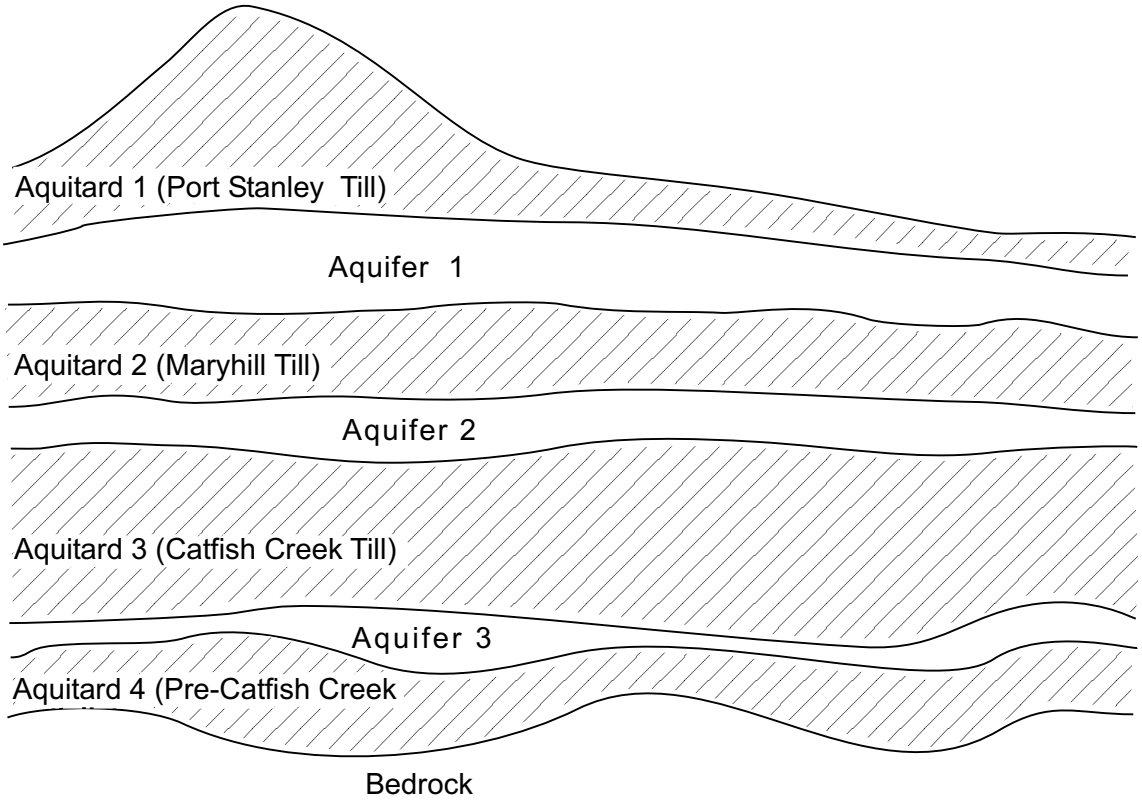

Figure 1.3: Hydrogeological conceptual model (adapted from Callow, 1996).

Chapter 2

Modelling Methodology

2.1 Introduction

Groundwater flow and transport simulations require an understanding of geology, hydraulics, and processes involved in the flow and transport. Groundwater flow models solve for the distribution of head in the model domain, whereas transport models solve for solute concentration as affected by advection, dispersion and chemical reactions. Transport modelling requires groundwater velocities (flow model output) to obtain solute concentrations, so a fundamental understanding of groundwater flow modelling is a prerequisite for the application of solute transport models.

WATFLOW is a advanced groundwater modelling tool, developed at the University of Waterloo, which is able to accommodate the geologic complexities found in the study area. Common, simplified modelling tools have been found to be ineffective for this heterogeneous environment [*Callow,* 1996]. In this study, modified version of WATFLOW [*Beckers et al.,* 2000] is used for flow simulation while for transport simulations, a new particle tracking code WATRAC [*Frind*, 2000, in preparation] and two advective-dispersive models (WTC and LTG) are applied using Wilson's approach and are discussed briefly in this chapter.

2.2 Flow Modelling

A new version of WATFLOW [*Beckers et al.,* 2000] with a pseudo-unsaturated module developed by *Beckers* [1998] is used to calculate the head and velocity distribution for the model domain using coarse as well as fine meshes. The finite element model (WATFLOW) is based on the solution of the 3D groundwater flow equation. The continuity equation for flow can be expressed as [*Bear*, 1972]:

$$\frac{\partial}{\partial x_i}\Big[K_{ij}\big(\frac{\partial \phi}{\partial x_j}\big)\Big] - \sum_{k=1}^{N} Q_k(t)\cdot\delta(x_k, y_k, z_k) = S_S\frac{\partial \phi}{\partial t} \tag{2.1}$$

where x_i and x_j represent the spatial dimensions, K_{ij} is the hydraulic conductivity tensor, ϕ is the hydraulic head, Q_k is the fluid volume flux for a source or sink located at (x_k, y_k, z_k), S_S is the specific storage, and t is time. In this study, only steady state groundwater flow is considered for which the time derivative on the RHS reduces to zero. Solution of equation (2.1) requires that the boundary conditions be specified all around the domain. This may be *Type 1* or *Dirichlet* boundary condition on boundary segment Γ_1

$$\phi = \phi_\Gamma \tag{2.2}$$

the *Type 2* or *Neuman* boundary condition on boundary segment Γ_2

$$K_{ij}\frac{\partial \phi}{\partial x_i}n_j = q_\Gamma \tag{2.3}$$

For the *Dirichlet* boundary condition (2.2), ϕ_Γ is the specified head along boundary segment Γ_1. For the *Neuman* boundary condition, given by equation (2.3), n_j is the component of the normal vector and q_Γ is the Darcy flux in the direction normal to boundary Γ_2.

In the numerical solution of equation (2.1), a standard Galerkin finite element method [*Huyakorn and Pinder*, 1983; *Kinzelbach*, 1986] was used. WATFLOW uses 3D triangular prisms to resolve the finite element domain. This type of element shape facilitates detailed discretization in both the vertical and horizontal dimensions and provides versatility in the domain design. These elements can have either constant or variable height in order to accommodate irregular layers.

Velocity calculations within WATFLOW are performed using elemental hydraulic conductivity and hydraulic head calculated at the six nodes of the element. For an element of constant height, the velocity calculations are performed as:

$$V_x = \frac{-K_{xx}}{2\Delta\theta} \sum_{i=1}^{6} \phi_i b_i \tag{2.4}$$

$$V_y = \frac{-K_{yy}}{2\Delta\theta} \sum_{i=1}^{6} \phi_i c_i \tag{2.5}$$

$$V_z = \frac{-K_{zz}}{\Delta\theta} \sum_{i=1}^{3} \left[\left(\phi_i \left(\frac{-a_i - b_i x_c - c_i y_c}{h} \right) \right) + \left(\phi_{i+3} \left(\frac{a_{i+3} + b_{i+3} x_c + c_{i+3} y_c}{h} \right) \right) \right] \tag{2.6}$$

where V_x, V_y, and V_z are the three-dimensional velocity components; K_{xx}, K_{yy}, and K_{zz} are the elemental hydraulic conductivities in the x, y, and z directions respectively; Δ is the surface area of the triangular element; θ is the elemental porosity value; ϕ_i is the calculated hydraulic head at each of the six nodes of the three-dimensional prismatic element; h is the average height of the element; x_c and y_c are the element centroid co-ordinates; and a_i, b_i, and c_i, are counter clockwise cyclic permutations derived from the shape of the plan-view projection of each element.

Equation (2.6) is applied only for non-deformed or mildly deformed elements; a numerical integration option is available for highly deformed elements as shown in Figure 2.1.

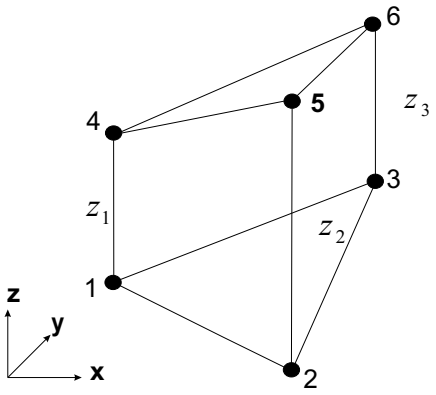

Figure 2.1: Prismatic element as used in WATFLOW.

Originally, WATFLOW was developed with a free-surface top boundary, where the water table was located iteratively based on the condition of zero pressure head, and the mesh was deformed accordingly. In the modified version of WATFLOW, rather than using the water table position as a parameter for the non-linear update of the solution, the saturation of the elements above the water table is computed through an ad-hoc exponential relationship between the pressure head p and the saturation of the porous medium S [*Beckers et al.,* 2000]:

$$\begin{aligned} S(p) &= S_r + (1 - S_r)e^{\epsilon p} \qquad p < 0 \\ &= 1 \qquad\qquad\qquad\qquad\quad p \geq 1 \end{aligned} \tag{2.7}$$

where S_r is the residual saturation of the porous medium, and ϵ is a parameter determining the extent of the zone between residual and full saturation. Partial saturation of the elements results in a lower hydraulic conductivity, impeding groundwater flow [*Beckers*, 1998]. This is accomplished by scaling the relative permeability of an element according to its saturation, i.e., $k_r = S(p)$. In this case, K_{ij} is replaced by $k_r K_{ij}$ in equation (2.1). By implementing this pseudo-unsaturated approach there is no need to deform the mesh and elemental conductivities do not have to be updated in each Picard iteration.

The final matrix equations for both the flow and mass transport problems are solved using an efficient preconditioned conjugate gradient (PCG) solution for symmetric matrices [*Schmid and Braess*, 1988]. In practice, the PCG solver has performed exceptionally well, even under highly heterogeneous conditions (with up to 5 orders of magnitude conductivity contrast between adjacent elements), with high accuracy and rapid convergence [*Waterloo Hydrogelogic, Inc.* 1998].

2.3 Delineation of Capture Zones

Capture zones associated with groundwater wells form the basis for defining wellhead protection areas. Conventionally, capture zones are created by particle tracking, often in 2D, to define isochrones of arrival time. For complex heterogeneous systems, this procedure can be problematic because 2D capture zones are rarely valid, and the particle tracks can be erratic due to large variations in the flow velocities. Also, reliable particle tracking methods for complex 3D systems are still relatively scarce. *Wilson and Liu* [1995] proposed another approach (Wilson's technique) to delineate the capture zone based on the solution of transport (advective-dispersive) equation.

In this study, particle tracking as well as Wilson's technique for advective-dispersive modelling are used and are discussed briefly in the next sections.

2.4 Particle Tracking

Particle tracking is used to trace pathlines by placing imaginary particles in the flow field and then tracking them in a forward or backward direction. This technique is highly efficient, because it does not involve solving the transport partial differential equation (2.1). Advective transport modelling may be used to delineate capture zones and wellhead protection areas based on a time-of-travel criterion [*U.S. Environmental Protection Agency*, 1987] for chemically conservative contaminants.

The advection of infinitesimal particles can represented by the following first-order ordinary differential equation:

$$\frac{dp}{dt} = v(p,t) \tag{2.8}$$

where $p = xi + yj + zk$ is the position vector (using the conventional unit vector notation), and $v = v_x i + v_y j + v_z k$ is the average seepage velocity vector, a function of particle position and time. The solution of equation (2.8) for particle location at any time t can be expressed by

$$p(t) = p(t_0) + \int_{t_o}^{t} v(p,t)dt \tag{2.9}$$

where $p(t_0)$ is the position of a particle at time t_o. When linear interpolation is used, the integral in the above equation can be evaluated analytically. *Pollock* [1988] applied the name "semi-analytical method" to this approach of pathline computation based on numerically calculated velocities and analytically derived pathlines [*Zheng and Bennett*, 1995].

A new particle-tracking code (WATRAC) developed by *Frind* [2000, in preparation] provides a basis of comparison without restrictions due to geometry for 3D systems. The code is based on prismatic finite elements for maximum flexibility, and uses a linear interpolation of velocities based on continuous interface fluxes across the five sides of the prism. This method was found to give better accuracy than conventional particle tracking methods [*Frind et al.,* 2000].

2.5 Wilson's Approach

An alternative approach for capture zone delineation is based on the adjoint method for advective-dispersive transport [*Wilson and Liu*, 1995; *Neupauer and Wilson*,

1999] . In this approach, one determines the location probability $f = f(x, y, z)$, i.e. the probability that a particle arriving at a well at a given time has originated at location (x, y, z) in the aquifer. To obtain the probability distribution, an advective-dispersive transport model is applied to the aquifer system with a source value of $C_s = 1.0$ at the well and a velocity of $-v(x, y, z)$. Although the dispersion coefficient is a function of velocity, no sign reversal is needed for the dispersion term. Dispersion is proportional to the magnitude of velocity; therefore reversing the direction of velocity does not affect the sign on the dispersion coefficient [*Neupauer and Wilson*, 1999]. *Uffink* [1989] states that dispersion is an irreversible process and therefore, results from the backward-in-time equation cannot be interpreted as concentration and can only be interpreted as probabilities. *Wilson and Liu* [1995], who first time derived expression for travel time probabilities, so this method referred as Wilson's Approach.

The advection-dispersion equation (ADE) is usually used to describe transport of a conservative solute in groundwater. Solute concentration as a function of space and time can be obtained by solving the ADE, for all times after the initial release of the solute. This form of the ADE is called a 'forward-in-time' model because the solute is located as it moves forward in time.

The advection-dispersion equation governing mass transport in the porous matrix is [*Bear*, 1972]:

$$\frac{\partial}{\partial x_i}(D_{ij}\frac{\partial c}{\partial x_j}) - v_i\frac{\partial c}{\partial x_i} - R\lambda c = R\frac{\partial c}{\partial t} \tag{2.10}$$

where $c = c(x, y, z, t)$ is the dissolved concentration of the solute (usually expressed as relative with respect to the source concentration c_o, or c/c_o; x, y, and z are spatial coordinates; D_{ij} is the hydrodynamic dispersion coefficient tensor; $v_i = q_i/\theta$ is the average groundwater velocity; R is the retardation coefficient; and λ is the first-order decay constant.

In three dimensions, the components of hydrodynamic dispersion tensor for an isotropic medium are given by [*Burnett and Frind*, 1987]:

$$D_{xx} = \alpha_L \frac{v_x^2}{v} + \alpha_{TH} \frac{v_y^2}{v} + \alpha_{TV} \frac{v_z^2}{v} + D^* \tag{2.11}$$

$$D_{yy} = \alpha_L \frac{v_y^2}{v} + \alpha_{TH} \frac{v_x^2}{v} + \alpha_{TV} \frac{v_z^2}{v} + D^* \tag{2.12}$$

$$D_{zz} = \alpha_L \frac{v_z^2}{v} + \alpha_{TH} \frac{v_x^2}{v} + \alpha_{TV} \frac{v_y^2}{v} + D^* \tag{2.13}$$

$$D_{xy} = D_{yx} = (\alpha_L - \alpha_{TH}) \frac{v_x v_y}{v} \tag{2.14}$$

$$D_{xz} = D_{zx} = (\alpha_L - \alpha_{TV}) \frac{v_x v_z}{v} \tag{2.15}$$

$$D_{yz} = D_{zy} = (\alpha_L - \alpha_{TV}) \frac{v_y v_z}{v} \tag{2.16}$$

where α_L, α_{TH}, and α_{TV}, are longitudinal, transverse horizontal, and transverse vertical dispersivities, respectively; $D^* = D_d \tau$ is the effective diffusion coefficient in the porous medium with D_d being the free solution diffusion coefficient of the solute; and τ is the tortuosity of the medium.

The transport equation (2.10) requires boundary conditions all around the domain for solution. This may be *Type 1* or *Dirichlet* boundary condition on boundary segment Γ_1

$$c = c_o(t) \tag{2.17}$$

the *Type 2* or *Neuman* boundary condition on boundary segment Γ_2

$$\frac{g_o(t)}{\theta} = -D_n \frac{\partial c}{\partial n} \tag{2.18}$$

Alternatively, the boundary condition can be specified in the form of a known mass flux, known as a *Type 3* or *Cauchy* boundary condition on boundary segment Γ_3 which takes the form:

$$\frac{q_o c_o(t)}{\theta} = vc - D_n \frac{\partial c}{\partial n} \tag{2.19}$$

where Γ=Γ_1+Γ_2+Γ_3 is the entire domain boundary, D_n is the dispersion coefficient in the direction normal to the boundary, g_o and q_o are normal components of dispersive vector and the Darcy fluid flux, respectively, prescribed on the boundary and c_o is a specified concentration.

The initial condition representing the concentration at $t = 0$ on the interior of the domain can be an arbitrary surface. For simplicity, it is be assumed that the domain is initially devoid of solute mass.

$$c(x, y, z, 0) = 0 \tag{2.20}$$

In Wilson's approach, the travel time cumulative distribution function (CDF), $F_\zeta(x, y, z, \zeta)$ describes the probability that a contaminant is captured by the pumping well in a period of time less than ζ, for a given location (x, y, z) [*Wilson and Liu*, 1995]. The three-dimensional travel time CDF, $F_\zeta(x, y, z, \zeta)$, for a travel time, ζ, from some location (x, y, z) to pumping well location can be expressed with the standard advection-dispersion equation (2.10) by replacing the concentration, c, with F_ζ and v by $-v$:

$$\frac{\partial}{\partial x_i}(D_{ij}\frac{\partial F_\zeta}{\partial x_j}) + v_i \frac{\partial F_\zeta}{\partial x_i} - R\lambda F_\zeta = R\frac{\partial F_\zeta}{\partial \zeta} \tag{2.21}$$

The boundary conditions are:

$$F_\zeta = 1.0 \qquad \text{as } \textit{Type 1} \text{ on boundary segment } \Gamma_1 \tag{2.22}$$

$$\frac{g_o(\zeta)}{\theta} = -D_n \frac{\partial F_\zeta}{\partial n} \qquad \text{as } \textit{Type 2} \text{ on boundary segment } \Gamma_2 \tag{2.23}$$

$$\frac{q_o F_o(\zeta)}{\theta} = v F_\zeta - D_n \frac{\partial F_\zeta}{\partial n} \qquad \text{as } \textit{Type 3} \text{ on boundary segment } \Gamma_3 \tag{2.24}$$

and initial condition is:

$$F_\zeta = 0 \qquad \text{at } \zeta = 0 \tag{2.25}$$

Applying this approach, prior contaminant locations can be determined using backward location and travel time probabilities. These probabilities can be used to improve characterization of known sources of groundwater contamination, to identify previously unknown contamination sources, and to delineate capture zones [*Neupauer and Wilson*, 1999].

Conceptually, this approach is also equivalent to applying the backward particle tracking with a random component added, where the random component (or the dispersion term in the transport model) represents the effect of high-frequency heterogeneities of the porous medium [*Frind et al.,* 2000].

Wilson's approach is applied in this study by using time-marching (WTC) and time-continuous (LTG) transport models.

2.5.1 Time-marching (Galerkin Finite Element) Technique

For solving transport equation (2.10), *Pinder and Frind* [1972] presented an approach which involves a finite element approximation in the spatial domain, and

finite difference for time derivative. The standard Galerkin weighted residual technique is applied to obtain an algebraic equation for every node in the grid. The development of the Galerkin finite element formulation is described by *Frind* [1993]. The numerical model WTC is based on a finite element time integration which generates a symmetric coefficient matrix while retaining second-order accuracy in time [*Molson et al.,* 1992]. WTC uses the symmetric conjugate solver, similar to WATFLOW, and results in a high degree of computational efficiency. Numerical errors were controlled by observing the grid Peclet and Courant criteria [*Daus et al.,* 1985] given by:

$$P_e = \frac{v\Delta x}{D} \leq 2 \tag{2.26}$$

$$C_r = \frac{v\Delta t}{\Delta x} \leq \frac{P_e}{2} \leq 1 \tag{2.27}$$

where Δx is the grid spacing and Δt is the size of the time step.

The presence of the advective term in the transport equation (2.10) can lead to numerical dispersion if these constraints are violated. Numerical dispersion may be difficult to identify, but it typically takes the form of a smeared concentration profile, a lagging concentration front or in oscillations resulting in negative concentrations or concentrations exceeding the source concentration [*Frind*, 1993]. A solution obtained in this way is inherently time marching because the response is advanced discretely through time from one time step to the next.

2.5.2 Laplace Transform Galerkin Technique

As described above, it is a common procedure to discretize time, using finite differences to approximately integrate the system of ordinary differential equations after the spatial discretization. This piecewise integration in time is performed even though the time domain possesses homogeneity and the governing equation and boundary conditions are linear [*Sudicky*, 1989].

It is generally well-known that certain choices for the time or improper selection of grid spacing or time step size can lead to artificial smearing or oscillations in the solution. In situations where the advective displacement of the solute dominates over the dispersive advance such that the solute front is relatively sharp, an exceedingly fine spatial and temporal discretization may be needed to ensure a reliable solution. Proper grid design and time step selection is further involved in natural geologic settings because the groundwater velocity may vary widely from point to point both in direction and magnitude.

If the governing equation and boundary conditions are linear and if the finite element coefficient matrices do not depend directly on time, it is then possible to obtain a closed-form analytical solution to the system of ordinary differential equations stemming from the spatial discretization step that is both continuous and exact in time [*Sudicky*, 1989]. The Laplace Transform Galerkin (LTG) technique was designed to use velocity vectors as element-wise constant (flow model output), recognizing that the velocity distribution produced is discontinuous at the element bounds. In this method, groundwater velocities and transport parameters can be variable in space, domain boundaries can be irregular and boundary conditions that are arbitrary functions of time can be easily accommodated. Because the Laplace domain solution is relatively smoother than the time domain solution, the use of relatively coarse grids or weakly dispersive problems is admissible without introducing problematic numerical dispersion [*Sudicky*, 1989]. LTG directly uses the velocity field and mesh configuration output from any groundwater flow model.

Laplace Transform and its Numerical Inversion

The Laplace transform, $f(p)$ of some function $f(t)$ is defined as:

$$L[f(t)] = \bar{f}(p) = \int_0^\infty \exp(-pt) f(t) dt = 0 \tag{2.28}$$

where L is the Laplace transform operator and p is the complex-valued Laplace

transform variable. The basic operational property of the Laplace transform is

$$L[\frac{df}{dt}] = p\bar{f} - f(t=0) \tag{2.29}$$

Application of the Laplace transformation equation (2.28) to the governing equation (2.10) and using the operational property equation (2.29) to eliminate the temporal derivative in equation (2.10) leads to:

$$\frac{\partial}{\partial x_i}(D_{ij}\frac{\partial \bar{c}}{\partial x_j}) - v_i\frac{\partial \bar{c}}{\partial x_i} - R(p+\lambda)\bar{c} = 0 \tag{2.30}$$

where $\bar{c} = \bar{c}(x, y, z, p)$ is the p space transformed concentration. Equation (2.30) now has the appearance of the steady state form of the advection-dispersion equation except for the introduction of the Laplace transform operator, p, in the decay term.

The boundary conditions (Equations 2.17- 2.19) must also be transformed and in p space, they become:

$$\bar{c} = \bar{c}_o(p) \qquad \text{on} \quad \Gamma_1 \tag{2.31}$$

$$\frac{\bar{g}_o(p)}{\theta} = D_n\frac{\partial \bar{c}}{\partial n} \qquad \text{on} \quad \Gamma_2 \tag{2.32}$$

$$\frac{q_o\bar{c}_o(p)}{\theta} = v\bar{c} - D_n\frac{\partial \bar{c}}{\partial n} \qquad \text{on} \quad \Gamma_3 \tag{2.33}$$

In the finite element method, a trial solution for equation (2.30) is assumed as:

$$\bar{c} \approx \hat{\bar{c}} = \sum_{j=1}^{m} \bar{c}_j(p) w_j(x, y, z) \tag{2.34}$$

where the w_j are basis functions, m is the number of nodes in the grid, and $\bar{c}_j(p)$ are unknown coefficient representing the p space concentrations at the node points.

Letting L^{-1}denote the inverse transformation, it can be written from equation (2.34):

$$\widehat{c}(x,y,z,t) = \sum_{j=1}^{m} L^{-1}[\bar{c}_j(p_k)]w_j(x,y,z) = \sum_{j=1}^{m} c_j(t)w_j(x,y,z) \tag{2.35}$$

where $c_j(t)$ is the concentration at node j in the time t domain. The numerical inversion algorithms require the value of the transformed variable for different values of $p = p_k, k = 1, 2, ..., 2K$, so the system of equations developed by applying Galerkin's method to equation (2.34) is solved anew for each p_k. *De Hoog* [1982] proposed an improved procedure for numerical inversion of Laplace transforms. There are many problems for which the Laplace transform of the solution is readily found, but the transform cannot be easily inverted analytically [*De Hoog*, 1982]. The proposed numerical method uses the trapezoidal rule for enhancing the convergence of the Fourier series that obtained from the inversion integral.

The nodal concentration $c_j(t)$ can be found from $\bar{c}_j(p_k)$:

$$c_j(t) = \frac{1}{T}\exp(p_o t)\Big\{\frac{1}{2}\bar{c}_j(p_o) + \sum_{k=1}^{2K} Re[\bar{c}_j(p_o + \frac{k\pi i}{T})\exp(\frac{k\pi i t}{T})]\Big\} + E \tag{2.36}$$

where $2T$ is the period of the Fourier series approximating the inverse on the interval $[0, 2T]$, Re denotes the real part of c_j, $i = \sqrt{-1}$, E is an error term and $p_o + k\pi i/T = p_k$. Usually, K=5 is adequate for convergence of the series [*Sudicky and McLaren*, 1992]. The parameter p_o is given by

$$p_o = \mu - \frac{\ln(E)}{2T} \tag{2.37}$$

Experience with large range of problems suggests that $\mu = 0, T = 0.8t_{\max}$ where $t_{\max}$ is the maximum time at which $c_j(t)$ is desired and E in the range of 10^{-4} and 10^{-6} yields accurate results [*Sudicky and McLaren*, 1992].

Chapter 3

Model Development and Parameterization

3.1 Model Development

Due to the complex nature of the Waterloo Moraine area, a fully three-dimensional model is the only option to get reliable flow and transport results. For flow simulations, a modified version of the 3D code WATFLOW [*Beckers et al.,* 2000] is used in this study. For capture zone delineation, the following three models are used:

1. WATRAC (particle-tracking advective transport code),
2. WTC (advective-dispersive time-marching transport code), and
3. LTG (advective-dispersive time-continuous transport code).

Some modifications are made in the LTG model developed by *Sudicky* [1989] to incorporate the dispersivity in all three directions. Prior to solving the transport equation, the flow equation is solved using WATFLOW to get the nodal head distribution and elemental velocities.

The particle-tracking code (WATRAC) requires hydraulic heads as an input while the advective-dispersive transport models (WTC and LTG) require velocities

along with the 3D mesh information. The development of this scheme is represented in Figure 3.1.

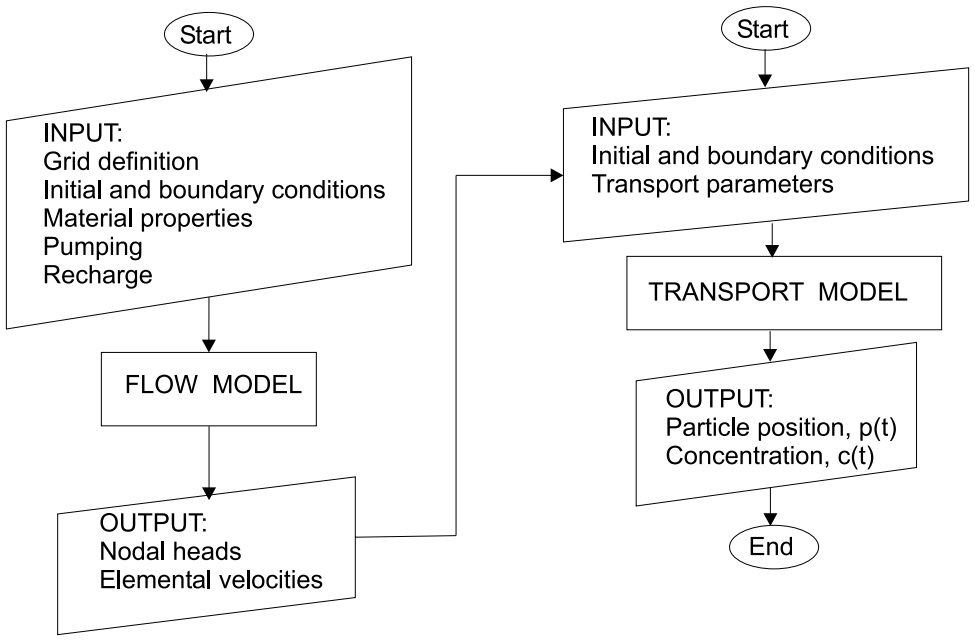

Figure 3.1: Algorithm for the solution of flow and transport equations.

3.2 Spatial and Temporal Discretization

One of the objectives of this study is to use LTG with coarse and fine meshes to compare the results with different mesh sizes, so two different spatial discretizations are needed within the model domain. The coarse mesh (Figure 3.2) is used for LTG only while the fine mesh is used for WTC, LTG, and WATRAC. For each case (coarse and fine mesh discretization), a two-dimensional finite element mesh is generated within the model domain using the preprocessor GRIDBUILDER [*McLaren*, 1999], and projected vertically to form a 3D mesh. The coarse element mesh has

elements ranging from 10 m close to the wells to a maximum of 500 m away from the well fields. Vertically, 8 hydrostratigraphic zones of aquifers and aquitards were resolved using 13 elemental layers by *Martin and Frind* [1998]. In the Gartner Lee Report [*GLL et al.,* 1998], the Greenbrook subdomain was resolved using 27 layers. The most recent simulations were made by *GLL et al.,* [1999] using a total of 30 layers (Figure 3.3) with the addition of 3 layers in Aquitard 1. The added refinement in Aquitard 1 was considered necessary because of the importance of resolving small-scale heterogeneities close to the recharge surface [*GLL et al.,* 1999]. Vertically, the hydrostratigraphy is divided as follows:

Aquitard 1: 5 equal layers;
Aquifer 1: 6 equal layers;
Aquitard 2: 4 equal layers;
Aquifer 2: 5 equal layers;
Aquitard 3: 3 equal layers;
Aquifer 3: 3 equal layers;
Aquitard 4: 2 equal layers;
Aquifer 4: 1 layer,

for a total of 29 elemental layers and 30 nodal surfaces. In addition, a thin recharge spreading layer (RSL; for definition see GLL, 1998) is present above the land surface in whole of the domain. This results in a total of 301,475 nodes and 567,360 prismatic elements in 3D system. This coarse mesh is refined twice in the area of all major well fields (Figure 3.4) which results in a 1,335,790 nodes and 2,568,900 elements for whole of the model domain.

Because the LTG model solves the transport equation continuous in time, there is no need for temporal discretization. For the WTC time-marching solution, time increments (Δt) of 5 days for earlier times and 10 days for later times are used.

3.3 Boundary Conditions

For the flow model, a *Type 1* (*Dirichlet*) boundary condition is applied in the surficial layers of nodes to the water elevation values of Grand River, Conestogo River, Boomer Creek, Nith River, and Roseville Swamp (Figure 3.5). A *Type 2* (*Neuman*) boundary is applied at the top of the model to represent the recharge to the system as a specified flux (mm/year), with some constant head nodes where surface bodies exist in direct contact with the saturated zone.

A no-flow boundary is designed for the base of the model. The bottom layer of the model (bedrock) is assumed to be uniformly fractured at the top portion and it was found that this layer is contributing some water to the Greenbrook wells [*Woeller*, 1982]. Other geochemical and isotopic studies for production wells throughout the Waterloo Moraine indicate that a significant amount of water is derived from the bedrock storage [*Terraqua*, 1992]. Below the upper fractured portion, the bedrock is assumed to be less fractured and to act as a no-flow boundary.

Pumping wells are represented by 1-D line elements as per *Sudicky et al.,* [1995] extending between a number of nodes depending upon their actual position in the respective aquifer. For transport modelling, wells are assigned as *Type 1* to be used for capture zone delineation by Wilson's technique. To determine the sources of contamination in the Greenbrook wells, nodes at the expected contaminated sites are also assigned as *Type 1.* Boundary conditions for flow and transport models are shown in Figure 3.5.

3.4 Pumping Wells and Pumping Rates

To calibrate the flow model, *GLL et al.,* [1999] used the 1990's pumping wells and pumping rates for Waterloo Moraine area. Presently, some of those wells are not in operation and some are replaced due to deterioration. Those wells and pumping rates are used in this study to determine the potential sources of contamination in

the wells. For the delineation of capture zones, projected pumping rates provided by the RMOW in November, 1999 are used. Table 3.1 shows the details of existing and expected pumping wells with their pumping rates.

3.5 Calibrated Hydraulic Conductivity

For flow and transport simulations, hydraulic conductivity (K) is the most fundamental parameter. Most groundwater text books list typical values and ranges of hydraulic conductivity for various rock types [i.e., *Freeze and Cherry*, 1979; *Domenico and Schwartz*, 1990; *Fetter*, 1994]. Hydraulic conductivity may exhibit extensive horizontal and vertical variations, especially in areas such as the Waterloo Moraine. *GLL et al.,* [1999] used point values of K (estimated from the available lithologic information) for calibration with observed surface and groundwater level records. In that study, a spatial statistical technique (3D kriging) was used for defining the intra-formational conductivity distribution in each aquifer and aquitard. The correlation lengths λ_x, λ_y, and λ_z were determined by semivariogram analysis and then used for the interpolation of K in all the lithologic units. Simulated versus observed heads for the assessment of the calibration are given in Figure 3.6. Final calibrated K distributions in Aquifer 1 and Aquitard 1 are shown in Figure 3.7 and Figure 3.8, respectively. It is very clear from these figures that the system is highly heterogeneous. There are high conductivity zones (windows) in the aquitard which act as a part of an aquifer, while low conductivity zones are present in the aquifer which locally act as an aquitard. The same kind of heterogeneity is present in the other aquitards and aquifers. Aquitard windows have a controlling influence on the capture zone delineation, and even small but strategically located windows can cause large changes in the capture zones [*Martin and Frind*, 1998].

3.6 Calibrated Recharge

An average groundwater recharge of 100 mm/year was estimated by *Rudolph* [1985]. *Fitzpatrick* [1993] assumed as average rate of 125 mm/year with higher rates of 275 mm/year in western rural areas. *Callow* [1996] applied 50 mm/year in urban areas and 250 mm/year in the rural areas. *Martin and Frind* [1998] used an average of 200 mm/year over their study area with 180 mm/year along the flanks, 220 mm/year in the core area of the Moraine, and to a high of 310 mm/year in the immediate vicinity of the Mannheim sandhills.

In this study, an average 'potential recharge' value of 535 mm/year is redistributed over the area of the model by the recharge spreading layer (RSL). This value was determined by *GLL et al.,* [1999] while calibrating the model with observed groundwater and stream levels in the Waterloo Moraine area. A recharge value of 296 mm/year is calculated for the Greenbrook fine meshed area using the vertical component of the velocity of elements which lie in the bottom layer of Aquitard 1. The distribution of recharge through this layer for Greenbrook area is shown in Figure 3.9. The remaining part of the 'potential recharge' (i.e., 239 mm/year) goes directly to the streams from the RSL as a surface runoff or as an interflow.

3.7 Transport Parameters

For simulations with fine grid, the values of 20, 5, and 0.02 m are used for the longitudinal, transverse horizontal and transverse vertical dispersivities, respectively. These values were used in the previous studies for the Greenbrook well field using time-marching transport techniques.

Scale may influence the magnitude of the dispersivity in the sense that in a simulation which uses a coarse mesh spacing, more and larger heterogeneities are included in each element or cell than in a simulation which uses a close spacing

[*Zheng and Bennett*, 1995]. Thus for the same field problem, the dispersivities needed to achieve agreement with observed solute movement may tend to be larger at larger spacings [*Zheng and Bennett,* 1995].

For the coarse mesh, values of horizontal macro-dispersivity are calculated using the formulations described by *Gelhar and Axness* [1983] for all the units (aquifers and aquitards). Statistical parameters that were determined by *Radcliffe* [2000, in preparation] for a selected area in the Waterloo Moraine are used for these calculations. A value of 50 m is selected for longitudinal macro-dispersivity that is close to the average value of the four aquifers. Also, this value is well within the range of results presented by *Gelhar, et. al.* [1992] for the scale of kilometers. Following parameter values are used for the transport modelling:

Porosity:	$f(K_x)$ [*Domenico and Schwartz*, 1990]
Longitudinal dispersivity:	20 m (fine mesh), and
	50 m (coarse mesh)
Transverse horizontal dispersivity:	5 m
Transverse vertical dispersivity:	0.02 m
Retardation factor:	1.0
Decay coefficient:	0.0

Table 3.1: Waterloo Moraine: Summary of pumping rates (m^3/sec).

Well Name	Well Field	Easting	Northing	Pumping Rate		Layers
				Existing	Expected	
B1	Baden	528446.8	4805790.5	1.55E-02		20-24
B2	Baden	528447.8	4805788.3	1.55E-02		20-24
HD1	Heidelberg	531220.0	4819153.6	1.23E-03	1.63E-03	5-6
HD2	Heidelberg	531218.8	4819138.5	8.52E-04	1.63E-03	5-6
K1	Greenbrook	540567.5	4808455.7	1.83E-02	2.04E-02	11-14
K2	Greenbrook	540545.0	4808299.6	2.06E-02	2.04E-02	11-14
K3	Greenbrook	540726.6	4808666.3	6.86E-04		5-6
K4b	Greenbrook	540773.8	4808694.2	4.61E-02	4.60E-02	11-14
K5	Greenbrook	540567.3	4808833.4	8.64E-03		11-14
K5A	Greenbrook	540539.8	4808799.9		4.09E-02	11-14
K6	Greenbrook	540521.0	4808808.4	7.18E-03		5-6
K8	Greenbrook	540437.0	4808249.4	2.70E-02	2.66E-02	11-14
K10a	Strange St.	538911.0	4810431.0	2.94E-03	1.16E-02	20-24
K11	Strange St.	537825.4	4810479.5	1.56E-02	3.25E-02	20-24
K12	Strange St.	539163.8	4811192.9	5.46E-03	5.91E-03	11-14
K13	Strange St.	537876.6	4810217.0	6.78E-03	2.36E-02	20-24
K17	Strange St.	539410.5	4810676.6	5.72E-03	5.32E-03	11-14
K18	Strange St.	537287.6	4810660.0	3.45E-02	3.55E-02	20-24
K21	Mannheim	538505.3	4806484.0	2.12E-02	4.60E-02	20-24
K22	Mannheim	536538.2	4805046.0	3.09E-02	3.55E-02	20-24
K23	Mannheim	536770.3	4804781.7	3.72E-02	4.96E-02	20-24
K24	Mannheim	537054.8	4803860.8	2.22E-02	3.43E-02	20-24
K25	Mannheim	538815.5	4805709.3	5.33E-02	5.91E-02	20-24
K26	Mannheim	537733.0	4803203.8	7.65E-02	8.04E-02	20-24
K29	Mannheim	538818.0	4805693.0	5.08E-02	4.81E-02	20-24
K31	Parkway	544542.0	4807032.9	4.50E-02	3.72E-02	5-6
K32	Parkway	544870.3	4806875.5	3.54E-02	3.72E-02	5-6
K33	Parkway	544523.8	4807049.6	3.62E-02	3.72E-02	5-6
K34	Parkway	544032.8	4804487.0	2.54E-02	4.47E-02	5-6
K36	Parkway	543952.7	4803923.9	2.45E-02	4.96E-03	5-6
K50	Wilmont	530898.7	4803907.1	5.11E-02	7.26E-02	20-24
K51	Wilmont	530889.3	4803901.8	5.11E-02	7.26E-02	20-24
K91	Mannheim	537687.7	4806010.5	4.89E-03	8.64E-03	20-24
K92	Mannheim	537714.2	4806040.0	4.89E-03	1.08E-02	20-24
K93	Mannheim	537573.4	4806489.2	4.61E-03	1.08E-02	20-24
K94	Mannheim	537691.1	4806543.6	4.61E-03	1.08E-02	20-24
ND2+ND4	New Dundee	537938.1	4800208.3	4.12E-05	4.47E-03	20-24
ND3	New Dundee	537926.6	4800202.3	2.43E-03		20-24
R4	Roseville	542779.4	4799031.5	8.23E-04		5-6
R5+R6	Roseville	542786.7	4799006.7		1.41E-03	5-6
SC1	St. Clement	528004.7	4819424.6	3.61E-04		20-24
SC2	St. Clement	527999.1	4819425.0	8.46E-04	8.04E-04	20-24
SC3	St. Clement	528026.1	4819420.4		7.27E-03	20-24
STA3+STA4	St. Agatha	530548.9	4809271.5	1.59E-04	4.72E-04	20-24
W1C	William St.	538847.0	4812319.0	2.33E-02	2.26E-02	11-14
W1B+W2	William St.	538877.8	4812290.6	4.15E-02	3.98E-02	11-14
W3	William St.	538884.8	4812303.4	1.53E-02		1-2
W4	Waterloo North	536868.0	4813010.7	1.08E-02	1.00E-02	20
W5	Waterloo North	535106.7	4814661.1		3.55E-02	11-14
W6A	Erb St.	532493.0	4809802.0		4.33E-02	20-24
W6B	Erb St.	532496.0	4809797.0	1.72E-02		20-24
W7+W8	Erb St.	533126.6	4809135.9	6.33E-02	1.01E-01	20-24
W10	Waterloo North	535307.3	4812505.8	1.38E-02	1.95E-02	20-24
W14	William St.	538412.5	4812175.5		7.56E-03	11-14
W15	William St.	538337.5	4812170.5		7.56E-03	11-14
WY1+WY5	Wellesley	518826.7	4813111.4	8.03E-04	2.36E-03	5-6
WY3	Wellesley	519113.2	4813193.0	3.71E-04		5-6
WY4	Wellesley	519488.2	4813934.5	8.23E-04		5-6
Private	Sunar1	537673.0	4812250.0		5.91E-04	11-14
Private	Sunar2	537704.0	4812270.0		5.91E-04	11-14

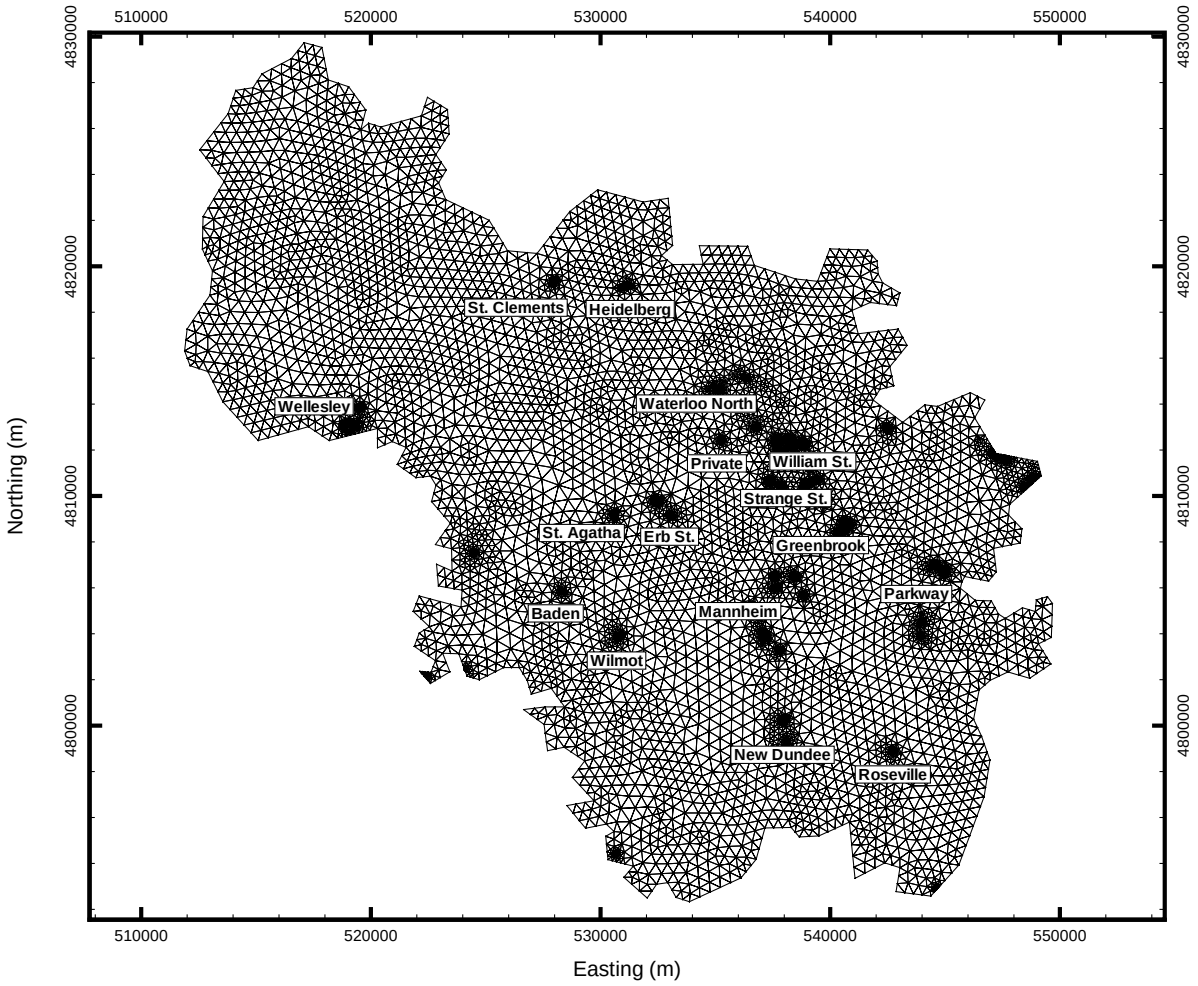

Figure 3.2: Finite element coarse mesh.

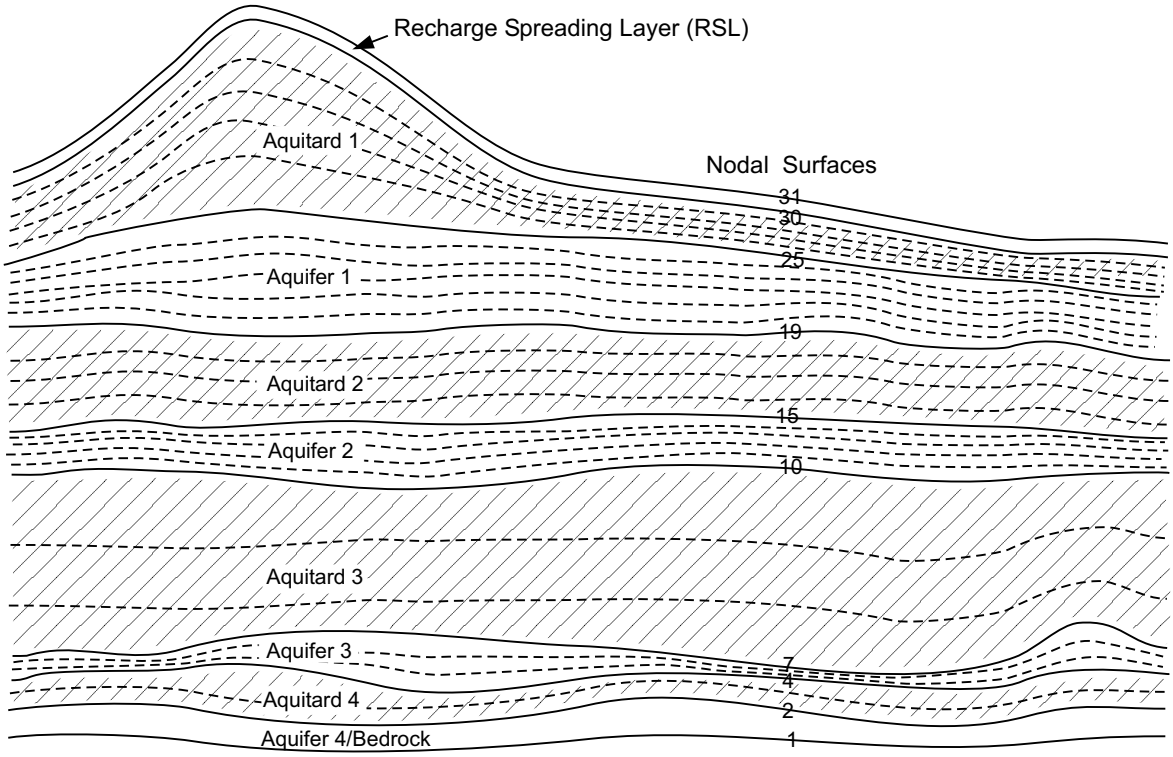

Figure 3.3: Finite element layering scheme (modified from Callow, 1996).

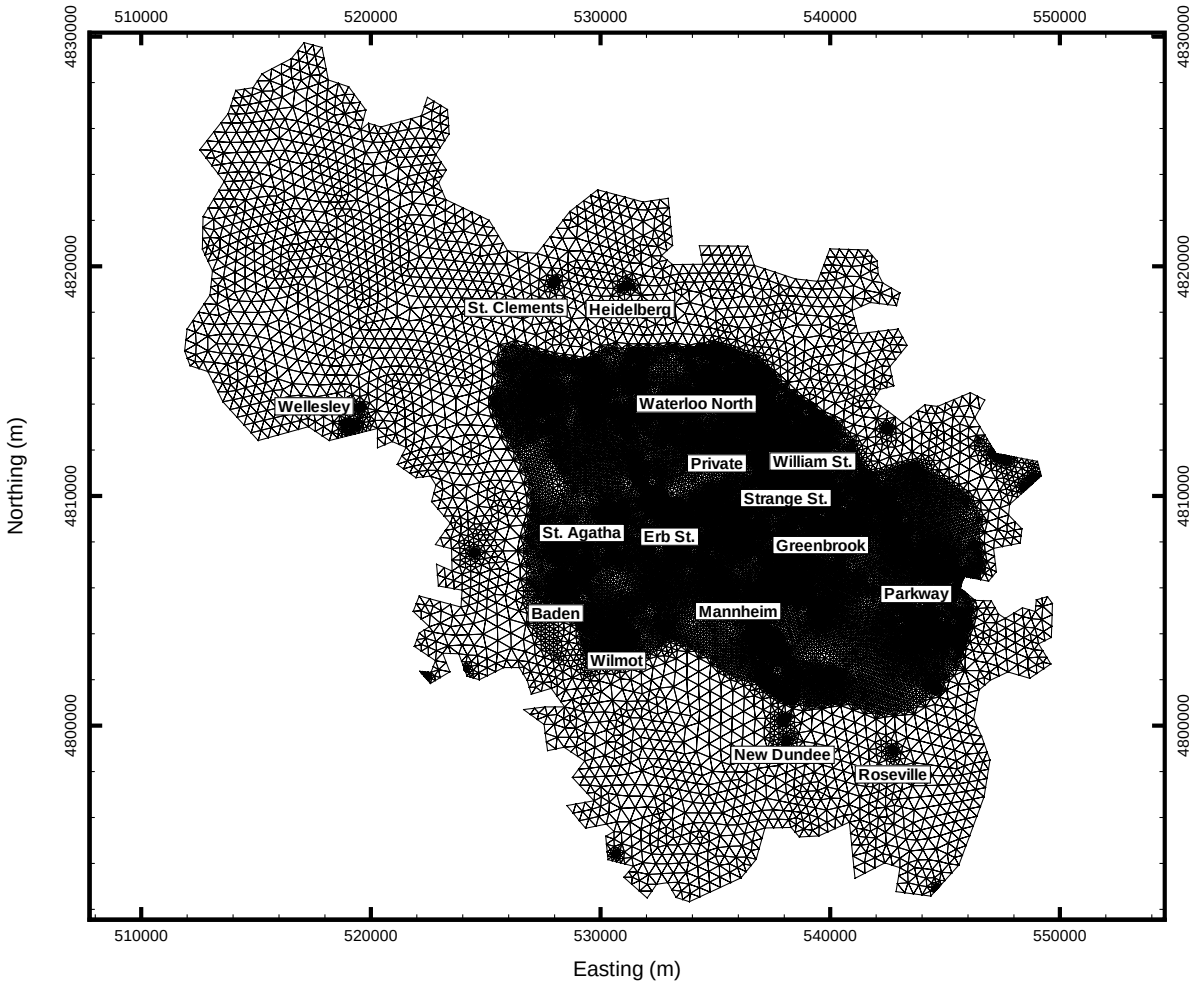

Figure 3.4: Fine mesh for major well fields embedded in coarse mesh.

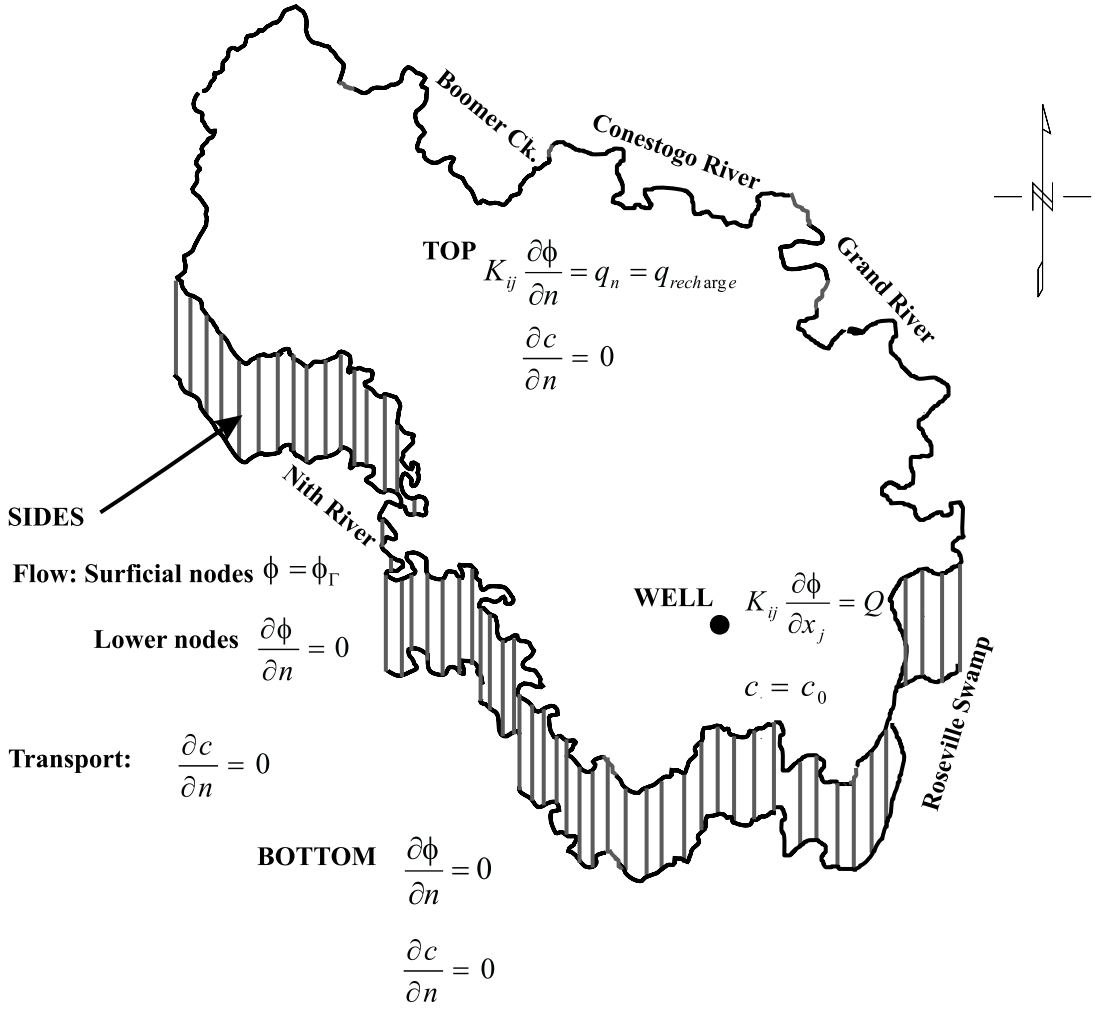

Figure 3.5: Boundary conditions for flow and transport models.

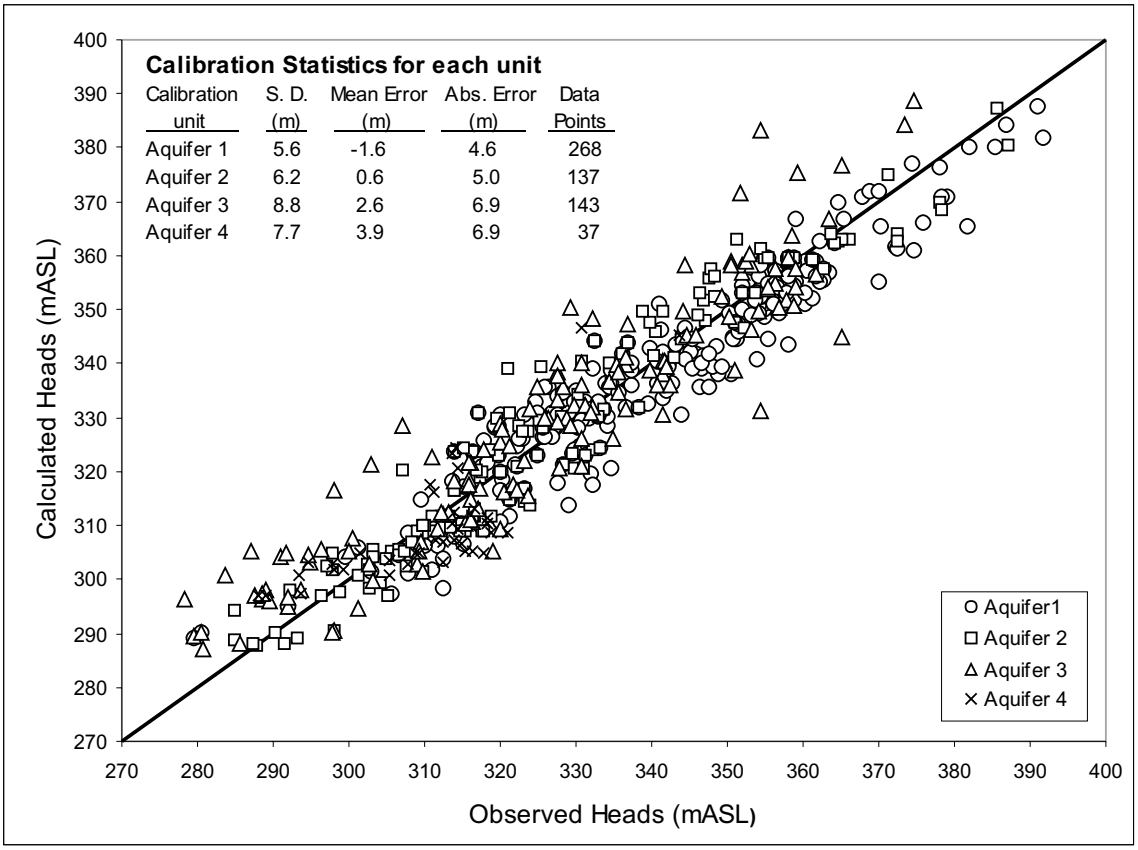

Figure 3.6: Assessment of flow model (WATFLOW) calibration (adapted from GLL, 1998).

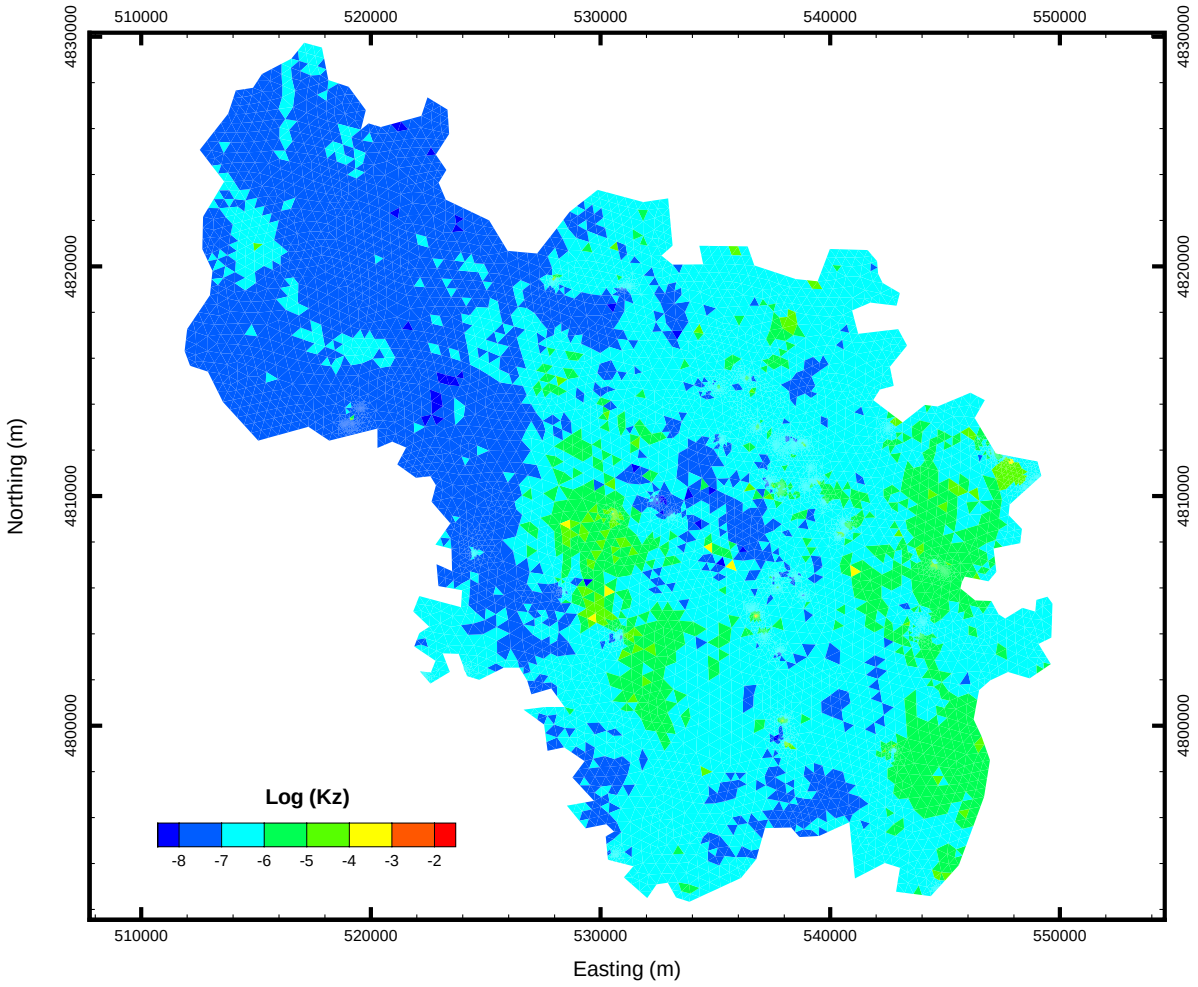

Figure 3.7: Distribution of hydraulic conductivity in Aquitard 1 (adapted from GLL, 1998).

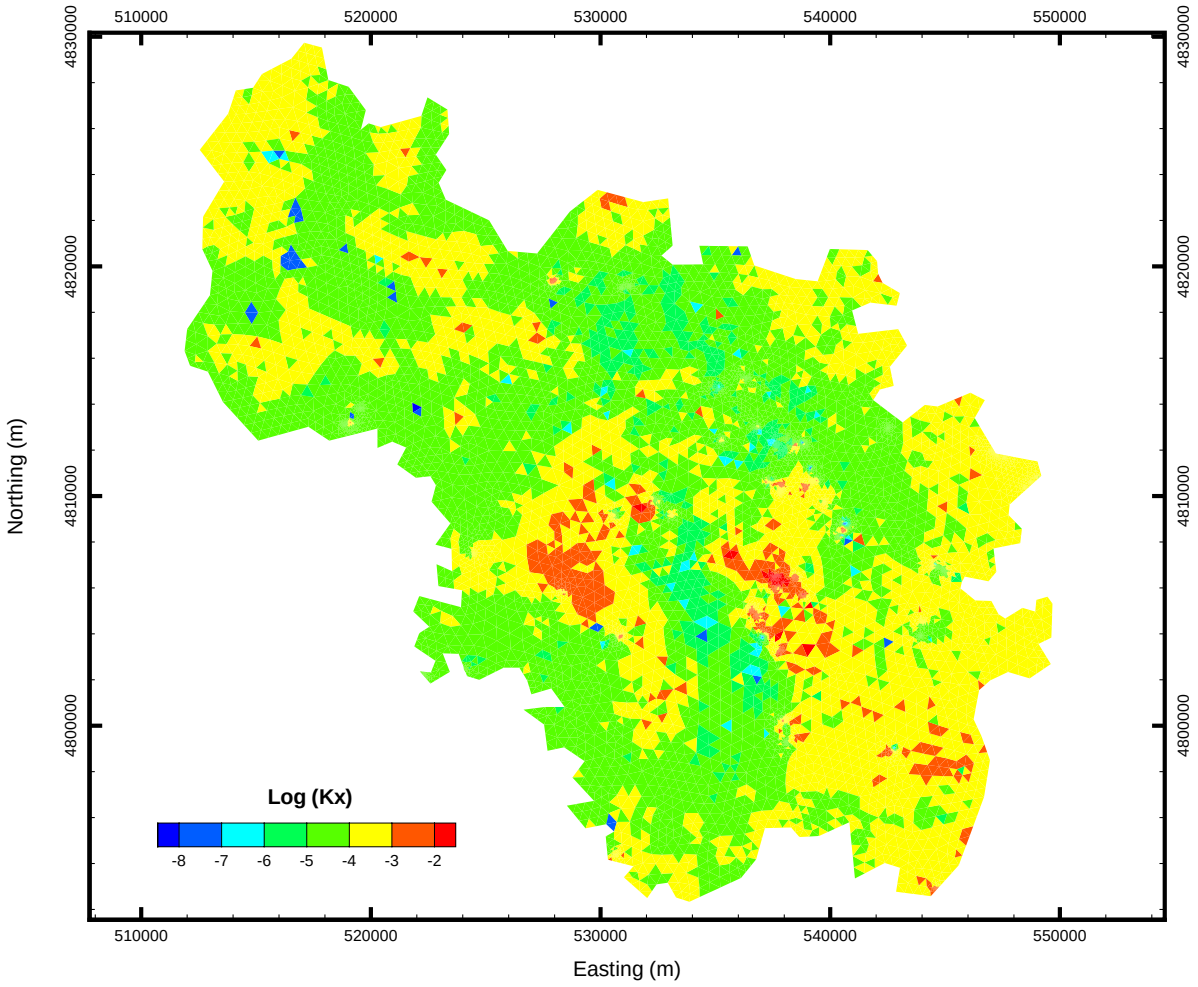

Figure 3.8: Distribution of hydraulic conductivity in Aquifer 1 (adapted from GLL, 1998).

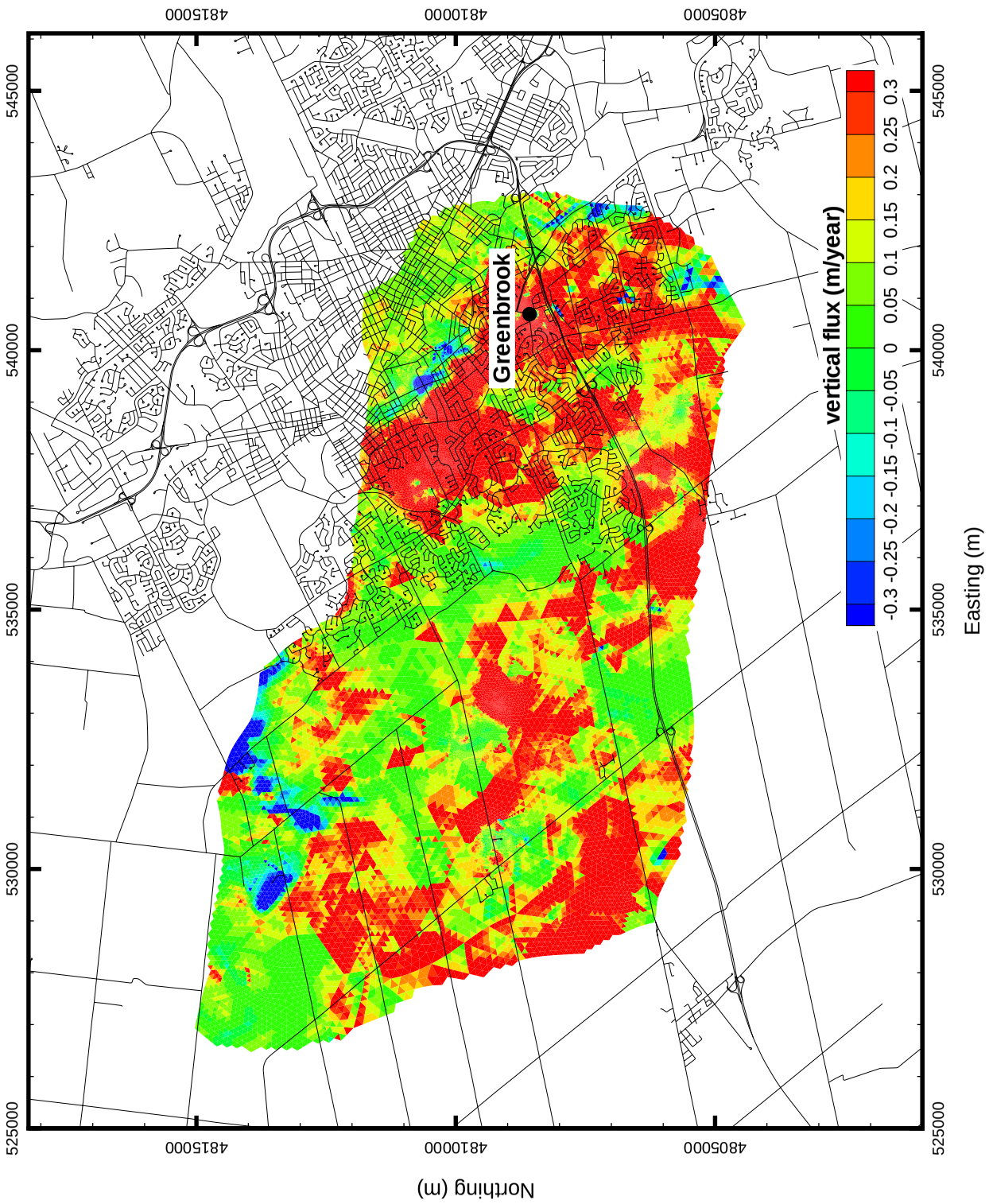

Figure 3.9: Vertical flux distribution in Greenbrook area.

Chapter 4

Flow Modelling Results

This chapter presents the results of the flow model (WATFLOW) under present, future and revised pumping conditions.

The flow model (WATFLOW) is used to simulate the steady state hydraulic head distribution for the following three cases:

i. Present pumping conditions for the determination of potential sources of contamination at some of the Greenbrook wells,

ii. Future pumping conditions (provided by RMOW) for delineation of capture zones, and

iii. Revised pumping conditions, after some adjustments in the future pumping rates at two well fields.

4.1 Present Pumping Conditions

Figures 4.1 through 4.3 show the hydraulic head distribution in three aquifers produced by the calibrated model under steady state pumping conditions using the present pumping rates as shown in Table 3.1. Generally, the groundwater flow

direction is from northwest to southeast along the core of the Moraine, and towards the Grand and Nith Rivers. Impact due to pumping is clear especially at the Greenbrook, Mannheim, and Erb Street wells in the respective aquifers in which these wells are screened. The execution of the fully 3D model with 1,335,790 nodal points required about 10 hours on a Pentium III 500 PC for steady state solution.

The system mass balance (m^3/sec.) calculations are:

Influxes at constant head nodes:	2.970986
Influxes due to recharge :	12.53186
TOTAL INFLUXES :	14.50256
Exit fluxes at constant head nodes :	15.50285
Exit fluxes at the pumping wells :	1.004245
TOTAL EXIT FLUXES :	15.50680
% SYSTEM MASS BALANCE ERROR:	-0.025

The percentage of mass balance error and calibration statistics (Figure 3.6) indicate that the model with the given parameters is representing the system quite well. The results of this case are used for transport modelling to determine the sources of contamination at some of the Greenbrook wells.

4.2 Future Pumping Conditions

RMOW expects an increase in water demand with respect to time due to population growth in the Region. Capture zones for all the major well fields are determined by using the future (expected) pumping rates (Table 3.1). Figures 4.4 to 4.6 show the hydraulic head distribution in three aquifers produced by using these pumping conditions. Generally, the flow trend is the same as in the previous case. It is clear from Figure 4.4 that the heads at the Erb Street well field are very low due to the increase in pumping rates (79 %) compared to the present pumping rates. This high pumping rate is creating a steep cone of depression for this well field, especially at well W6A. This well has a pumping rate of 3741 m^3/day which is

expected to replace the existing well W6B which is pumping at a rate of 1486 m^3/day; an increase of 152 %. This excess simulated drawdown may be due to the lack of observed groundwater levels used for calibration. On the other hand, the simulated results suggest that the proposed rate increase may not be realistic. The hydraulic head at Greenbrook well K5A is also low due to the high pumping rates of 3534 m^3/day, that replaced K5 with the existing pumping rate of 746 m^3/day (an increase of about 400%).

The increase in the pumping rates (42 %) at Wilmot well field has a profound effect on the hydraulic heads in Aquifer 1. The increase in the Waterloo North well field's pumping rate is due to the operation of W5, presently considered as an abandoned well. The effect of W5 is clear in Figures 4.5 and 4.6 representing the hydraulic head distribution in Aquifer 2 and Aquifer 3, respectively.

The system mass balance (m^3/sec.) calculations for this case are:

Influxes at constant head nodes:	3.061326
Influxes due to recharge :	12.53186
TOTAL INFLUXES :	15.59319
Exit fluxes at constant head nodes :	14.31315
Exit fluxes at the pumping wells :	1.276873
TOTAL EXIT FLUXES :	15.590023
% SYSTEM MASS BALANCE ERROR:	0.02

There is an overall increase of 27% in pumping rate for this case. The change in pumping rates for the major well fields is given in Table 5.1. Two private wells (Sunar-1 and Sunar-2) which are situated close to the William Street well field are also included in this case with a total pumping rate of 102.12 m^3/day.

4.3 Revised Pumping Conditions

As described in the previous section, the simulated hydraulic heads using the future pumping rates are unrealistic, therefore another flow solution is obtained by using the revised pumping rates. In this case, the future pumping rates provided by the RMOW are used except for the Erb Street wells and W5A of the Greenbrook well field. The pumping rates for these wells are kept the same as present (existing) rates. Figures 4.7 to 4.9 show the heads in Aquifer 1, 2, and 3, respectively.

The system mass balance (m^3/sec.) calculations for this case are:

Influxes at constant head nodes:	3.037834
Influxes due to recharge :	12.53186
TOTAL INFLUXES :	15.56970
Exit fluxes at constant head nodes :	14.38888
Exit fluxes at the pumping wells :	1.181213
TOTAL EXIT FLUXES :	15.57009
% SYSTEM MASS BALANCE ERROR:	-0.003

The head values at Erb Street wells and at K5A are now normal compared to the values computed by using the future (expected) pumping rates.

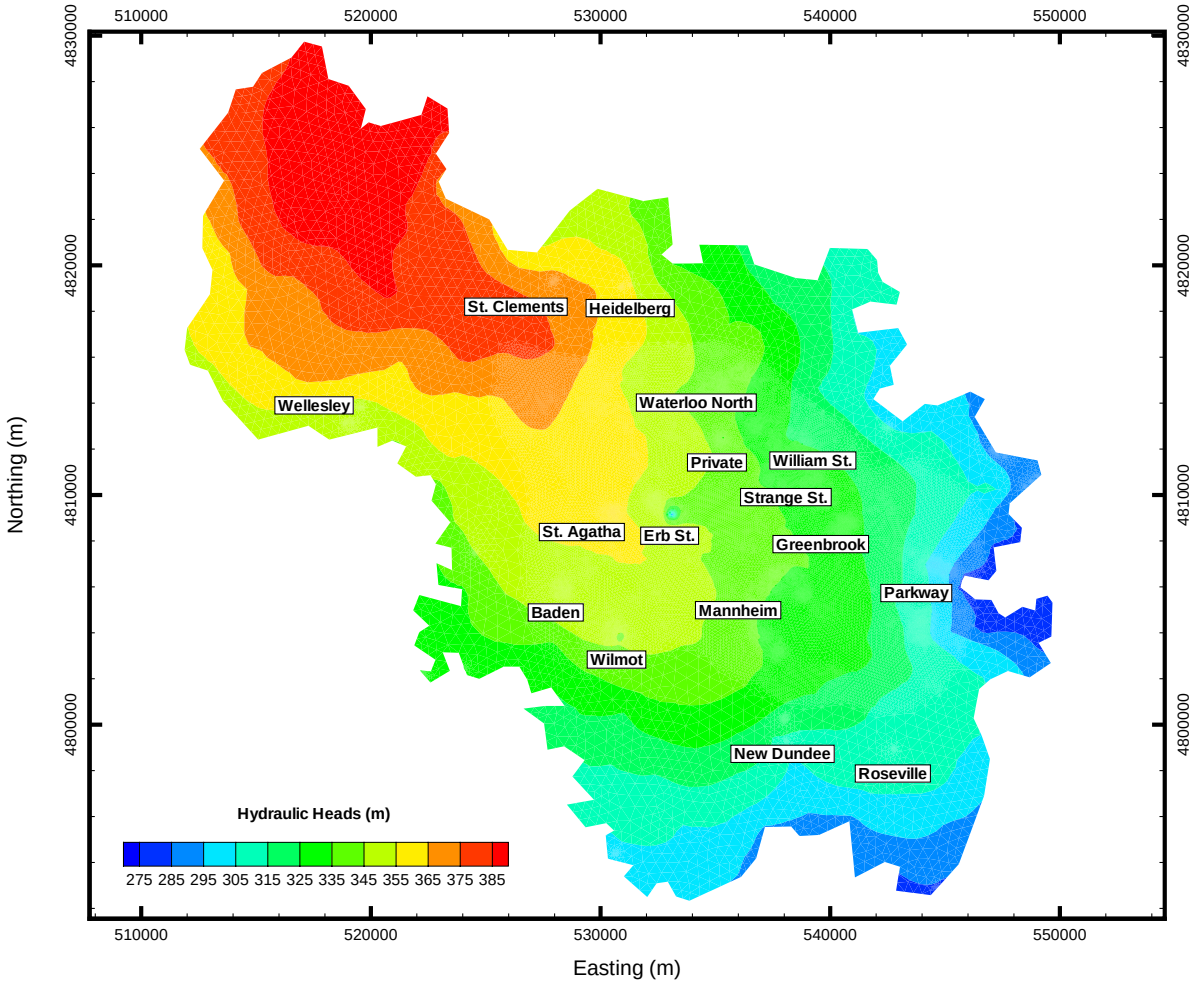

Figure 4.1: Head distribution under present pumping conditions in Aquifer 1.

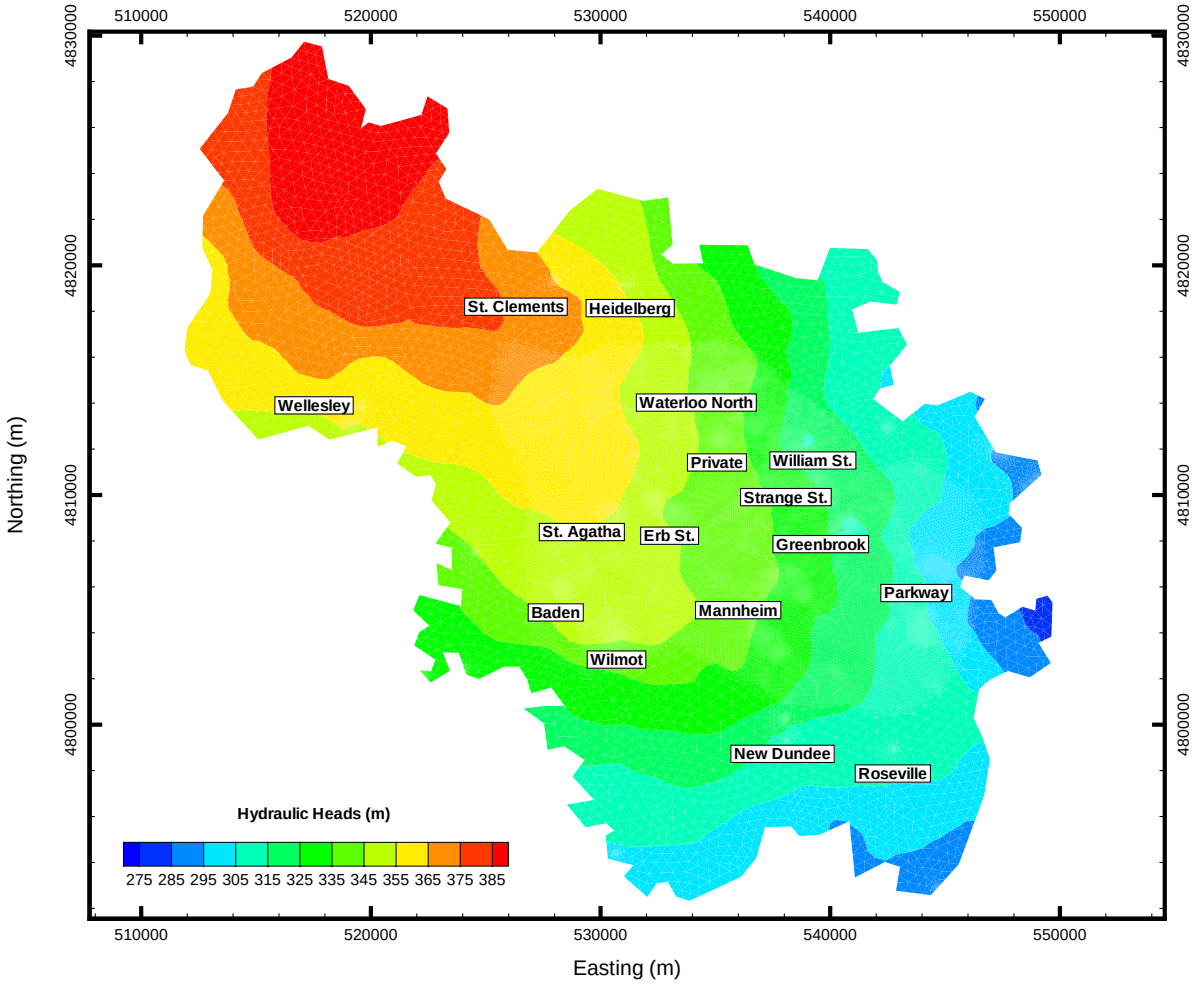

Figure 4.2: Head distribution under present pumping conditions in Aquifer 2.

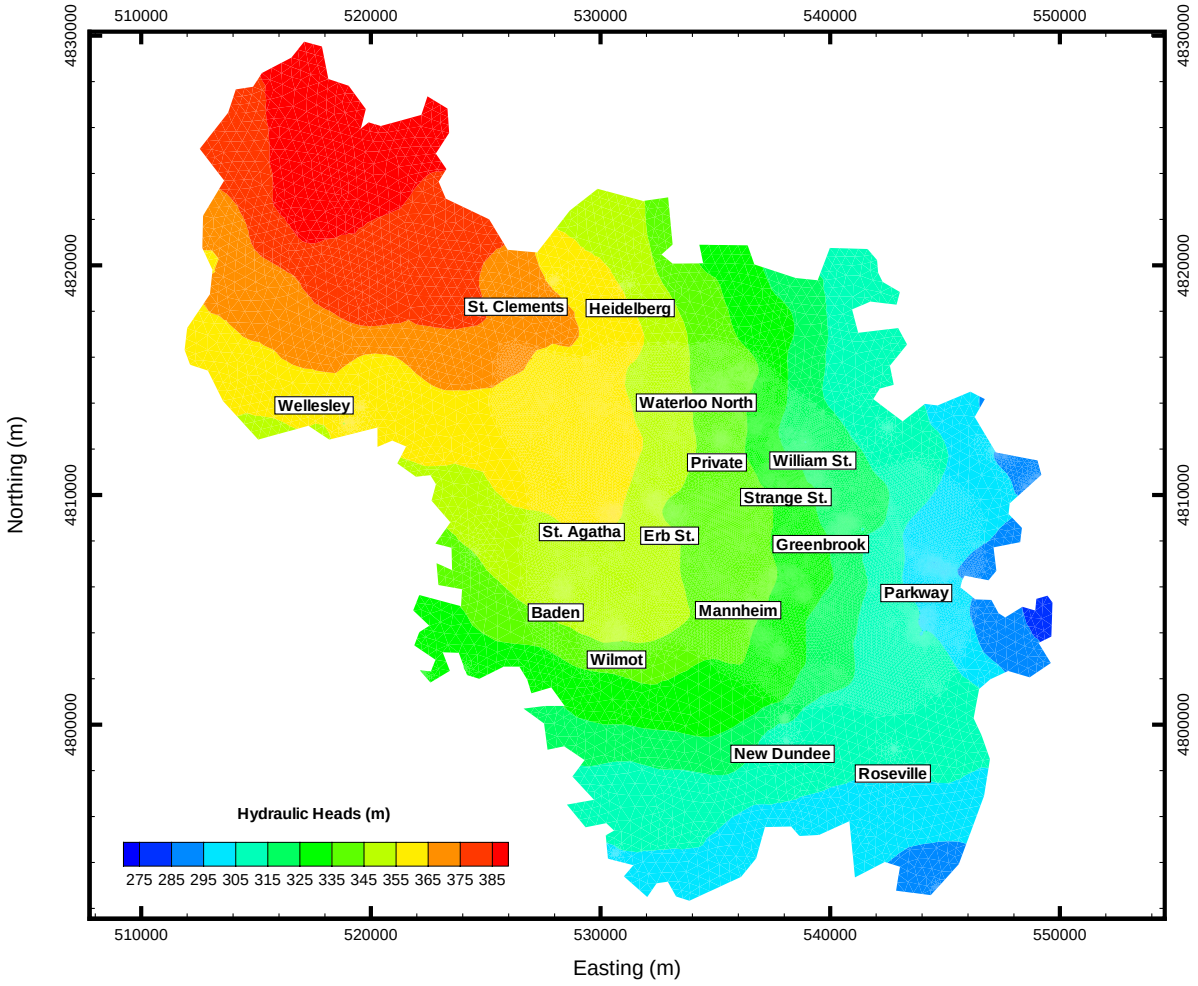

Figure 4.3: Head distribution under present pumping conditions in Aquifer 3.

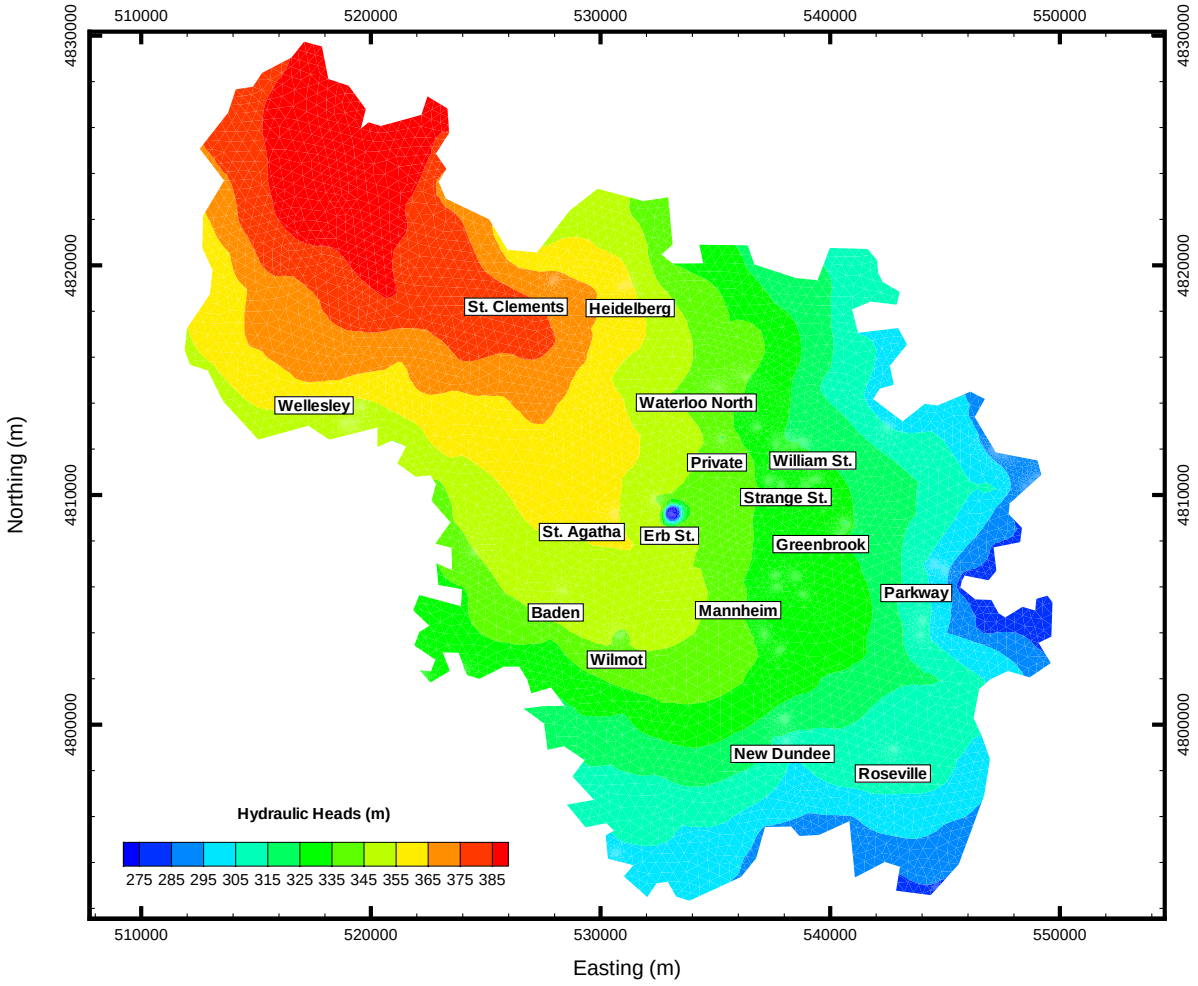

Figure 4.4: Head distribution under future pumping conditions in Aquifer 1.

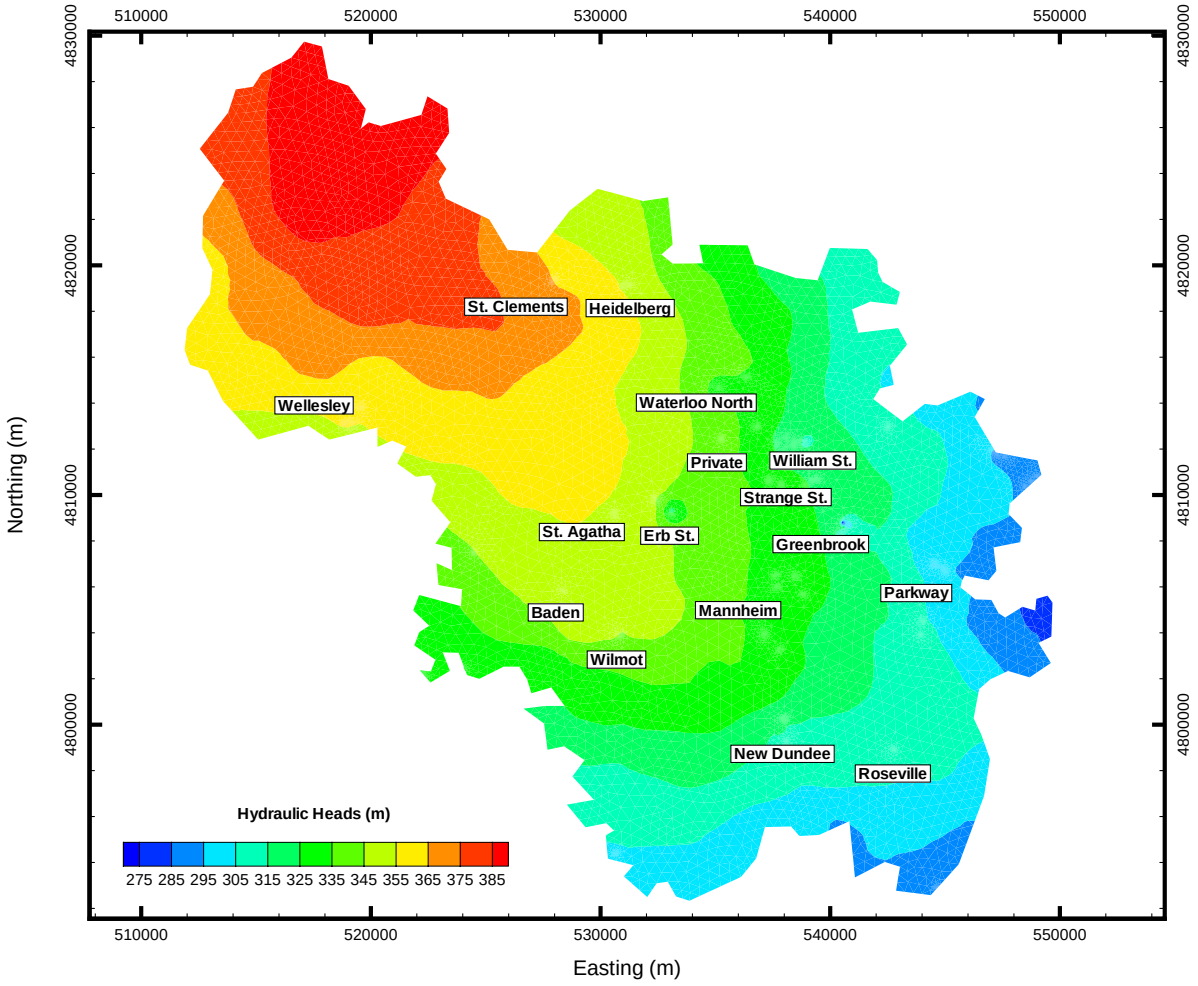

Figure 4.5: Head distribution under future pumping conditions in Aquifer 2.

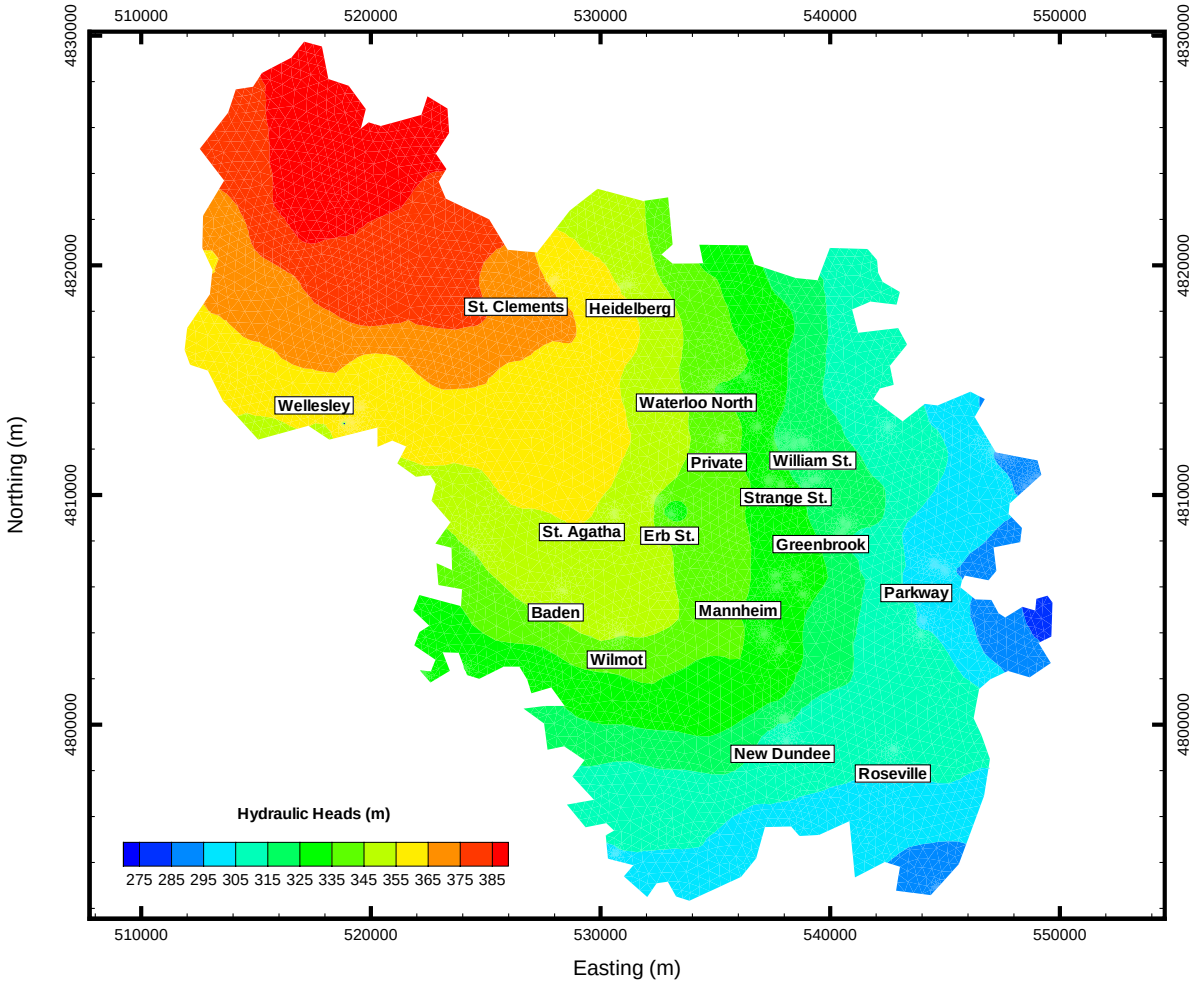

Figure 4.6: Head distribution under future pumping conditions in Aquifer 3.

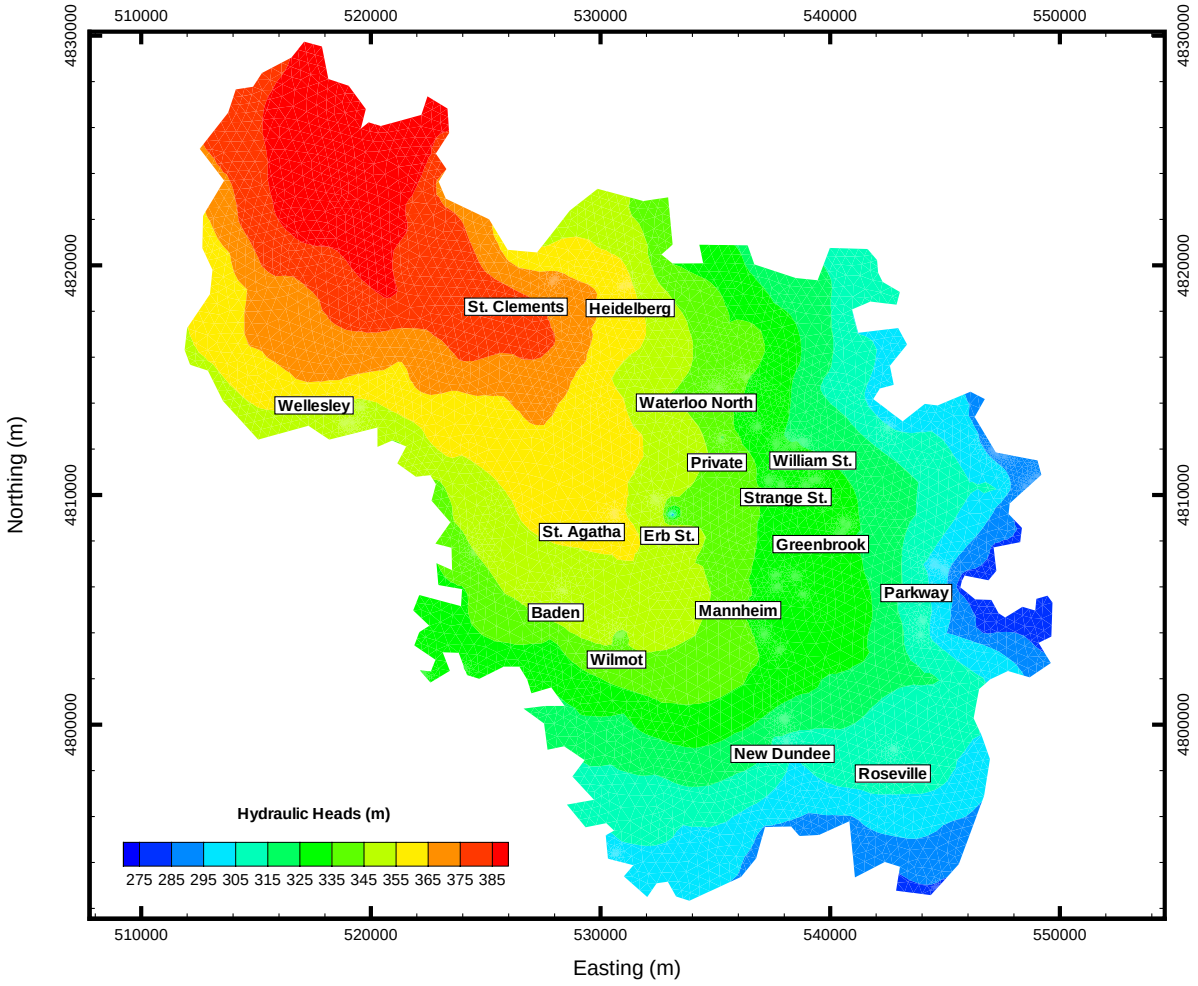

Figure 4.7: Head distribution under revised pumping conditions in Aquifer 1.

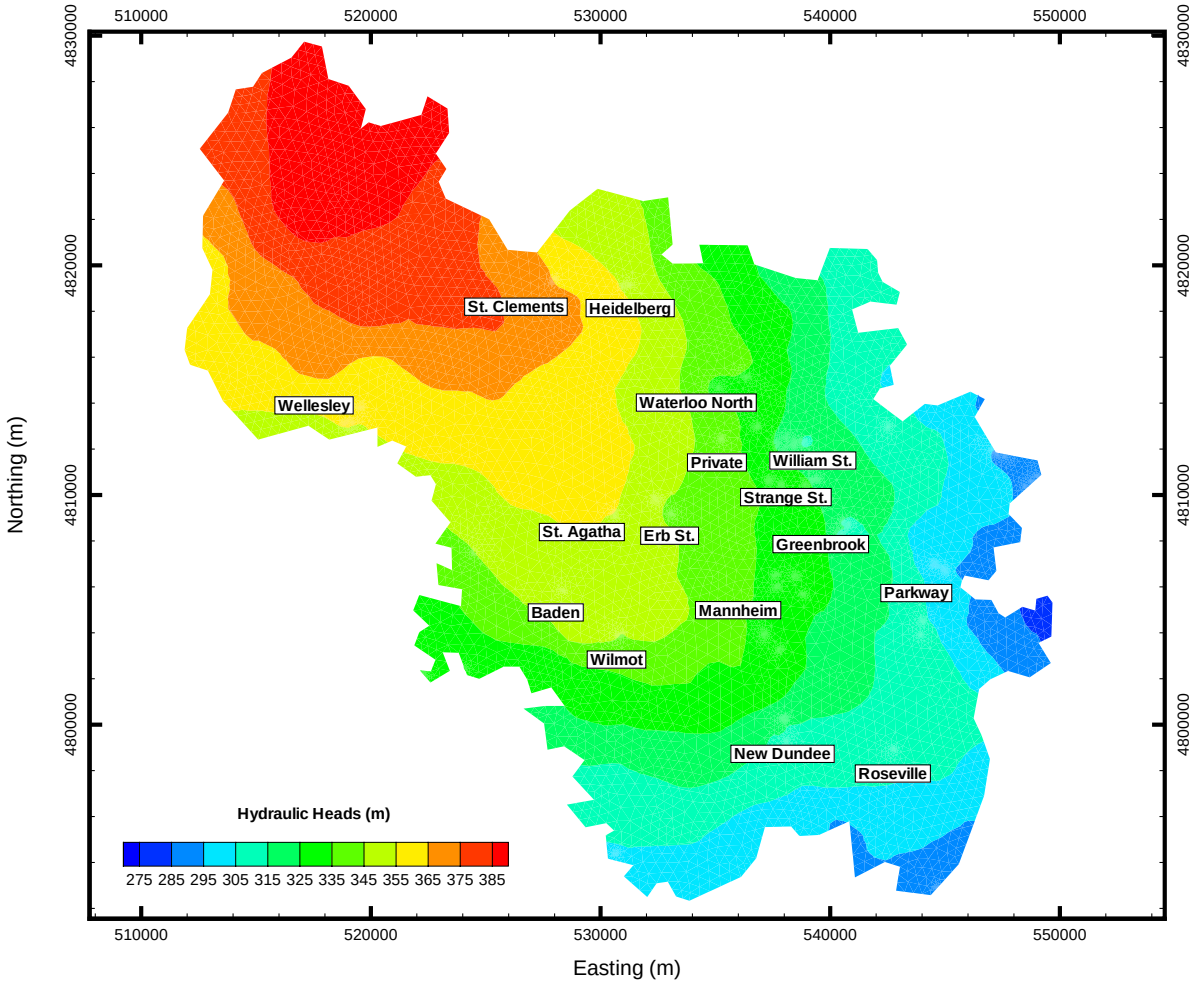

Figure 4.8: Head distribution under revised pumping conditions in Aquifer 2.

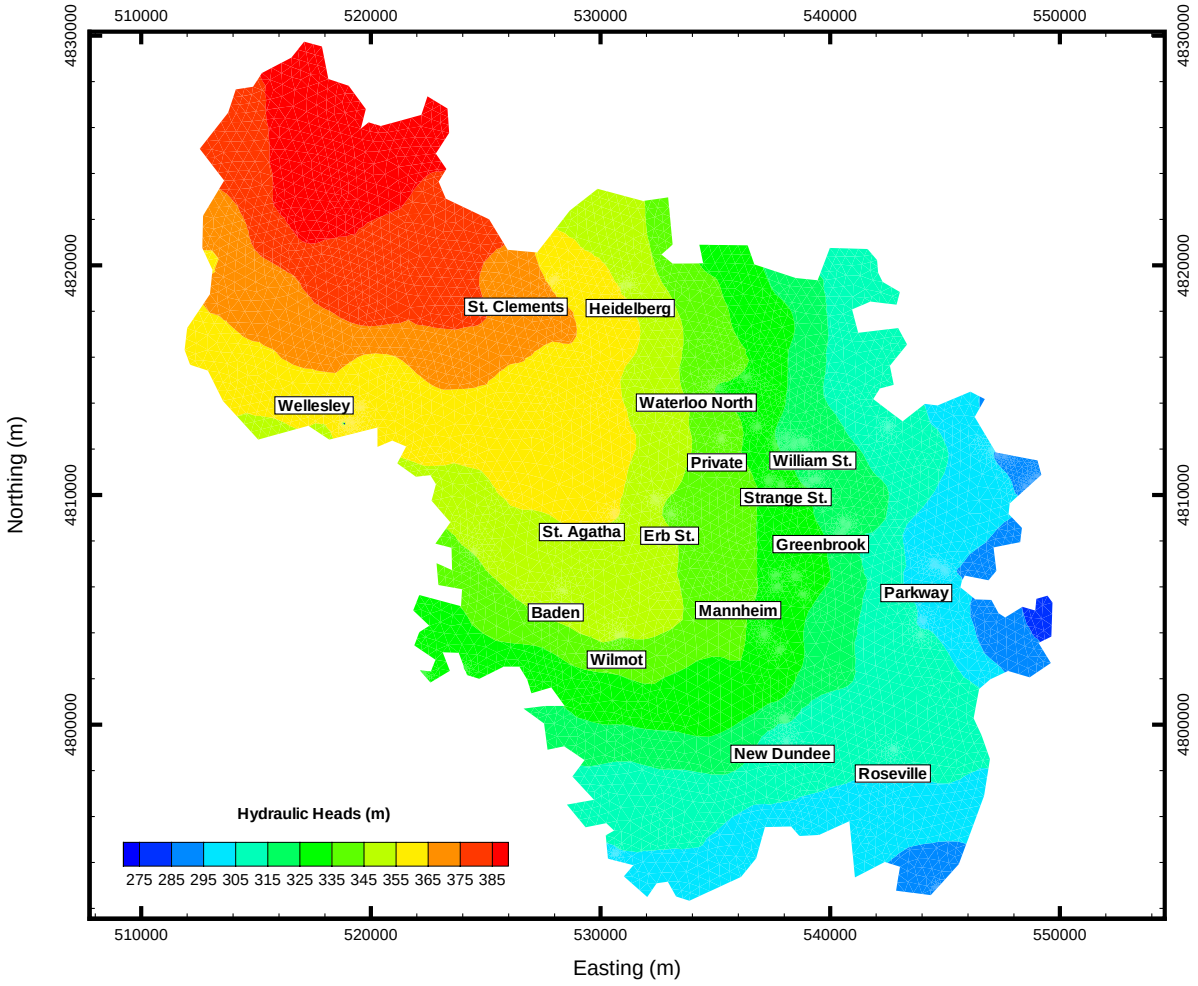

Figure 4.9: Head distribution under revised pumping conditions in Aquifer 3.

Chapter 5

Delineation of Capture Zones

Wellhead protection areas can be defined on the basis of capture zones associated with the groundwater wells. For the comparison of the different transport techniques to delineate capture zones, the Greenbrook well field is selected and is discussed here in detail.

As the technique for the delineation of the capture zones is the same for all well fields, plots for other major well fields are given in Appendix A. The summary of methods applied to individual well fields with the present and future pumping rates is given in Table 5.1.

The Greenbrook well field area lies on the eastern flanks of the Waterloo Moraine and has gently to moderately rolling topography. Surface elevation vary from 350 mASL west and south of the Greenbrook area along the crest of the Waterloo Moraine to 320 mASL in the vicinity of the Grand River. Historically, the Greenbrook area was the primary water supply source for the city of Kitchener prior to the establishment of the Mannheim well field in 1958-59 [*Callow*, 1996]. Presently, five out of seven wells are in operation, all are pumping from Aquifer 2. Aquifer 1 is minor and in places is dry at Greenbrook. K3 and K6 were screened in Aquifer 3 and are not in operation due to the problem of deterioration.

Table 5.1: Summary of methods applied to major well fields.

Well Field	Present Q (m^3/sec)	Future Q (m^3/sec)	ΔQ (%)	WATRAC	WTC	LTG Fine	LTG Coarse
Mannheim	3.111E-1	3.940E-1	26.7	Yes		Yes	Yes
Parkway	1.665E-1	1.613E-1	-3.1	Yes			Yes
Greenbrook	1.285E-1	1.543E-1	20.1	Yes	Yes	Yes	Yes
Wilmot	1.022E-1	1.452E-1	42.1	Yes		Yes	Yes
Erb Street	8.050E-2	1.439E-1	78.8	Yes		Yes	Yes
Strange St.	7.100E-2	1.144E-1	61.2	Yes			Yes
William St.	8.010E-2	7.752E-2	-3.2	Yes			Yes
Waterloo N.	2.460E-2	6.500E-2	164.2	Yes		Yes	Yes

The backward particle tracking technique and Wilson's approach using advective-dispersive transport models are applied and their results are compared. In the particle tracking model (WATRAC), a specified number of particles are initially positioned around the well for all the layers that were screened. The particles are tracked backward for a specified length of time (2 years, 10 years, and steady state) for all the well fields. Wilson's approach is used in the advective-dispersive models to obtain different time-of-travel capture zones. In this approach (probabilistic capture zone method), a source concentration of 1.0 is specified at the well nodes and the transport equation is solved with a reversed velocity field using the WTC and LTG codes.

Comparison of the capture zone outlines for Greenbrook well field is made for the following:

1. Particle-tracking technique (WATRAC):

   2, 10, and 280 years of time-of-travel,

2. Time-continuous technique (LTG):

   Coarse-mesh: 2, 10, 40, 70, 100, 130, and 160 years,

Fine-mesh: 2, 10, 40, 70, 100, 130, and 160 years,

3. Time-marching technique (WTC):

   2, 10, 40, 70, 100, 130, 160, 190, 220, 250, and 280 years,

4. LTG-WTC:

   (2, 10, 40, 70, and 100 years) - (130, 160, 190, 220, 250, and 280 years).

5.1 Particle Tracking (WATRAC) Results

Figures 5.1 to 5.3 show the results of particle tracking for 2, 10, and 280 years, respectively for the Greenbrook well field. At early times (2 and 10 years), most of the particles reach their travel-time limit, so all the capture zones are at unsteady state condition. At 280 years for the Greenbrook well field, 78 % of the particles reach the surface within the specified time period, while 22 % reach the time limit of 280 years without reaching the surface. It is clear from Figure 5.3 that almost all the particles at the extreme points are at the top. The cloud of particles is split into two distinctive parts around the Erb Street well field. The particles north of Erb Street well field move farther then the particles at the south. There are some particles that are probably stuck in the low-K zones, and reached their time limit before reaching the top. Particle tracking takes only a few minutes of computer time for simulation.

5.2 Wilson's Technique (LTG and WTC) Results

Figures 5.4 and 5.5 are 160-year peak concentration plots for the coarse and fine mesh, respectively. 160 years is about the limit for the LTG solution of the Greenbrook system; after this time, the solution becomes unstable and gives oscillatory results. The comparison of the two plots shows that the results obtained with the coarse mesh are essentially the same as those obtained with the fine mesh.

Figure 5.6 and Figure 5.7 show the 280-year peak capture zones in the horizontal plan view produced by the WTC, and by the combined approach of LTG-WTC, respectively. In the combined approach, the results of LTG at 100 years are used as an initial condition for the WTC model to obtain the steady state (280-year) capture zone. The comparison of these two figures indicates that the combined approach (LTG-WTC) is producing the same results as WTC alone. However, using WTC for the entire 280 year period takes about 2 weeks of execution time, while the combined approach takes only 1 day on a Pentium III 500 PC.

A mass balance check is performed on the basis that the vertical recharge through some control surface multiplied by the probability must equal the pumping rate, Q, at the wells. The centre of layer 25 (just above Aquifer 1) is chosen as a control surface. The vertical flux through this control surface is 296 mm/year on the average and Q is $4.9 * 10^6$ m^3/year. The mass balance equation takes the form:

$$Q = \int_A (vertical\,flux * A_P * probability) dA \tag{5.1}$$

where A_P is an increment of area (see Figure 5.8).

Figure 5.9 shows that the calculated contribution of recharge integrated over the entire area is very close to the pumping rate, Q. The 280-year capture zone is therefore essentially at steady state.

A capture zone outline can be selected from the probability contours by choosing any suitable probability level. For example, a probability contour of 0.05 means that the well field will get 95% of its water from the outlined area at steady state.

An alternative way to interpret the probability contours deterministically, i.e., in terms of capture vs. no capture, may be made by simply selecting an area of sufficient extent to supply the recharge required to balance the pumping. Figure 5.10 shows a plot of Q/A_P vs. the capture probability (i.e., the value of the contour enclosing area A_P). From the plot, the average recharge of 296 mm/year corresponds

to a probability contour of 0.25. This contour can then be taken as a capture zone outline.

Figures 5.11 and 5.12 show plots of the 0.25 probability contours for different times (2, 10, 40, 70, 100, 130, and 160 years) resulting from the LTG simulations using the coarse and fine mesh, respectively. The contour outlines are not so smooth in the case of coarse mesh due to the element size, but the extent of the capture zone is almost the same for both cases. This kind of behavior is also present for other well fields, especially the Mannheim well field (Appendix A).

Figure 5.13 shows the capture zone outlines determined by a time-marching technique (WTC), as defined by the 0.25 probability contour, for 2, 10, 40, 70, 100, 130, 160, 190, 220, 250, and 280 years. The capture zone is seen to advance with time mainly in the westerly direction and split into two lobes surrounding the Erb Street well field. The comparison between the 250-year and the 280-year capture zone contours indicates that the capture zone is almost at steady state, except at extreme tips, which still advances at a very slow rate.

Figure 5.14 shows the results (0.25 probability contours) obtained by a combined use of LTG and WTC models. Comparison with Figure 5.13 shows that the results are identical.

For the case of the revised pumping rates, Figure 5.15 shows the capture zone outlines for different times. Comparing these results with Figure 5.14, it is clear that there is an effect of heavy expected pumping rates at Erb Street wells on the shape of the capture zone. In this case, the lobes of the probability plume are not much separated around the Erb Street wells; also the extent of the capture zone is relatively less.

The particle tracks agree well with the 0.25 probability contour (Figures 5.16), except at the far end of capture zone in the north of Erb Street wells. A few particles travel ahead of the 0.25 contour, but most the particles are within the limit of 0.25. Also, the 0.25 contour is wider than the particle tracks. The difference between the two types of results is due to dispersion, which is considered in the transport

solution but not in the particle tracking solution. Transverse dispersion tends to spread the mass (or probability in this case) and reduce the maximum advance of a plume.

In Figures 5.17, 280-year particle tracks are projected onto the vertical plane of section BB$'$ (for location, see Figure 5.13). The top boundary of the section is ground surface. The particles that appear to extend above or below the top boundary are located off the section where surface topography may be higher or lower than in the section itself.

Figures 5.18 to 5.20 show three vertical cross-sections which provide a 3D interpretation of the 280-year capture zone in this complex multi-aquifer system. The location of these cross-sections is shown in Figure 5.13. From this 3D perspective, two distinct capture subzones are identified. The first, located around the well field and extending approximately 3 km upgradient, shows a continuous region of high capture probability extending throughout the multi-aquifer system. This indicates direct recharge from ground surface with numerous windows. The 3D plot (Figures 5.17) of particle tracks indicates that some particles are stuck in Aquitard 2 in this subzone.

A second subzone, approximately 5 km upgradient (see Figures 5.18 and 5.19), indicates the influence of windows in the upper aquitards. High probability contours cross Aquitard 2 and Aquitard 1 through these windows and reach at the surface. Even though all 3D particle tracks are shown on one vertical cross-section, the correlation between tracks and probability contours is quite good. Cross-section CC$'$ (Figures 5.20) indicates that the high probability contours are in the bottom of Aquifer 3 in this subzone. Particles in this area of subzones are probably stuck in the low-K materials.

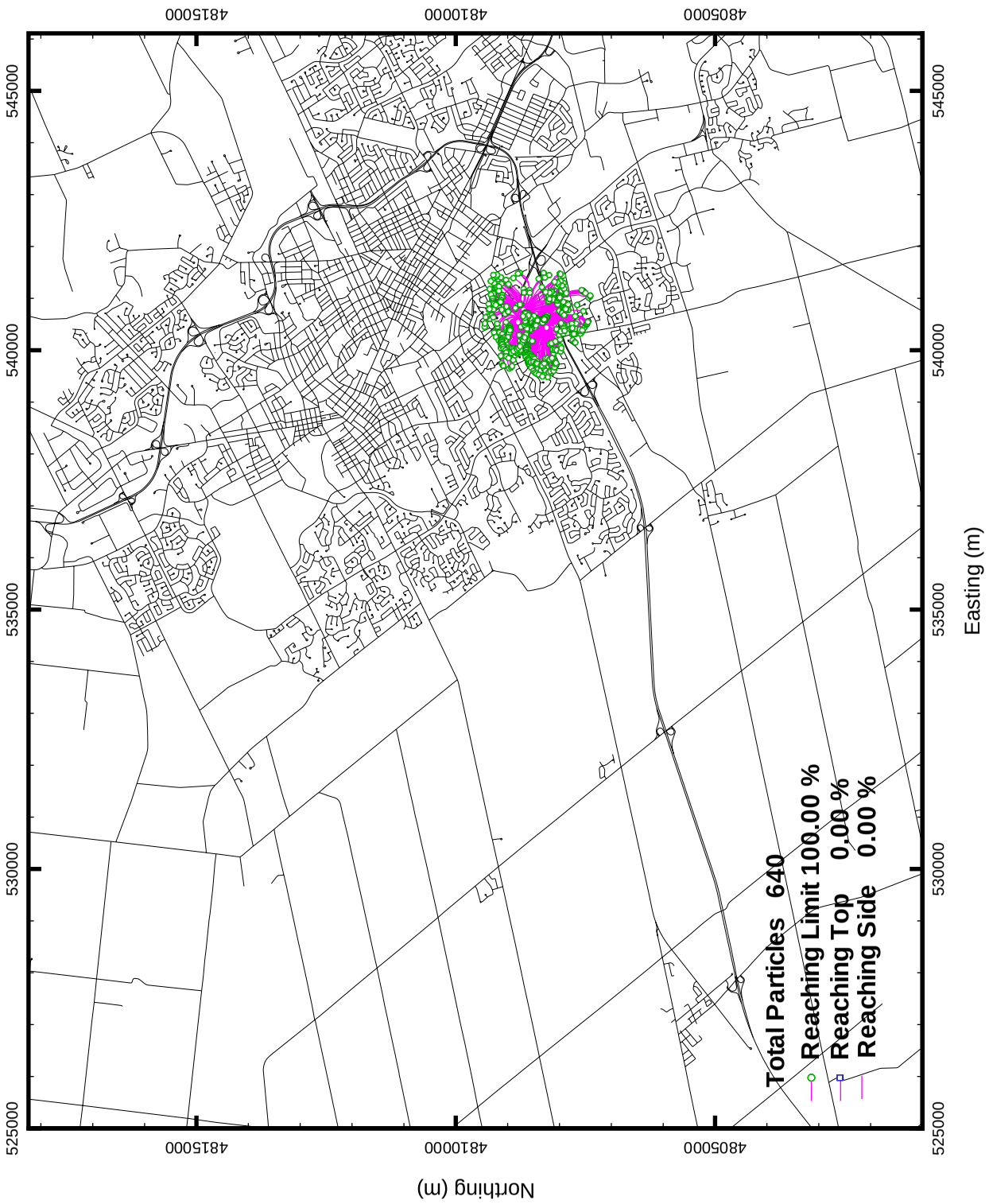

Figure 5.1: Greenbrook well field: 2-year particle tracks.

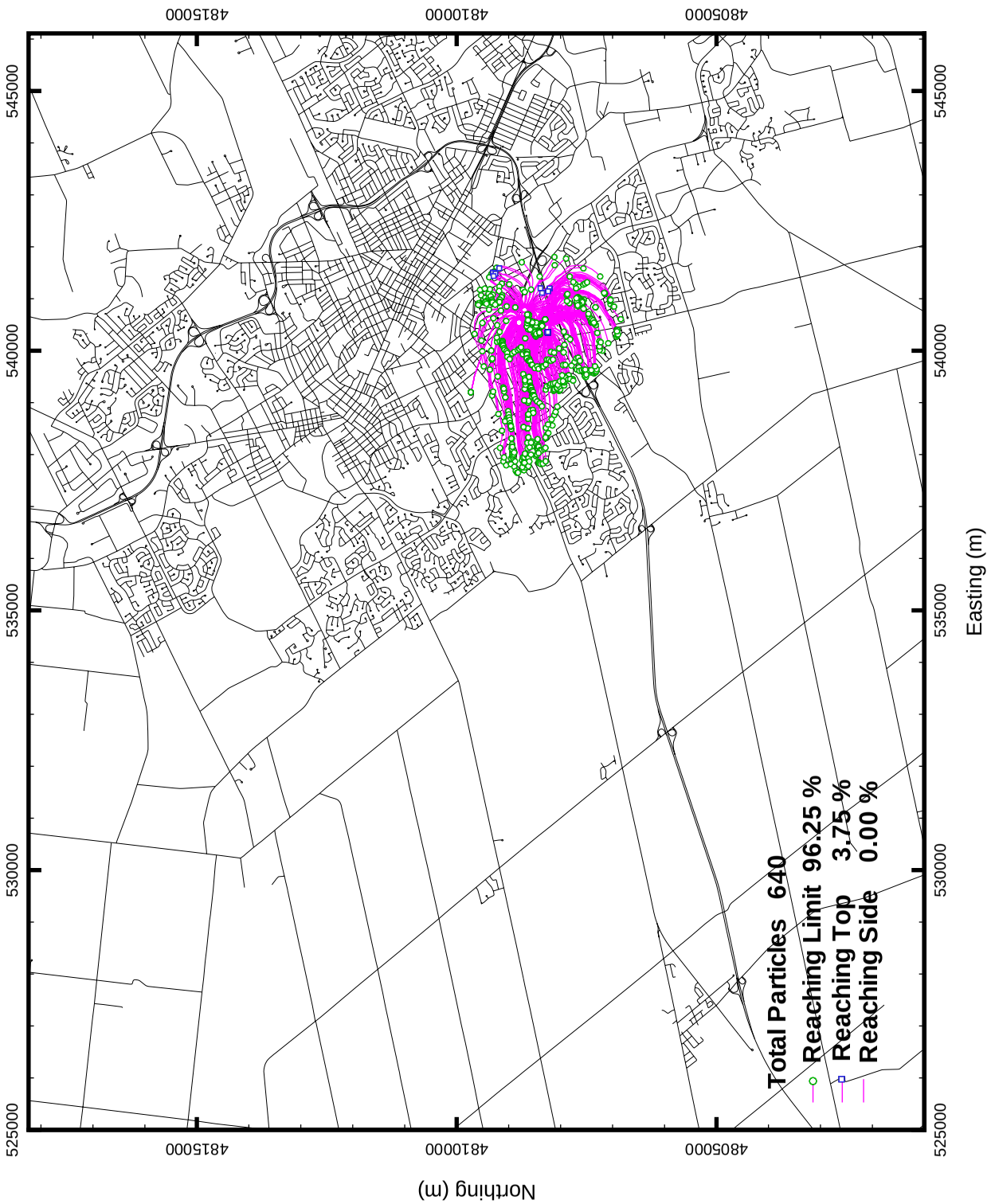

Figure 5.2: Greenbrook well field: 10-year particle tracks.

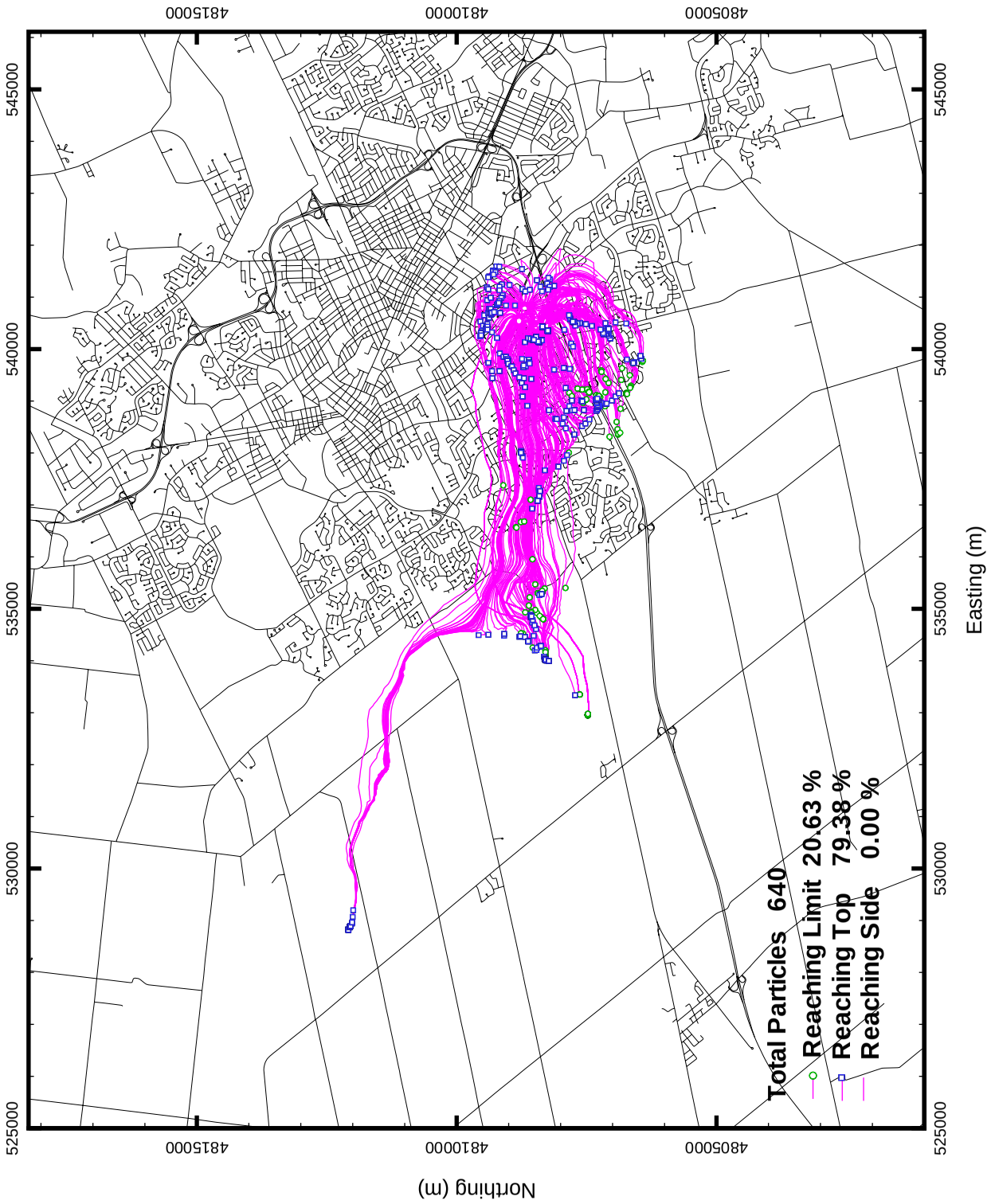

Figure 5.3: Greenbrook well field: 280-year particle tracks.

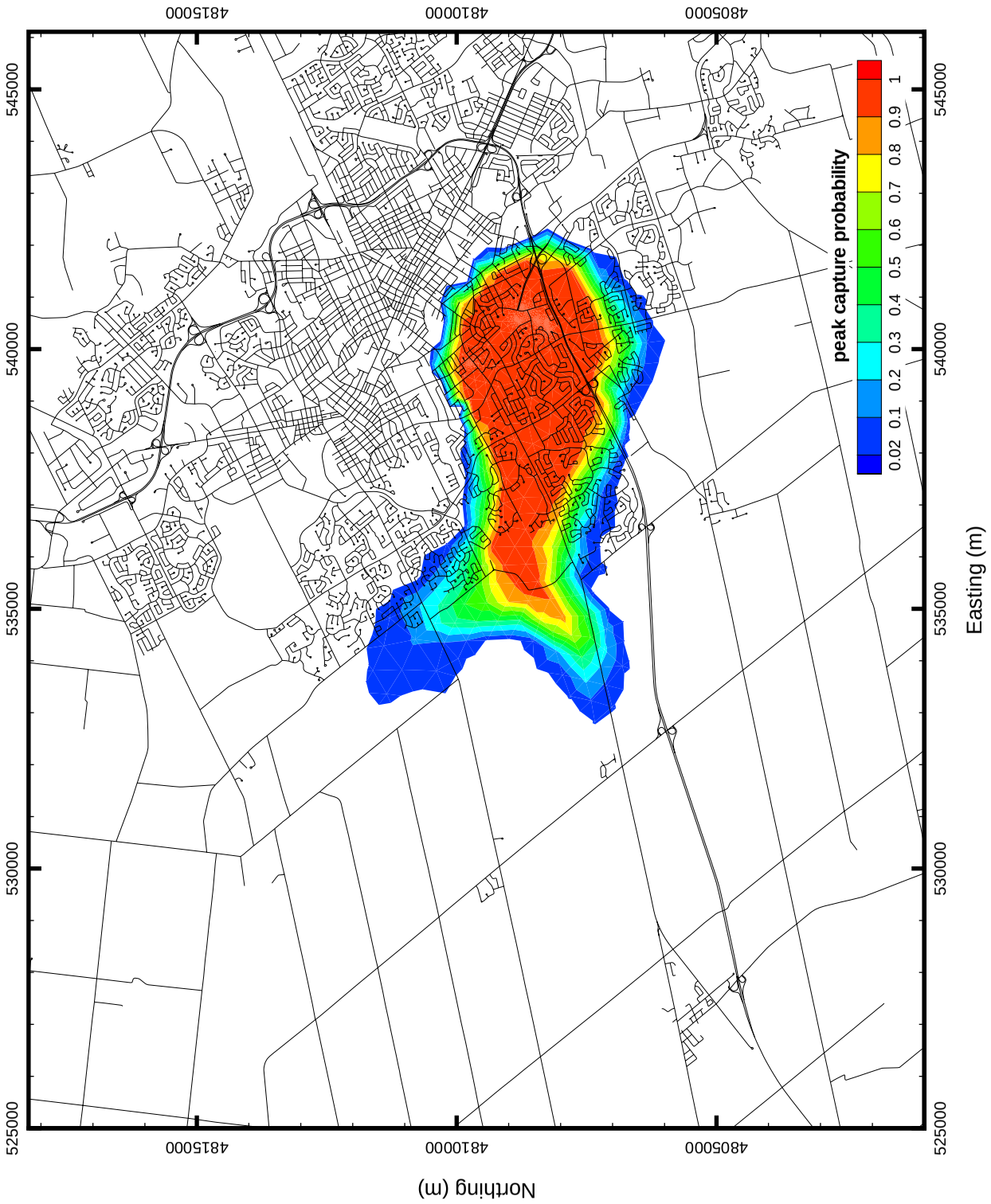

Figure 5.4: LTG (coarse mesh): 160-year peak capture probability.

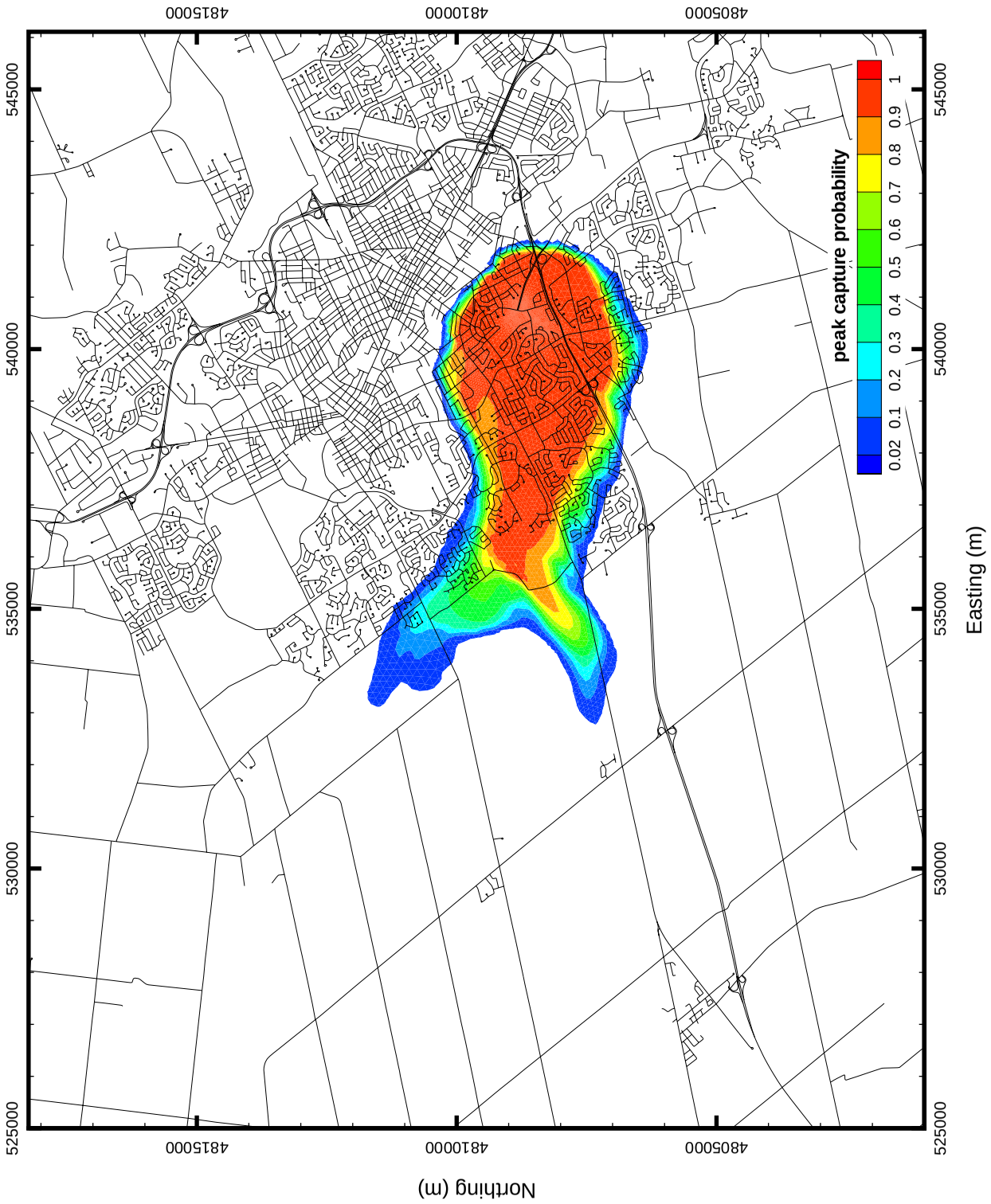

Figure 5.5: LTG (fine mesh): 160-year peak capture probability.

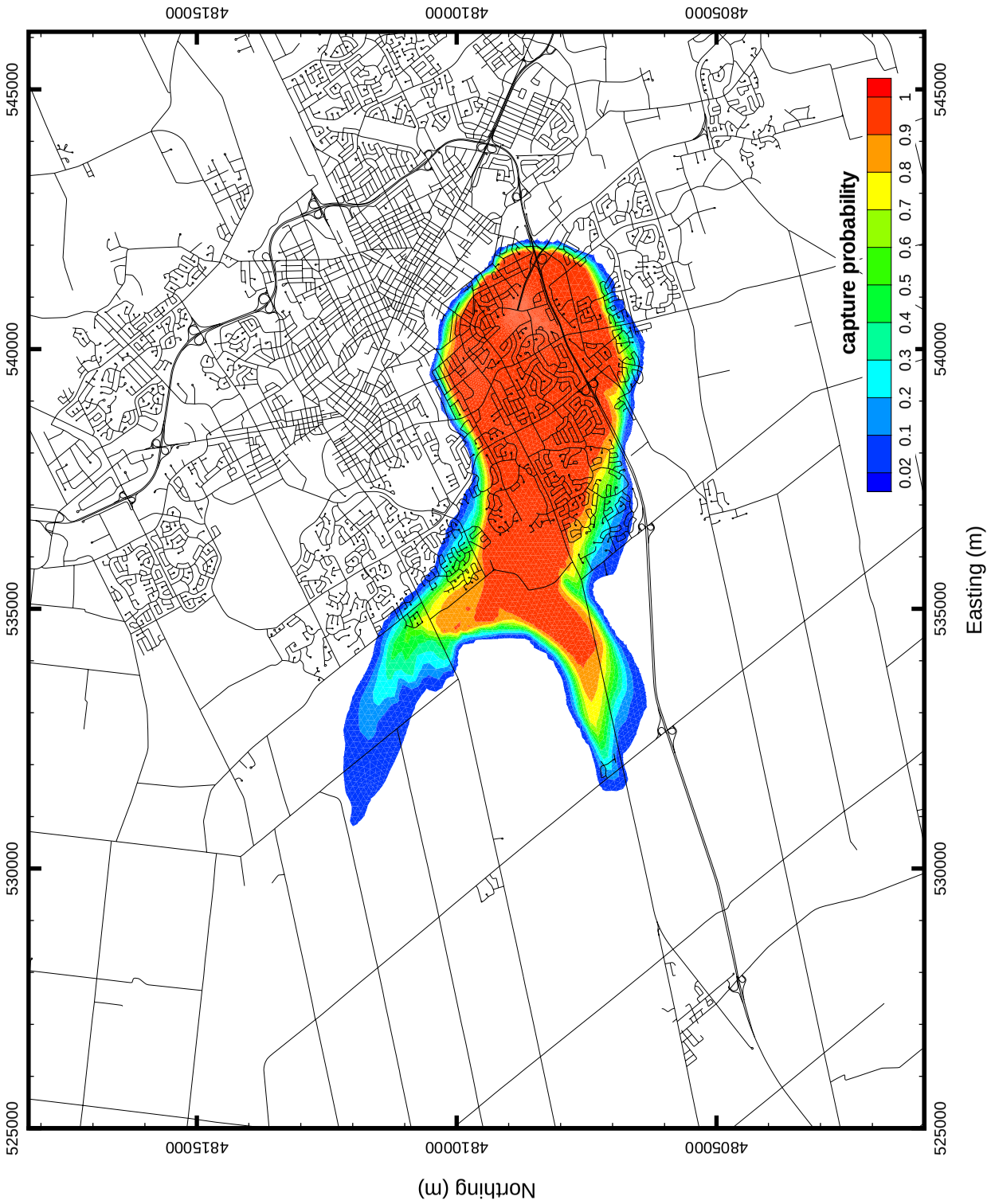

Figure 5.6: WTC: 280-year peak capture probability.

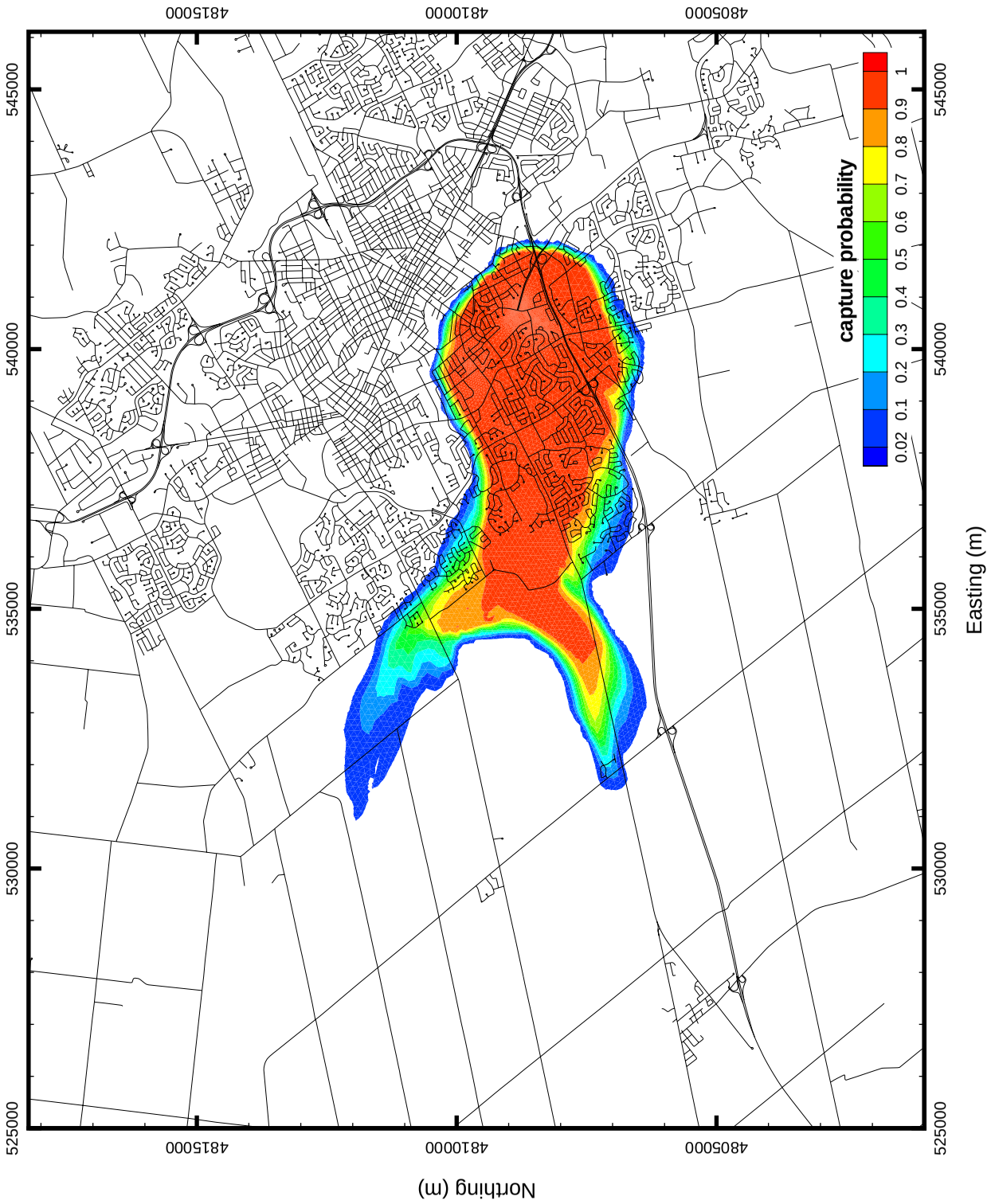

Figure 5.7: LTG-WTC: 280-year peak capture probability.

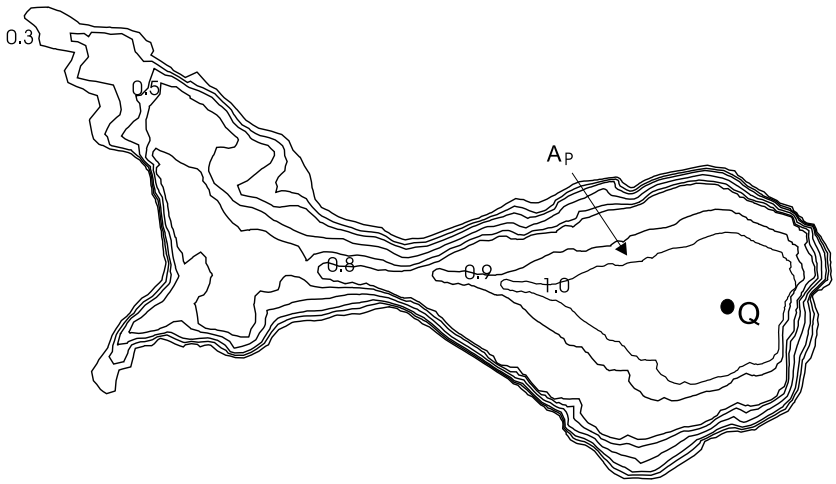

Figure 5.8: Determination of A_P for different capture probability contours.

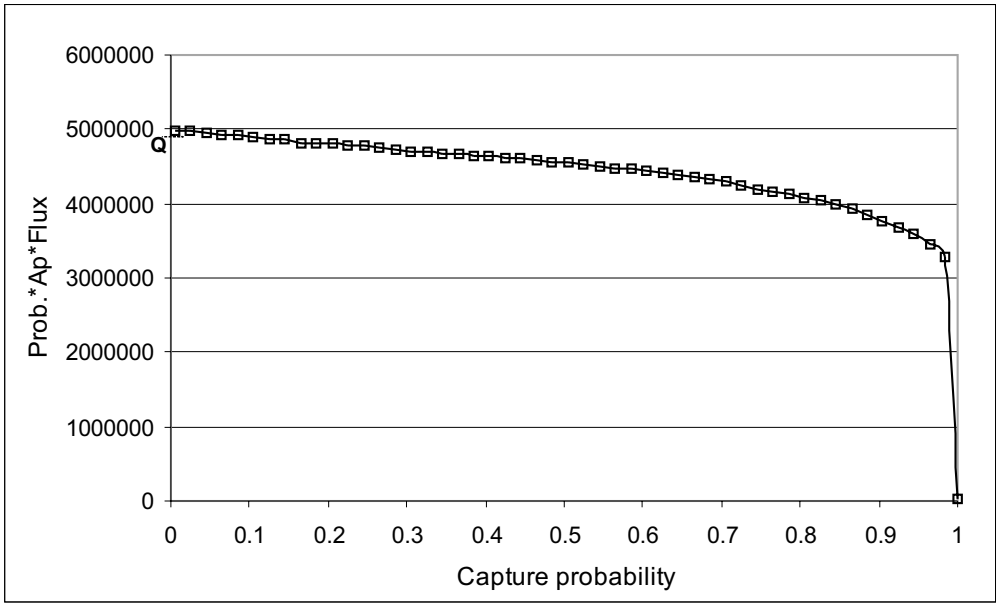

Figure 5.9: Contribution of recharge (m^3/year) at steady state (280 years) for different probability contours.

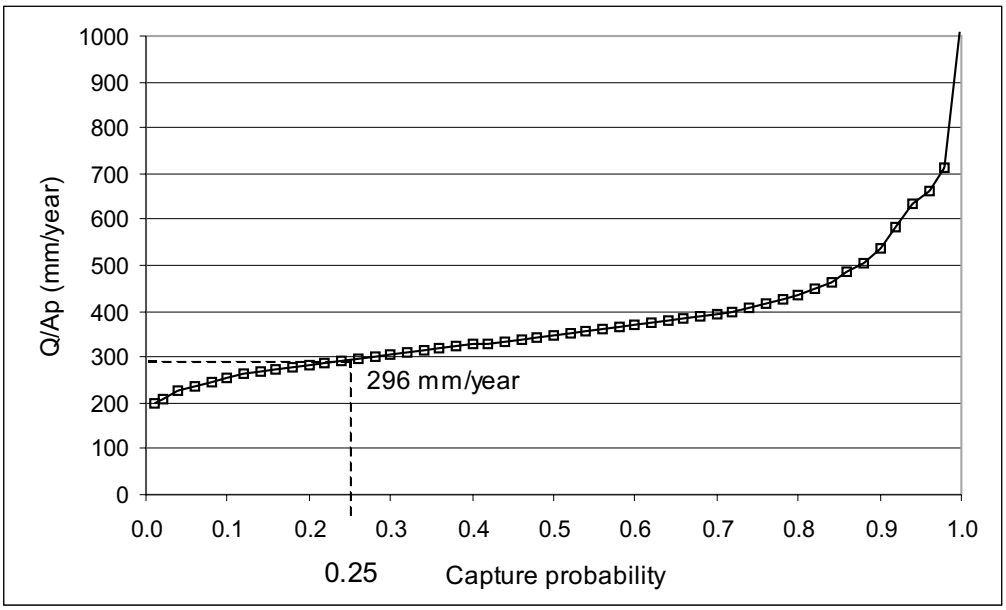

Figure 5.10: Q/A_P vs. capture probability to determine the outline of capture zone.

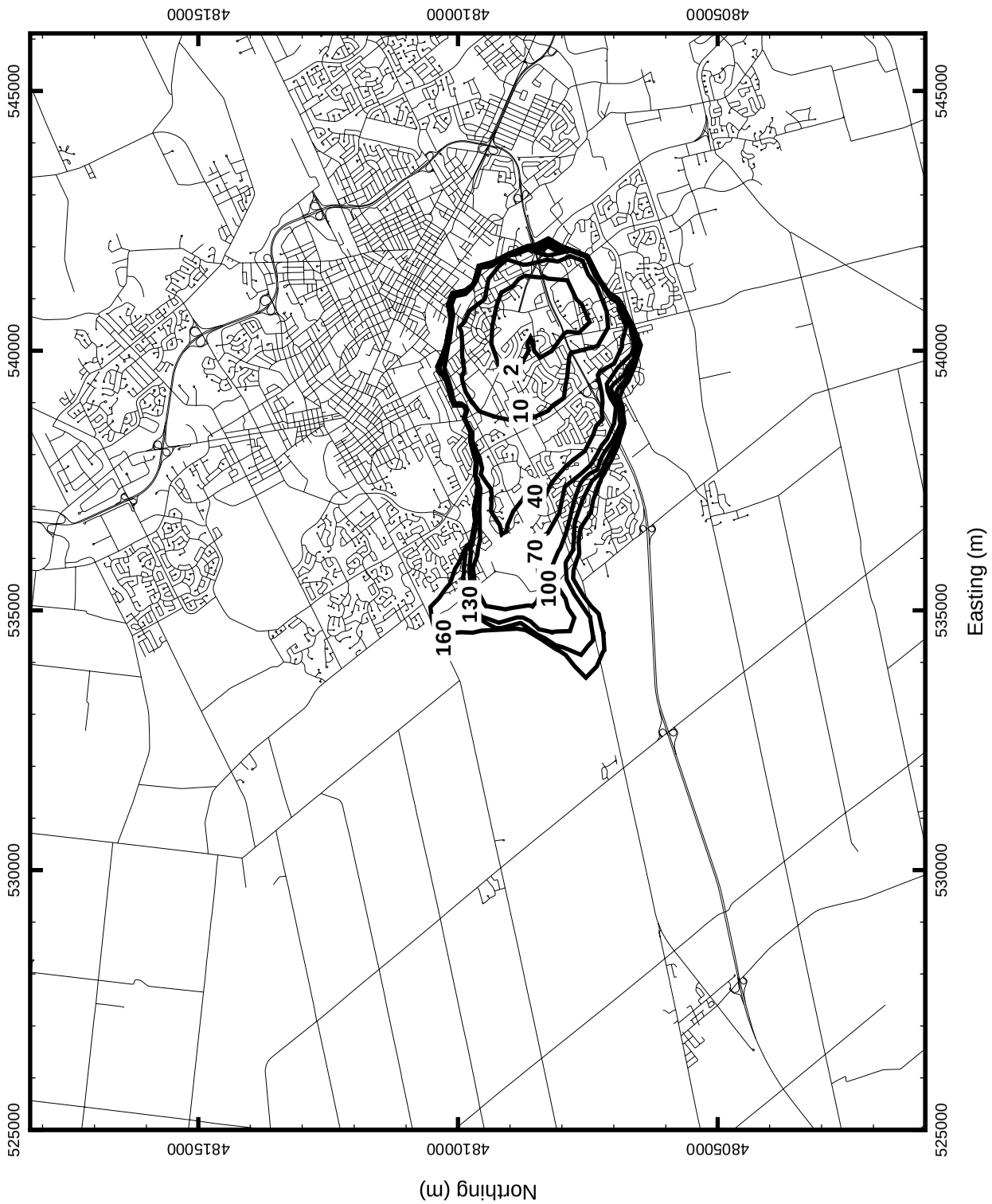

Figure 5.11: LTG (coarse mesh): 0.25 peak capture probability contours; 2, 10, 40, 70, 100, 130, & 160 years.

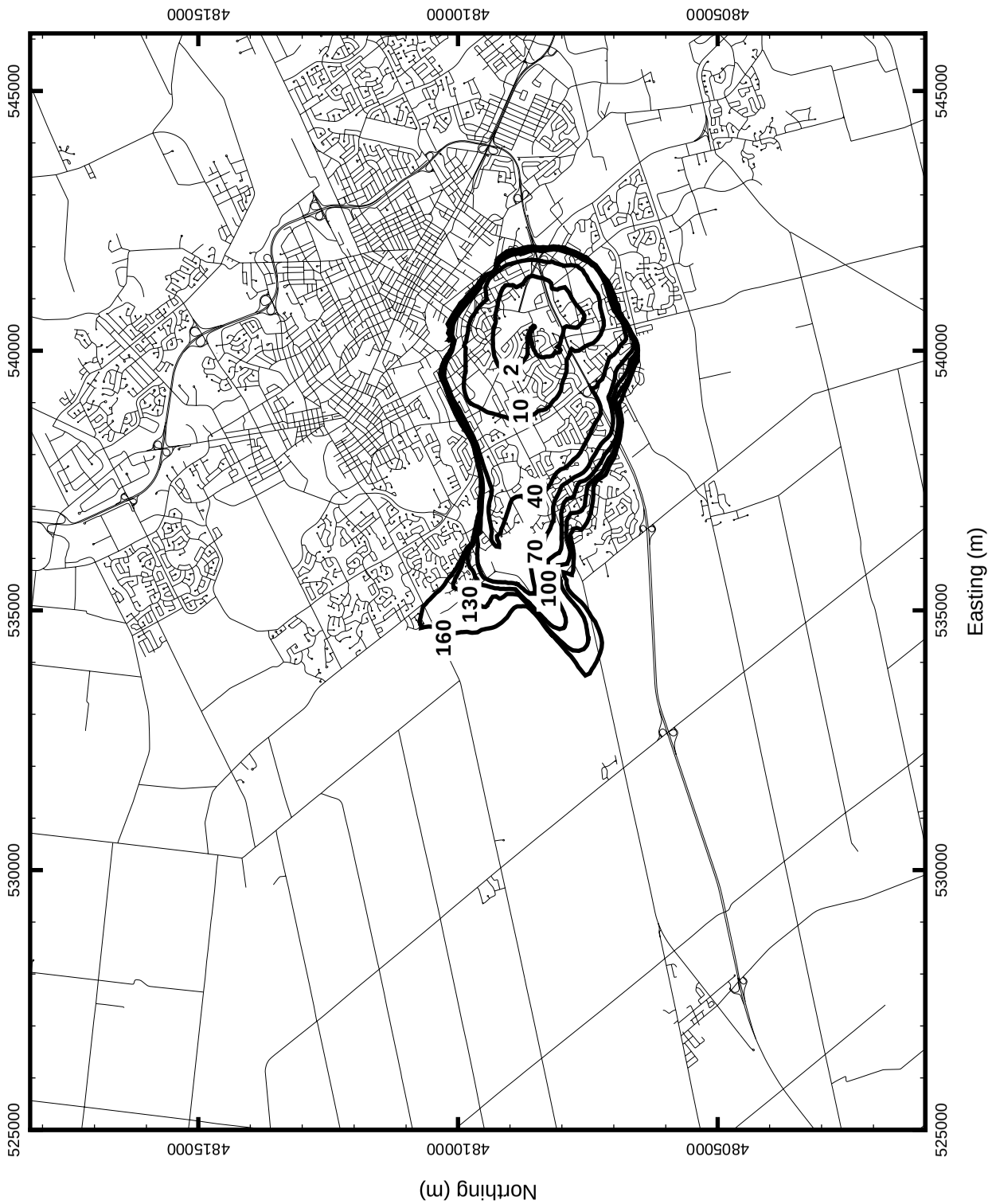

Figure 5.12: LTG (fine mesh): 0.25 peak capture probability contours; 2, 10, 40, 70, 100, 130, & 160 years.

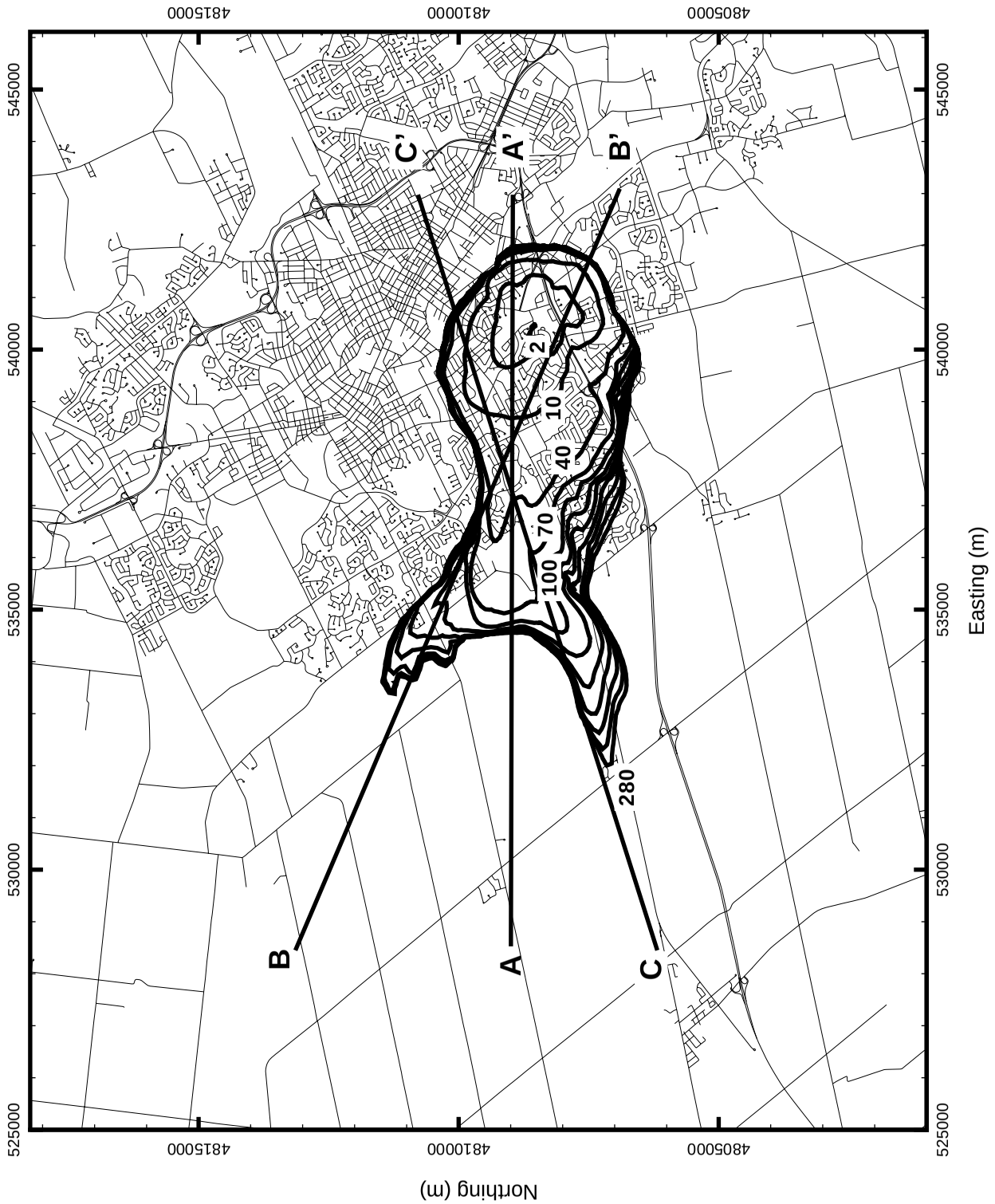

Figure 5.13: WTC: 0.25 peak capture probability contours; 2, 10, 40, 70, 100, 130, 160, 190, 220, 250, & 280 years (for sections AA′, BB′, and CC′, see Figures 5.18 to 5.20).

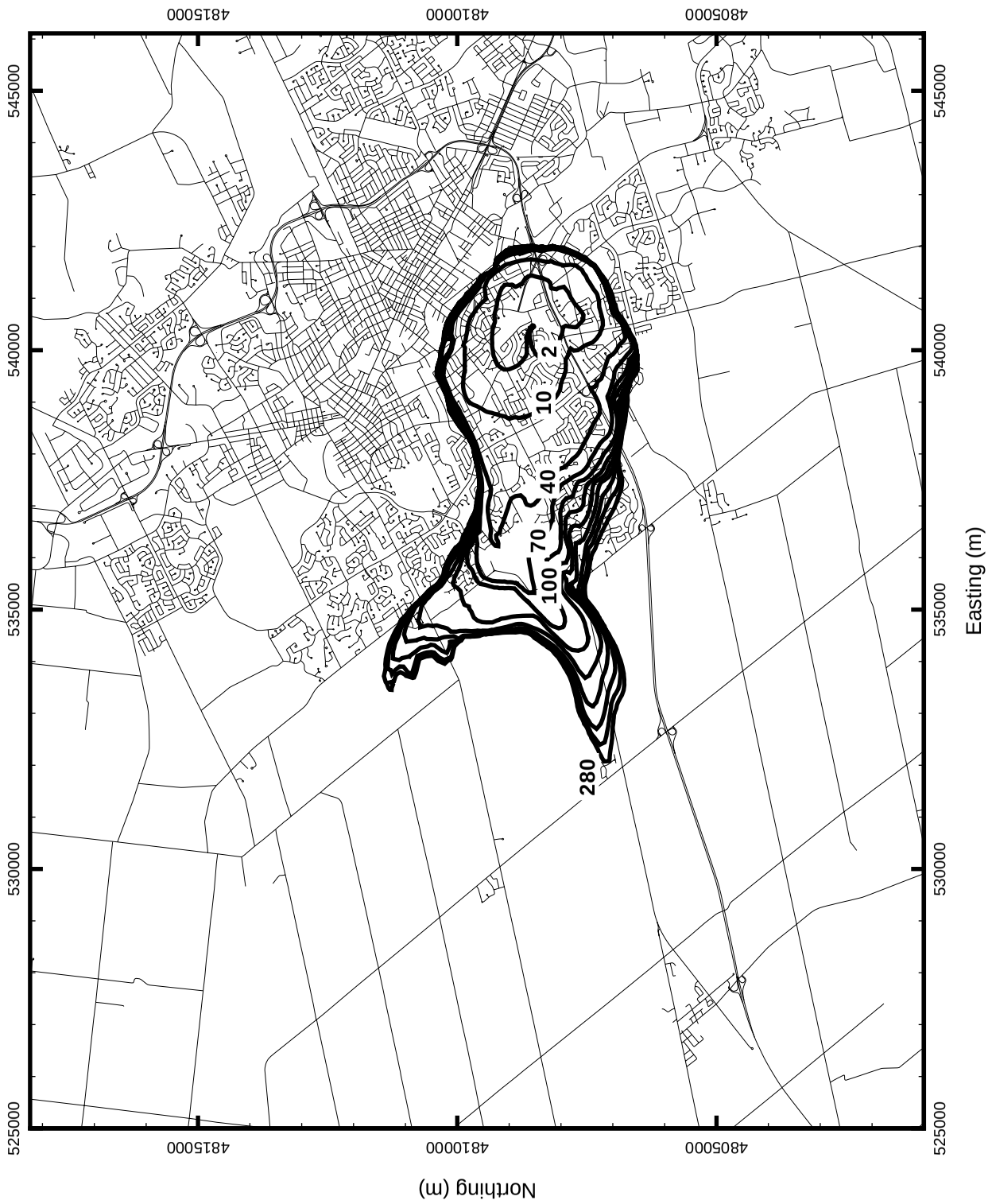

Figure 5.14: LTG-WTC: 0.25 peak capture probability contours; 2, 10, 40, 70, 100, 130, 160, 190, 220, 250, & 280 years.

Figure 5.15: Revised pumping rates: 0.25 peak capture probability contours; LTG: (2, 10, 40, 70, & 100 years); WTC: (130, 160, 190, 220, 250, & 280 years).

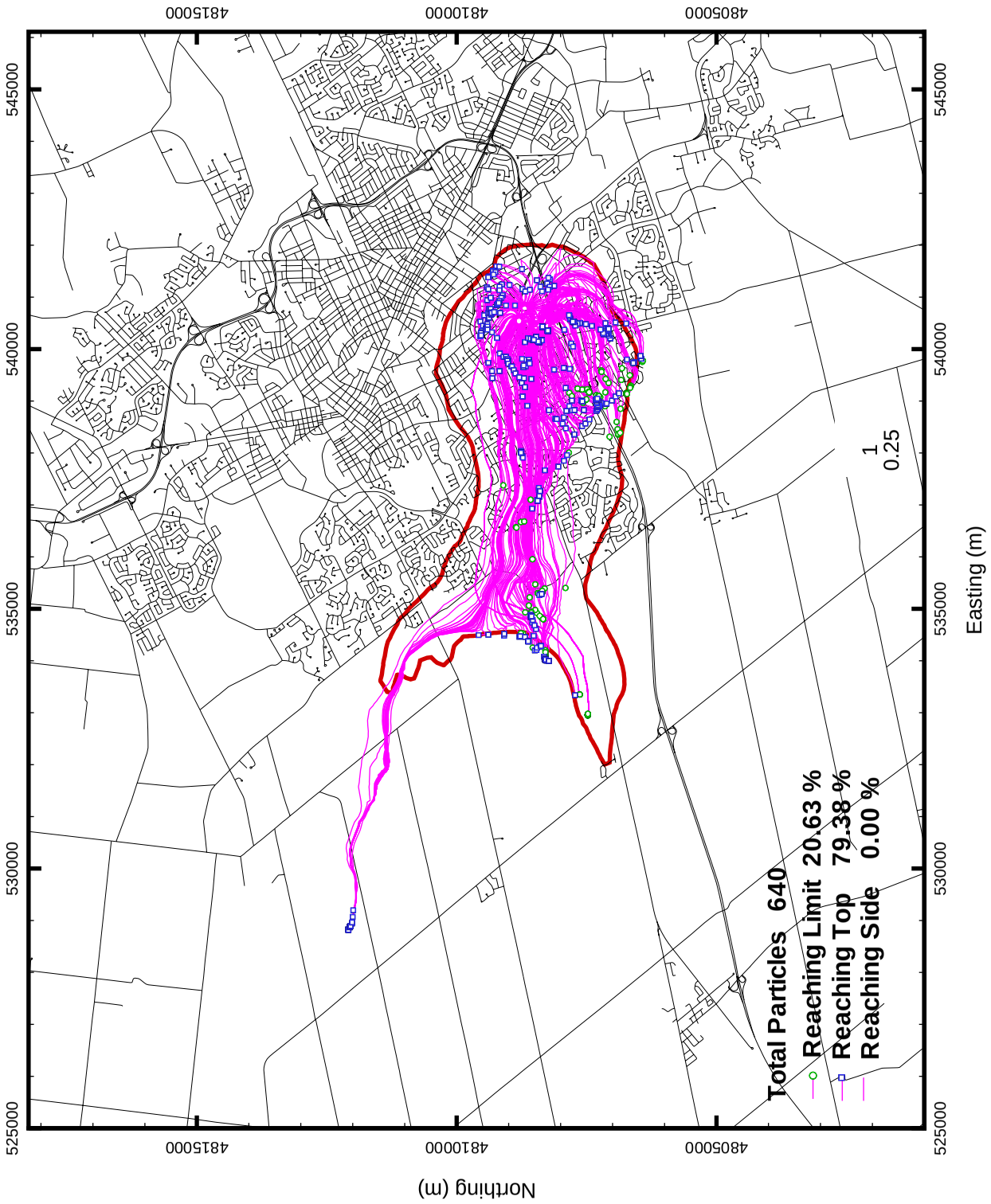

Figure 5.16: Greenbrook well field: 280-year particle tracks and 0.25 probability contour.

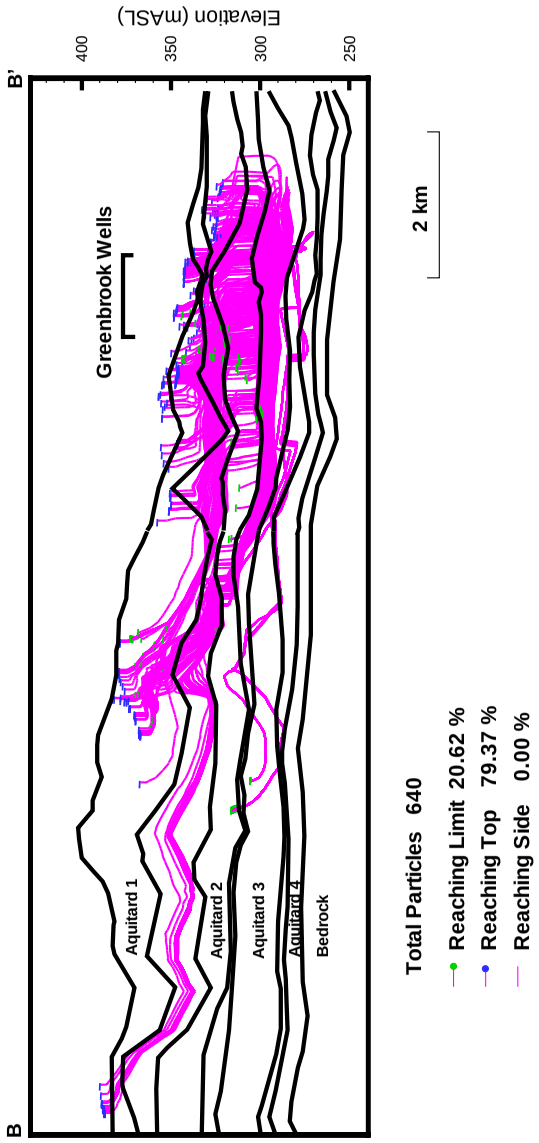

Figure 5.17: Greenbrook well Field: 280-year particle tracks projected onto cross-section BB$'$ (for location of section see Figure 5.13).

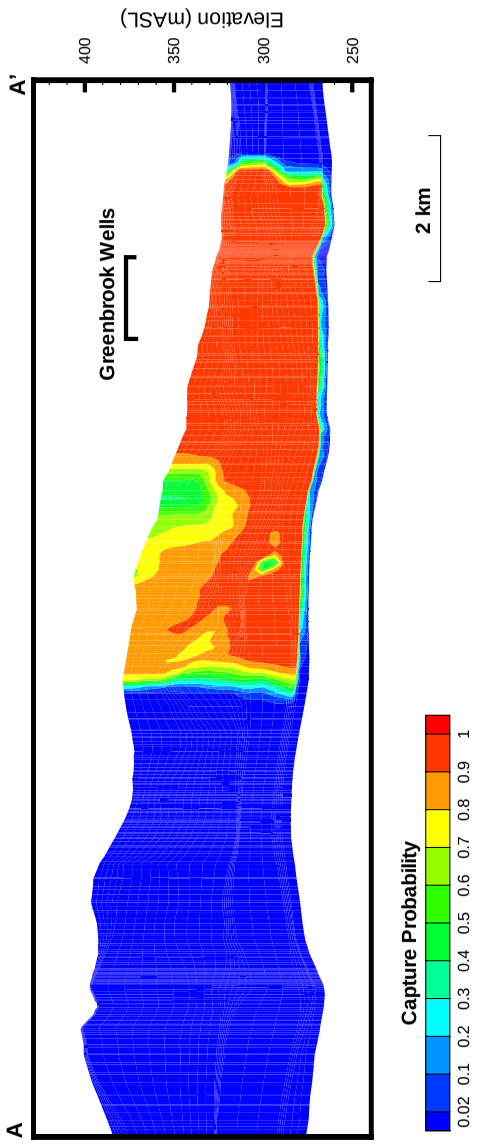

Figure 5.18: Greenbrook well field: vertical cross-section at AA′ (for location of section see Figure 5.13).

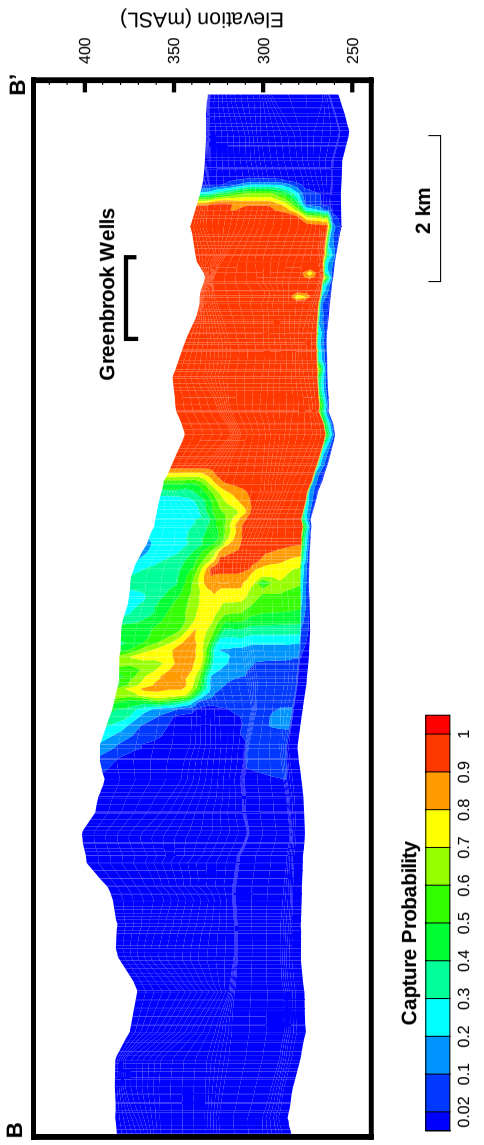

Figure 5.19: Greenbrook well field: Vertical cross-section at BB′ (for location of section see Figure 5.13).

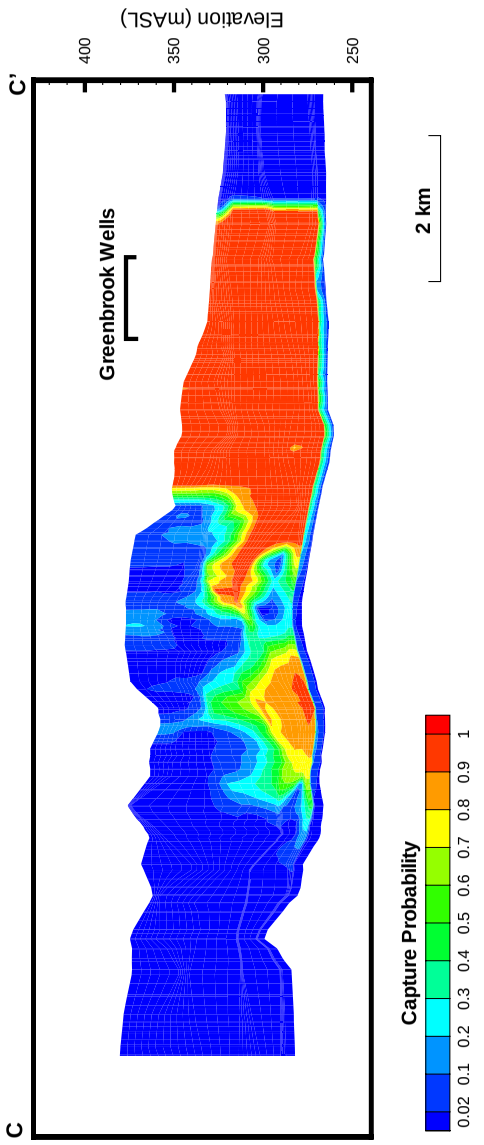

Figure 5.20: Greenbrook well Field: vertical cross-section at CC′ (for location of section see Figure 5.13).

Chapter 6

Potential sources of contamination

This chapter presents some preliminary findings on chloride contaminants that can potentially reach the Greenbrook wells.

Water quality data shows that chloride concentrations in the Greenbrook wells are increasing with respect to time except for wells K6 and K8. Table 6.1 shows the observed chloride concentration at all the Greenbrook wells.

One of the objectives of this study is to determine the possible sources of these chlorides. By reviewing previous literature (i.e., *Woeller*, 1982) and with some personal communications (RMOW professionals, *Johnston* and *Rudolph*), three potential contaminant sources can be identified:

i. Bedrock water,

ii. The former Kitchener landfill at Ottawa Street, and

iii. Road salt.

In addition to this, snow dumping north-east of Greenbrook well field has taken place for about 50 years (1940's-1990), however the effect of this activity may be combined with the road salt and is not treated as a separate source in this study.

Table 6.1: Observed chloride concentration (mg/l) at Greenbrook wells.

Year	K-1	K-2	K-3	K-4B	K-5	K-6	K-8
1973	47.3	9.0	35.0		71.4	6.0	
1974	42.3	9.0	37.0		72.4	6.0	
1975	62.3	12.0	21.0		92.4	11.0	
1976	93.3	11.0	21.0		99.4	10.0	
1977	111.3	13.0	40.0		105.4	10.0	
1978	71.3	11.0	60.0		98.4	6.0	
1979	65.3	13.0	44.0		107.4	8.0	
1980	61.3	14.0	65.0		117.4	7.0	
1981	85.3	19.0	68.0		127.4	8.0	
1982	97.3	20.6			131.8		
1983	90.3	20.6			132.0		
1984	93.3	18.2			133.2		
1985	81.5	16.4	61.8	164.9	143.8	19.6	
1986	92.4	18.1	63.3	177.9	158.4	24.8	
1987	89.8	19.5	109.5	139.9	173.4	12.4	
1988	110.3	25.4	109.5	150.9	169.4	13.2	
1989	102.3	50.2	116.0	149.9	182.4	24.1	2.0
1990	111.3	53.1	127.0	164.9	193.4	31.1	2.7
1991	158.3	58.1	111.0	179.9	215.4	33.6	3.9
1992	141.3	69.0	206.0	156.9	186.4	24.0	8.5
1993	201.3	80.2		216.9	196.4	21.0	13.0
1994	146.3	58.0		156.9	186.4	16.0	8.6
1995	231.3	110.0		176.9	246.4	58.0	24.0

Accidental spills present another intangible source which will also not be considered here.

Unfortunately, it is not straightforward to determine the chloride input concentrations for these sources. The determination of the exact quantitative contribution of these potential sources on the individual wells is left for future studies. In present study, some preliminary results are obtained to give a direction for further study on this aspect.

6.1 Bedrock Water

Contribution from the bedrock is determined by applying the *Type 1* boundary condition to all the nodes of bottom layers. With the maximum observed chloride concentration of 30 mg/L [*Johnston*, 1994], the results of the transport model (LTG) indicate that the system approaches steady state within 8 years. Figure 6.1 is a cross-sectional view of the steady state condition which clearly indicates that there is upconing of bedrock water below the Greenbrook wells, especially below K1. Figure 6.2 shows the breakthrough curves for all the Greenbrook wells, indicating that the system is almost at steady state with the prevailing conditions. K3 and K6 are getting more water from the bedrock, because these wells are pumping from Aquifer 3. From the wells that are screened in Aquifer 2, K1 is receiving the highest proportion from bedrock than the other wells. K8 is likely to be least affected from this source. Because the chloride concentration simulated at the wells is much lower than that observed, it may be concluded that the bedrock water will not create any serious problem for the pumping wells. Water quality in the Greenbrook wells is not expected to deteriorate further due to this source under present flow conditions. Upconing below K1 indicates that there is a 'window' (high K zone) in Aquitard 3 beneath this well.

6.2 Landfill Leachate

The Ottawa Street landfill site encompasses an area of approximately 30 hectares, and was operated during a 20-year period from 1958 to 1978 as a municipal sanitary landfill. It has been estimated that approximately two million tonnes of refuse was disposed of at the landfill [*RMOW*, 1991]. Some investigations were carried out to determine the impact of landfill leachate on the Greenbrook well field by *CH2M Hill Eng. Ltd.* [1993, 1995]. The contaminant plume in the subsurface due to landfill leachate was first described by *Farvolden* and *Weitzman* [1980]. Even though Aquitard 1 is laterally continuous and maintains a minimum thickness of 15

m in the landfill area, it is not homogeneous and is composed of both high and low hydraulic conductivity materials. Normally, the flow direction in this area is from west to east, away from the Greenbrook wells, however, due to the heavy pumping from the wells it may be expected that the wells will be contaminated with the landfill leachate. The geochemical data of contaminants at different depths below the landfill site is available in the reports. By applying the *Type 1* boundary for the top surface nodes at the landfill site with the concentration of 540 mg/l (observed at BMW 201 [*CH2M*, 1992]), breakthrough curves are obtained using the LTG method, as shown in Figure 6.3. Figure 6.4 shows the peak relative concentration at 36 years in the year 1995 by taking 1959 as a starting time of simulation. It is clear from the figures that only one well, K2, is being affected by the plume generated by the landfill. Presently, the effect of the landfill at this well is small, but the sharp rise in the breakthrough curve indicates that this well is in danger due to landfill leachate and there is a need to monitor this well on regular basis for the landfill contaminants. The other wells are getting negligible contamination from this source and are probably not in danger under the prevailing flow conditions.

6.3 Road Salt

During the snow season, RMOW is using about 30 tonnes/km of salt for deicing on the roads for the last 50 years, starting from about 1950. This salt contains about 60% of chloride and it is estimated that 20% of this goes to the groundwater [*Johnston,* Pers. comm.]. Using these quantities, it is calculated that along the roads the groundwater may have approximately 1000 mg/l of chlorides.

In order to determine the contribution of the road salt to the observed chlorides in the Greenbrook wells, transport modelling with the LTG method is carried out for two scenarios.

In the first scenario, all the top surface nodes are considered as *Type 1* boundary with a concentration of 1000 mg/l of chloride. For the second simulation of road

salt effects, a *Type 1* boundary condition is applied for the top surface nodes along the main roads with $c = 1000$ mg/l (Figure 6.5).

As the origin of contaminated water is unknown, the result of the first simulation shows higher chloride values than the observed at all the wells except at K3 as shown in Figure 6.6. Figure 6.6(c) shows the breakthrough curve at K3 with a lag of 6 years along with the observed chloride concentrations after subtracting the contribution of the bedrock source (i.e., 24 mg/l). The fit between the observed (points) and computed (line) concentrations is excellent for this kind of heterogeneous material. It indicates that the unknown location of this contaminated water has chloride concentration of about 1000 mg/l. Fit with the lag of 6 years means probably the source was originated in 1956 instead of 1950 as given in the simulation or it took 6 years for the salt to migrate through the unsaturated zone. The computed chloride concentrations are very high for all the other wells.

The results of the second simulation are also given in Figure 6.6. Breakthrough plots (Figure 6.6 a, d, & e) show an excellent agreement between observed and computed concentration except at the latter times for K1 and K5. Changes in the external stresses may result in different flow conditions as simulated for this case, consequently resulting in different outputs for latter times. It may be concluded that after 1990, the flow condition has changed due to abandoning of K3, K5, and K6 and installation of the K5A. Computed chloride concentrations on K2 and K6 are also close to those observed at latter times. Low observed values of chloride at K8 means that this well is not being contaminated from any of these probable sources of contamination investigated.

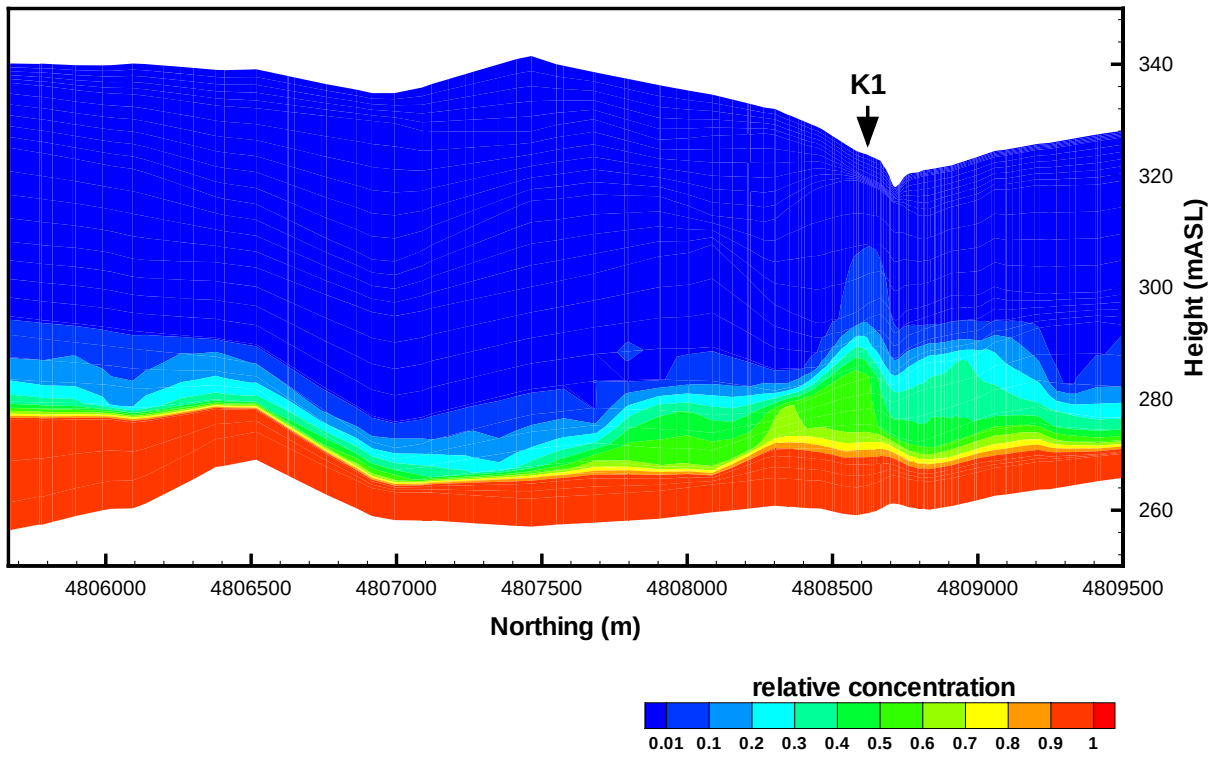

Figure 6.1: Cross-section at x=540800 m; upconing of bedrock water below Greenbrook wells.

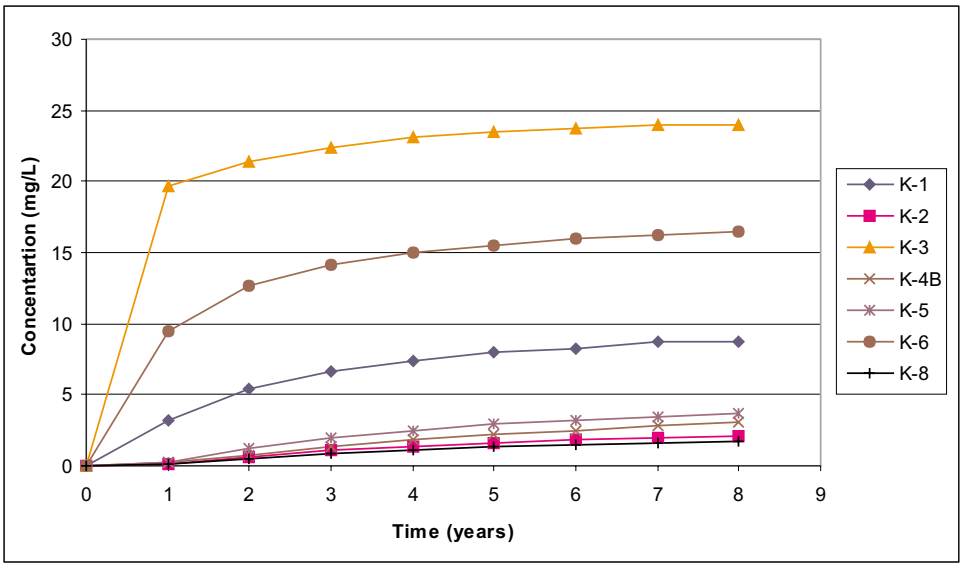

Figure 6.2: Breakthrough curve at Greenbrook wells (bedrock case).

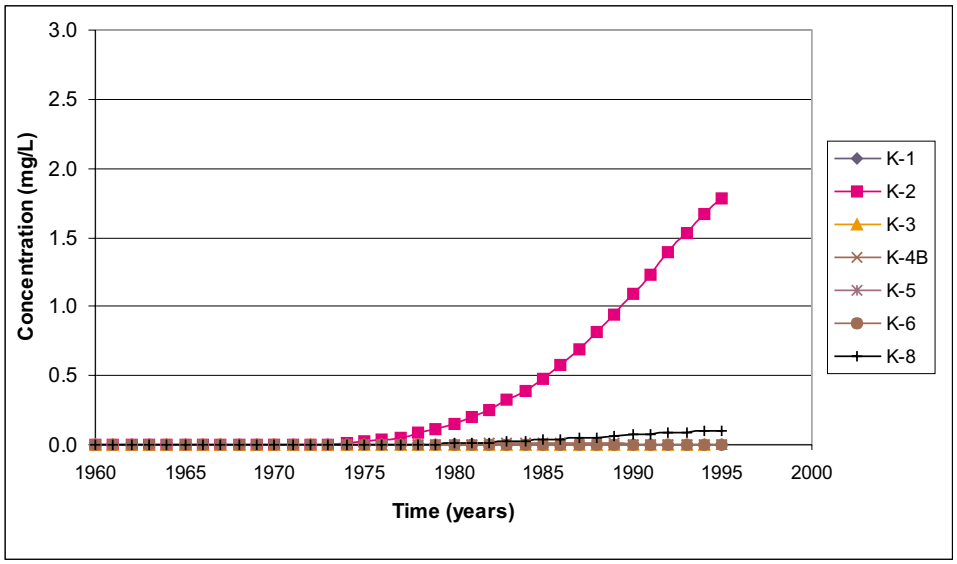

Figure 6.3: Breakthrough curve at Greenbrook wells (landfill case).

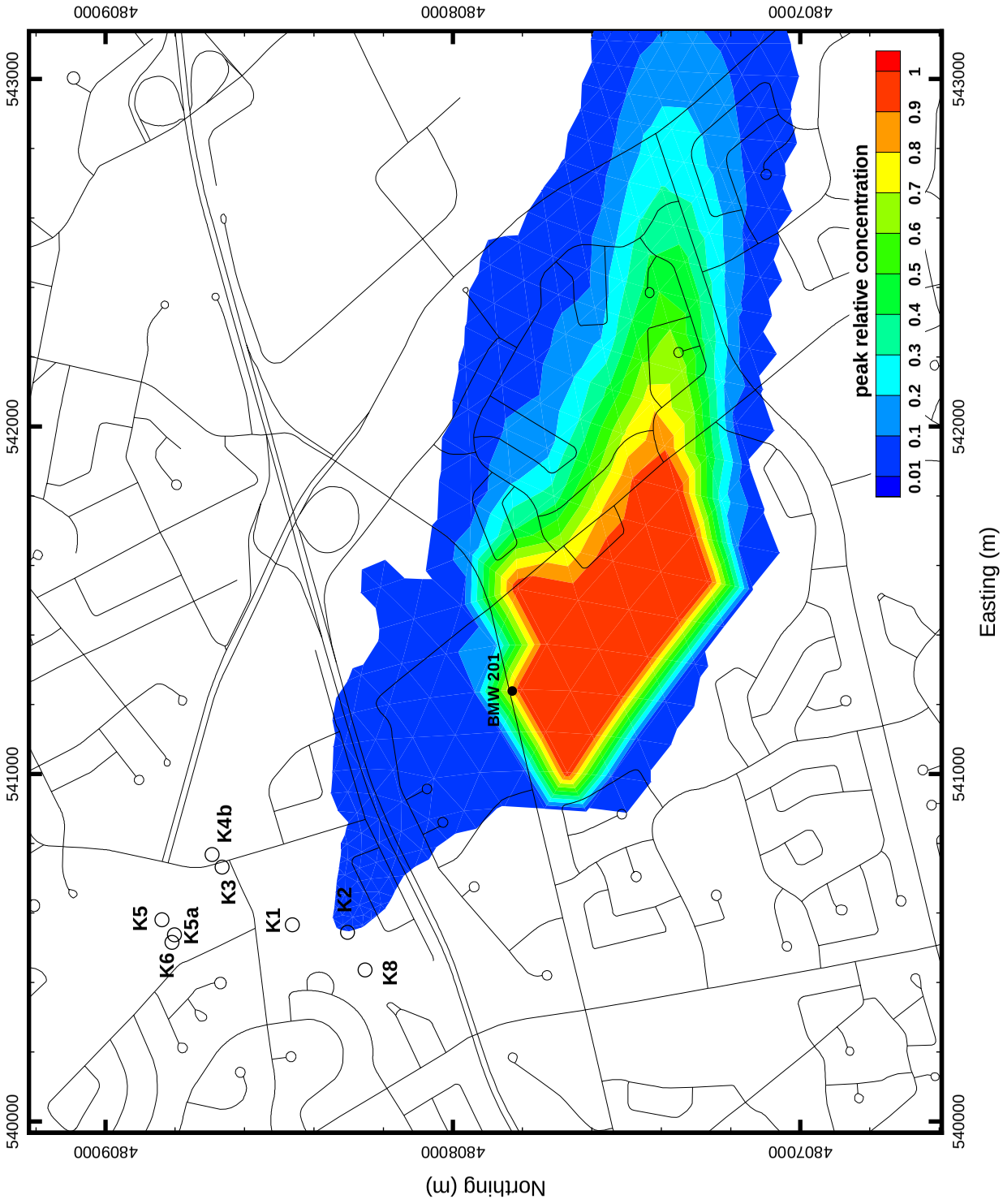

Figure 6.4: Peak relative concentration (landfill case).

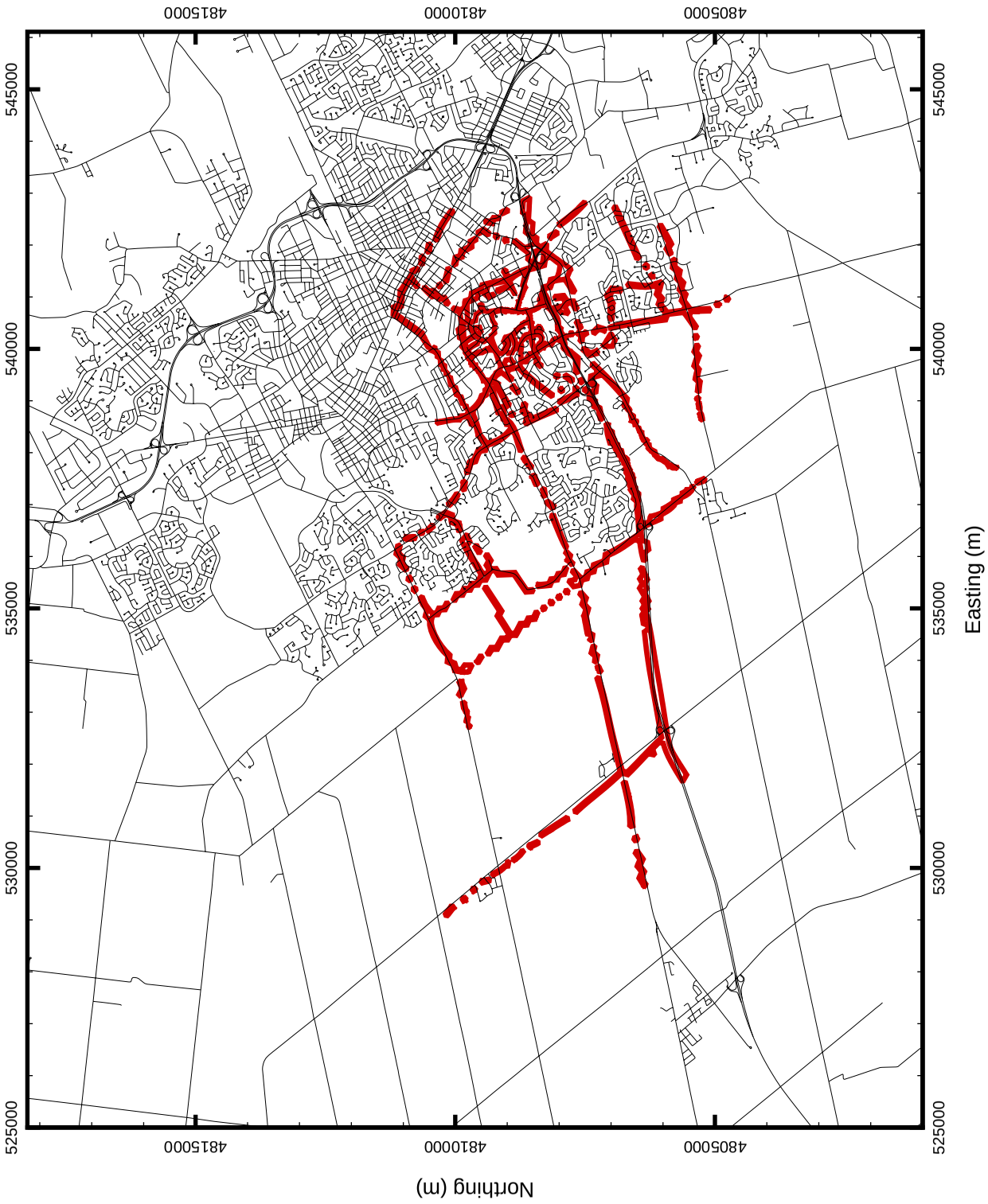

Figure 6.5: Road salt case; boundary nodes with c=1000 mg/l.

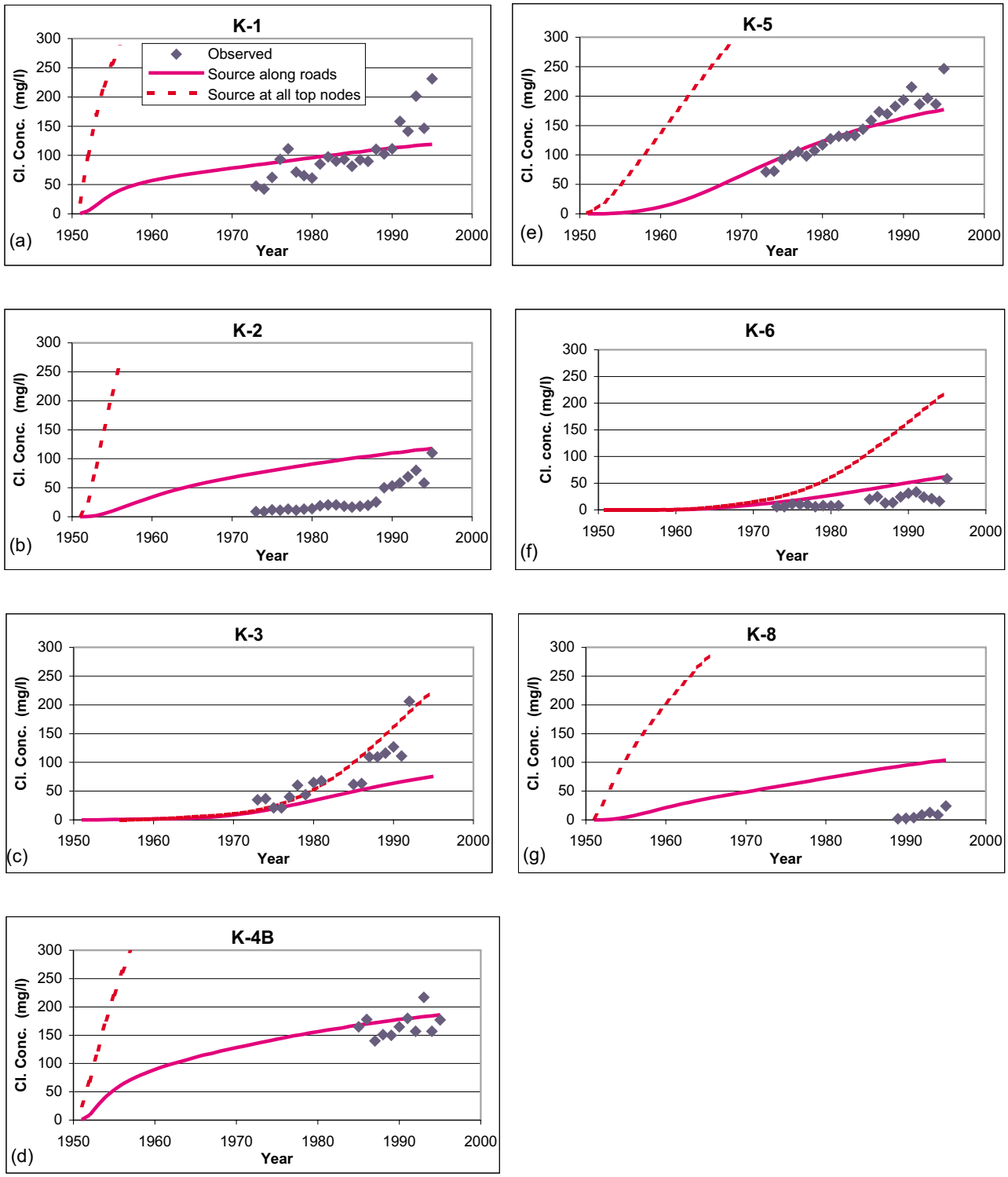

Figure 6.6: Road salt case; breakthrough curves at Greenbrook wells.

Chapter 7

Conclusions and Suggestions

The main objective of this study was to compare different methodologies for capture zone determination. This objective is achieved by comparing the results of particle tracking with two advective-dispersive transport models, i.e., a conventional time-marching transport model (WTC) and a time-continuous (LTG) model.

The LTG method is found to have certain advantages over the time-marching model (WTC) in the sense of efficiency and its ability to handle coarser grids, however it yields oscillatory results when approaching steady state. The time-marching method (WTC) has a disadvantage in that it requires small time steps especially at the beginning due to the Courant criterion resulting in significantly more execution time. This leads to the conclusion that the best approach to generate the steady state capture zone is by the combined application of LTG and WTC. The pseudo-steady state results from the LTG can be used as an initial condition for WTC to get the steady state capture zones.

Particle tracks and transport methods together are clearly more informative and give better insight than each by itself. While the particle tracks represent the conventional and easy approach for capture zones, the probability plume is more realistic in that it considers the uncertainty due to heterogeneities present in the system, and it eliminates the need to draw an envelope curve around the bundle of

particle tracks based on personal judgment. The agreement between the results of two different but compatible methodologies increases the credibility of the results.

This study provided valuable information on the application of different methodologies for the delineation of capture zones. These capture zones can be used to define the wellhead protection areas.

With respect to existing sources of contamination, preliminary results indicate that the major part of present observed chloride contamination is due to the application of road salt. Bedrock water is not expected to lead to any further deterioration of water quality at the Greenbrook wells. Leachate from the former Kitchener landfill may create a problem for one of the Greenbrook wells (K2).

The findings of this study reveal that there is a need for detailed sampling to get the exact locations of the chloride sources for the Greenbrook wells as well as for the other well fields. The assumption of steady state flow conditions for determining the contaminant sources may be removed in future studies by using the actual historical stress periods.

Bibliography

[1] Anderson, M.P., and W.W. Woessner (1992). *Applied groundwater modeling*, Academic Press, New York, NY.

[2] Bagtzoglou, A.C., D.E. Dougherty, and A. F. B. Thompson (1992). Application of particle methods to reliable identification of groundwater pollution sources. *Water Resour. Manage.*, 6, pp.15-23.

[3] Bear,J. (1972). *Dynamics of fluids in porous media*, American Elsevier, New York, NY.

[4] Beckers, J. (1998). Modelling the Ore Moraine multi-aquifer system: Role of geology, numerical model, parameter estimation, and uncertainty. Ph.D. thesis, University of Waterloo.

[5] Beckers, J., J.W. Molson, P.J. Martin and E.O. Frind (2000). WATFLOW/3D Version 2.0: A three-dimentional groundwater flow model with modules for automated calibration and parameter sensitivity analysis. User's guide, Department of Earth Sciences, University of Waterloo.

[6] Bester, M.L. (1999). Transport modelling: A comparison of the Laplace Transform Galerkin technique to time-marching methods. B.Sc. thesis, University of Waterloo.

[7] Burnett, R.D., and E.O. Frind (1987). An altenating direction Galerkin technique for simulation of groundwater contaminant transport in three dimen-

sions, 1: the alternating direction Galerkin technique. *Water Resour. Res.*, Vol. 23, No. 4, pp. 695-705.

[8] Callow (1996). Optimizing aquifer production for multiple well field conditions in Kitchener, Ontario. M.Sc. thesis, University of Waterloo.

[9] Chapnam, L.J. and D.F. Putnam (1984). The physiography of Southern Ontario, Third edition, Ontario Geological Survey, Special Volume 2.

[10] Crump, K.S. (1976). Numerical inversion of Laplace transform using a Fourier series approximation, *J. Assoc. Comput. Mach.*, Vol. 23, No. 1, pp. 89-96.

[11] CH2M Hill Engineering Ltd. (1993). Hydrogeological investigation of the former Kitchener landfill site, Volume 1. Prepared for Regional Municipality of Waterloo, Waterloo, Ontario.

[12] CH2M Hill Engineering Ltd. (1995). Draft annual report for Greenbrook Well Field monitoring program. Prepared for Regional Municipality of Waterloo, Waterloo, Ontario.

[13] Chin, D.A. and P.V.K. Chittaluru (1994). Risk management in wellhead protection, *J. Water Resour. Plan. Manage.*, 120 (3), pp. 294-315.

[14] Daus, A.D., E.O. Frind, and E. A. Sudicky (1985). Comparative error analysis in finite element formulations of the advection-dispersion equation, *Advances in Water Resources*, 8, pp. 86-95.

[15] De Hoog, F.R., J.H. Knight, and A. N. Stokes (1982). An improved method for numerical inversion of Laplace transforms, *SIAM J. Sci. Stat. Comput.*, Vol. 3, No. 3, pp. 357-366.

[16] Dixon, V.R. (1963). Groundwater Survey - City of Kitchener, Ontario Water Resources Commission.

[17] Domenico, P.A., and F.W. Scwartz (1990). *Physical and chemical hydrogeology*, John Wiley & Sons, New York.

[18] Farvolden, R.N., and M.J. Weitzman (1980). Greenbrook well filed study, Department of Earth Sciences, University of Waterloo, Ontario.

[19] Farvolden, R.N., J.P. Greenhouse, P.F. Karrow, P.E. Pehme, and L.C. Ross (1987). Subsurface Quaternary stratigraphy of the Kitchener-Waterloo area using borehole geophysics, Open file report 5623, Ontario Geological Survey.

[20] Fetter, C.W. (1994). *Contaminant hydrogeology*, Maxwell Macmillan Canada, Inc.

[21] Fitzpatrick, P.N. (1993). Groundwater flow and contamination at Kitchener-Waterloo, Ontario. M.A.Sc. thesis, University of Waterloo.

[22] Freeze, R.A. and J.A. Cherry (1979). *Groundwater*, Prentice-Hall, Englewood Cliffs, NJ.

[23] Frind, E.O. (1997). *Groundwater modelling (numerical methods)*. Lecture notes, Department of Earth Sciences, University of Waterloo.

[24] Frind, E.O. (2000, in preparation). WATRAC, Version 1.2: Particle tracking for 3D delauney prisms, Department of Earth Sciences, University of Waterloo.

[25] Frind, E.O., M. Shahid, J. W. Molson, and J. Beckers (2000). Methodologies for the delineation of well capture zones in complex aquifer systems, *Groundwater Research*, Rosbjerg et al., (eds), Balkema, Rotterdam.

[26] Gelhar, L.W., and C.L. Axness (1983). Three-dimensional stochastic analysis of macrodispersion in aquifers, *Water Resour. Res.*, Vol. 19, No. 1, pp. 161-180.

[27] Gelhar, L.W., C. Welty, and K.R. Rehfeldt (1992). A critical review of data on field-scale dispersion in aquifers, *Water Resour. Res.*, Vol. 28, No. 7, pp. 1955-1974.

[28] GLL, M.M. Dillon. Ltd., J.M. Molson and E.O. Frind (1998). Detailed delineation of capture zones, Greenbrook well field, Kitchener, Ontario.

[29] GLL, M.M. Dillon. Ltd., J.M. Molson and E.O. Frind (1999). Greenbrook well field capture zone simulations. Supplement to the report: Detailed delineation of capture zones, Greenbrook well field, Kitchener, Ontario (GLL 96-326).

[30] Huyakorn, P.S., G.F. Pinder (1983). *Computational methods in subsurface flow*, Academic Press, Orlando, Fla.

[31] Huyakorn, P.S., E.P. Springer, V. Guvanasen, and T. D. Wadsworth (1986). A three-dimensional finite-element model for simulating water flow in variably saturated porous media, *Water Resour. Res.*, Vol. 22, No. 13, pp. 1790-1808.

[32] Johnston, C.T. (1994). Geochemistry, isotope composition and age of groundwater from the Waterloo Moraine: Implication for groundwater protection and management. M.Sc. thesis, University of Waterloo.

[33] Karrow, P.F. (1987). Quaternary geology of the Hamilton-Cambridge area, Southern Ontario, Ontario Geological Survey. Report 255.

[34] Karrow, P.F. (1993). Quaternary geology, Stratford-Conestoga area, Ontario Geological Survey. Report 283.

[35] Kinzelbach, W. (1986). *Groundwater modelling*, Elsevier, Amsterdam.

[36] Li, S, F. Ruan, and D. McLaughlin (1992). A space-time accurate method for solving solute transport problems, *Water Resour. Res.*, Vol. 28, No. 9, pp. 2297-2306.

[37] Linderfelt, W.R.J.L. Wilson and S. Leppert (1989). Abstr., EOS, 70, pp. 971.

[38] Liu, J. and J.L. Wilson (1996). Validation and demonstration of backtracking to find the source of pollution. Technical Completion Report, Project WERC 01-4-23233. Department of Earth and Environmental Science, New Mexico Institute of Mining and Technology, Socorro, New Mexico.

[39] Martin, P.J. (1994). Modelling of the North Waterloo multi-aquifer system. M.Sc. thesis, University of Waterloo.

[40] Martin, P.J. 1995. Volume of Interpreted Cross Section Throughout the Waterloo Moraine. Waterloo Centre for Groundwater Research, University of Waterloo.

[41] Martin, P.J. (1996).WTC-TRAC: Waterloo transport code for particle tracking. Waterloo Hydrogeologic Inc., Waterloo, Ontario.

[42] Martin, P.J. and E.O. Frind (1998). Modeling a complex multi-aquifer system: The Waterloo Moraine, *GROUNDWATER*, Vol. 36, No. 4, pp. 679-690.

[43] McLaren, R.G. (1999). GRIDBUILDER, Version 5.5. A pre-processor for 2D, triangular element, finite-element programs. User's guide, Department of Earth Sciences, University of Waterloo.

[44] Molson, J.W., E.O. Frind and C.D. Palmer (1992). Thermal energy storage in an unconfined aquifer 2. Model development, validation, and application, *Water Resour. Res.*, Vol. 28, No. 10, pp. 2857-2867.

[45] Molson, J.W., P. J. Martin, and E.O. Frind (1992). WATFLOW: A three-dimensional groundwater flow model. User's guide, Department of Earth Sciences, University of Waterloo.

[46] Molson, J.W., P.J. Martin, and E.O. Frind (1996). WTC-TRAC: Waterloo Transport Code. User's guide, Department of Earth Sciences, University of Waterloo.

[47] Moridis, G.J. and D.L. Reddell (1991). The Laplace transform finite method for simulation of flow through porous media, *Water Resour. Res.*, Vol. 27, No. 8, pp. 1973-1884.

[48] Neupauer, R.M. and J.L. Wilson (1999). Adjoint method for obtaining backward-in-time location and travel time probabilities of a conservative groundwater contaminant, *Water Resour. Res.*, Vol. 35, No. 11, pp. 3389-3398.

[49] Paloschi, G.V.R. (1993). Subsurface stratigraphy of the Waterloo Moraine. M.Sc. project, University of Waterloo.

[50] Petrie, J.M. (1985). Field response of a clay till in a layered aquifer system at Waterloo, Ontario. M.Sc. project, University of Waterloo.

[51] Pinder, G.F., and E.O. Frind (1972). Application of Galerkin's procedure to aquifer analysis, *Water Resour. Res.*, Vol. 8, No. 1, pp. 108-120.

[52] Pollock, D.W. (1988). Semianalytical computation of path lines for finite-difference models, *GROUNDWATER*, Vol. 26, No. 6, pp. 743-750.

[53] Radcliffe, A.J. (2000, in preparation). Modelling the Waterloo west side and the affect of the urbanization on the regional groundwater flow system. M.Sc. thesis, University of Waterloo.

[54] Regional Municipality of Waterloo (1991). Information package - hydrogeologic investigation of the former Kitchener landfill site.

[55] Rudolph, D.L. (1985). A quasi three-dimensional finite element model for steady-state analysis of multiaquifer system: B. Application to the Greenbrook well field, Kitchener, Ontario. M.Sc. thesis, University of Waterloo.

[56] Rudolph, D.L. and R.N. Farvolden (1989). Numerical analysis of regional groundwater flow in a complex multi-aquifer system in Kitchener, Ontario. Waterloo Centre for Groundwater Research.

[57] Schmid, G., and D. Braess (1988). Comparison of fast equation solvers for groundwater flow problems. In *Groundwater flow and quality modelling*, NATO-ASI Series C, Vol. 224, (Eds. E. Custodio et al,.) pp. 173-188.

[58] Skaggs, T.H. and D.A. Barry (1996). Sensitivity methods for time continuous, spatially discrete groundwater contaminant transport models, *Water Resour. Res.*, Vol. 32, No. 8, pp. 2409-2420.

[59] Sudicky, E.A. (1989). The Laplace transform Galerkin technique: A time-continuous finite element theory and application to mass transport in groundwater, *Water Resour. Res.*, Vol. 25, No. 8, pp. 1933-1846.

[60] Sudicky, E.A. (1990). The Laplace transform Galerkin technique for efficient time-continuous solution of solute transport in double-porosity media, *Geoderma*, 46, pp. 209-232.

[61] Sudicky, E.A and R.G. McLaren (1992). The Laplace transform Galerkin technique for large-scale simulation of mass transport in discretely fractured porous formations, *Water Resour. Res.*, Vol. 28, No.2, pp. 499-514.

[62] Sudicky, E.A, A.J.A. Unger and S. Lacombe (1995). A noniterative technique for the direct implementation of well bore boundary conditions in three-dimensional heterogeneous formations, *Water Resour. Res.*, Vol. 31, No. 2, pp. 411-415.

[63] Terraqua Investigations Ltd. (1992). Waterloo north aquifer system study. Unpublished report to the Regional Municipality of Waterloo.

[64] Terraqua Investigations Ltd. (1995). Study of the hydrogeology of the Waterloo Moraine. Unpublished report to the Regional Municipality of Waterloo.

[65] Uffink, G. J. M. (1989). Application of Kolmogorov's backward equation in random walk simulations of groundwater contaminant transport. In *Contaminant transport in groundwater*. Edited by H. E. Kobus and W. Kinzelbach, A.A. Balkema, Brookfiled, Vt.

[66] U.S. Environmental Protection Agency (1987). Guidelines for delineation of wellhead protection areas.

[67] Waterloo Hydrogeologic Inc. (1995). Preliminary delineation of well field capture zones, Volume 1 & 2.

[68] Waterloo Hydrogeologic Inc. (1996). Visual MODFLOW, User's mannual, 180 Columbia Street West, Unit 1104, Waterloo, Onatrio.

[69] Waterloo Hydrogeologic Inc. (1998). Capture zone delineation modelling, Technical Appendix I. Draft Report to The Regional Municipality of Waterloo.

[70] Waterloo Hydrogeologic Inc. (1999). Delineation of Well Field Capture Zones Within the Waterloo Moraine. DRAFT Unpublished report to the Regional Municipality of Waterloo.

[71] Wilson, J.L. and W.R. Linderfelt (1991). Groundwater quality in pumping wells located near surface water bodies. Technical Completion Report 261, New Mex. Water Resour. Res. Inst., Las Cruses.

[72] Wilson, J.L. and J. Liu (1995). Backward tracking to find the source of the pollution in waste management. In *Waste Management: From Risk to Reduction.* Eds. R. Bahda et al., pp. 181-199, ECM Press, Albuquerque, NM.

[73] Woeller, R.M. (1982). Greenbrook well field management study 1981-1982. M.Sc. thesis, University of Waterloo.

[74] Woeller, R.M., and R. N. Farvolden (1989). The past, present and future of groundwater development in the tri-cities of Kitchener, Waterloo and Cambridge, Ontario, Canada. Proceedings of the NWWA FOCUS Conference on Eastern Regional Groundwater Issues Kitchener, Ontario.

[75] Zheng, C. and G.D. Bennet (1995). *Applied contaminant transport modeling.* Van Nortrand Reinhold, A division of International Thomson Publishing Inc., Toronto.

Appendix A

Capture Zones

The flow model of the study area was not fully calibrated for all the well fields except the Greenbrook well field. The capture zones in the following figures are shown only for the purpose of comparing the methodologies of particle tracking and Wilson's approach for the major well fields of the Waterloo Moraine given in Table 5.1. Capture zones are defined in terms of the 0.02 probability contour.

The advective-dispersive transport model (LTG) is used for all these well fields using the coarse mesh. For some of the well fields, a fine mesh is also used to compare the results using different discritization. The particle tracking code (WATRAC) is used for all the well fields using the fine mesh. 2- and 10-year particle tracks and peak probability capture zones for all the major well fields are given at the beginning (Figures A.1 to A.4).

William Street, Strange Street, and two private wells (Sunar-1 and Sunar-2) are simulated simultaneously due to the overlapping of individual capture zones.

The wells within Waterloo North well field are treated separately due to their depths and screen position in different aquifers. Capture zone for W4 and W10 is determined separately from W5, as these wells are screened in Aquifer 1 while W5 is screened in Aquifer 2. The time to reach the steady state capture zone is different for these wells.

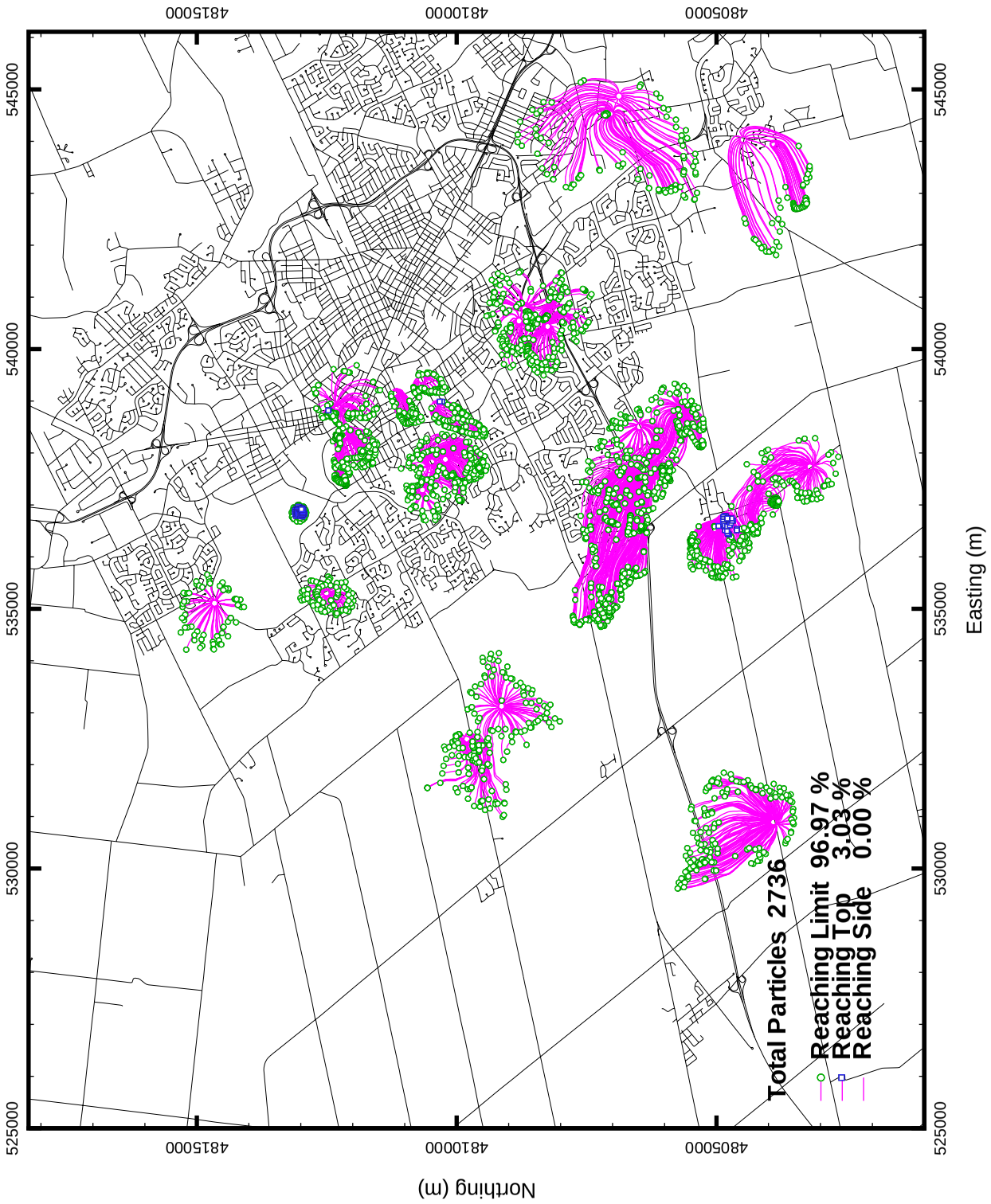

Figure A.1: All major well fields: 2-year particle tracks.

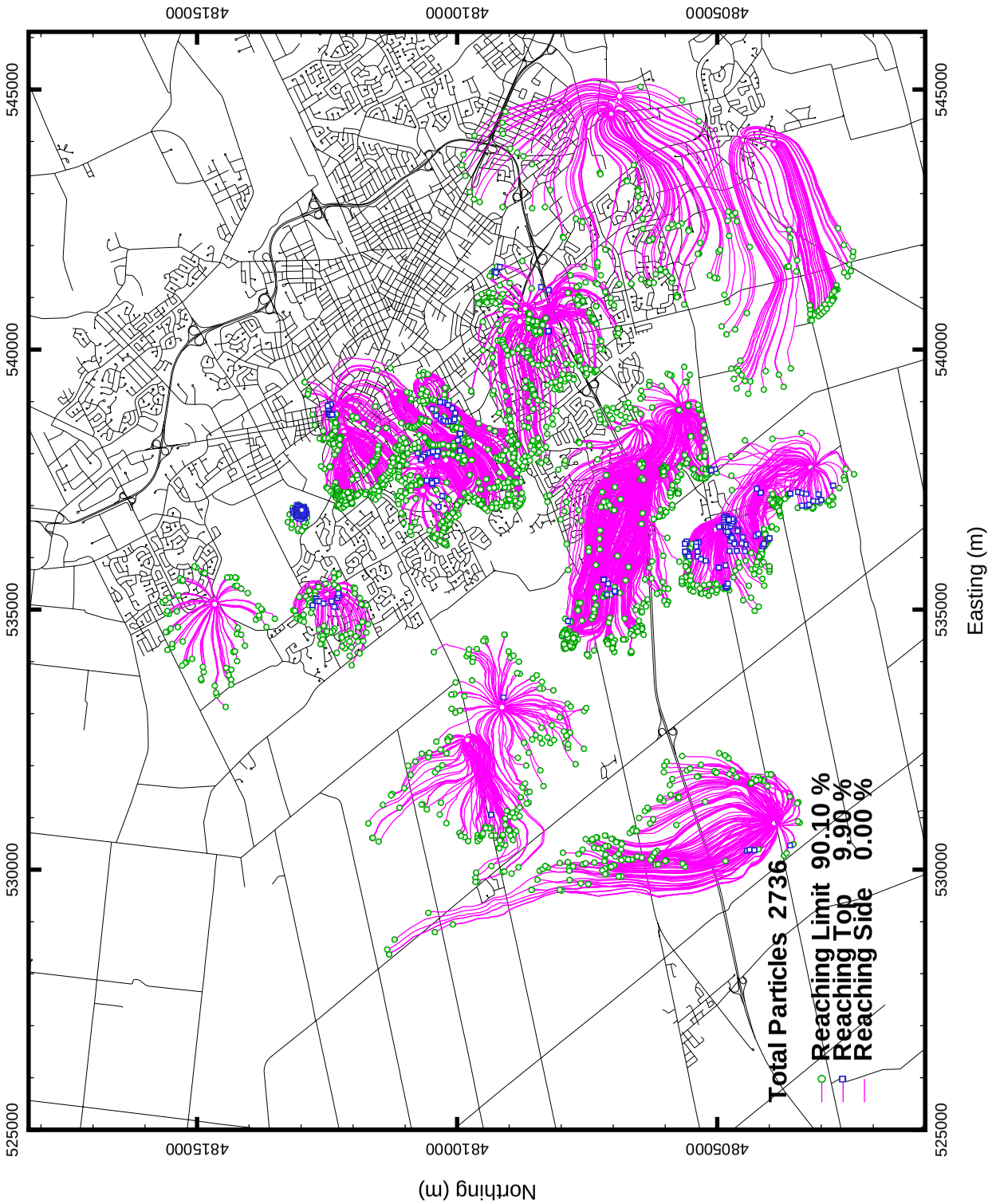

Figure A.2: All major well fields: 10-year particle tracks.

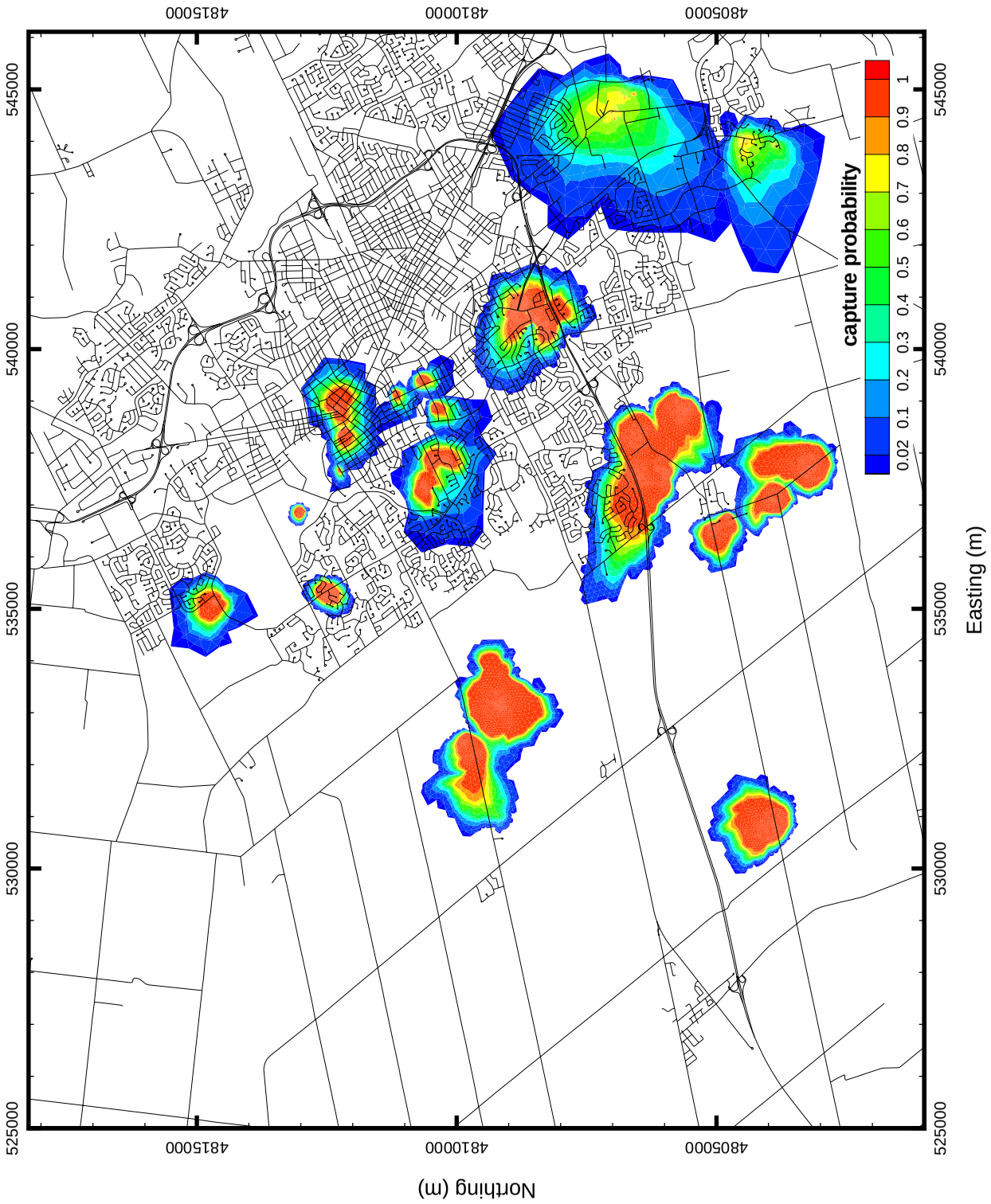

Figure A.3: All major well fields: 2-years peak capture probability.

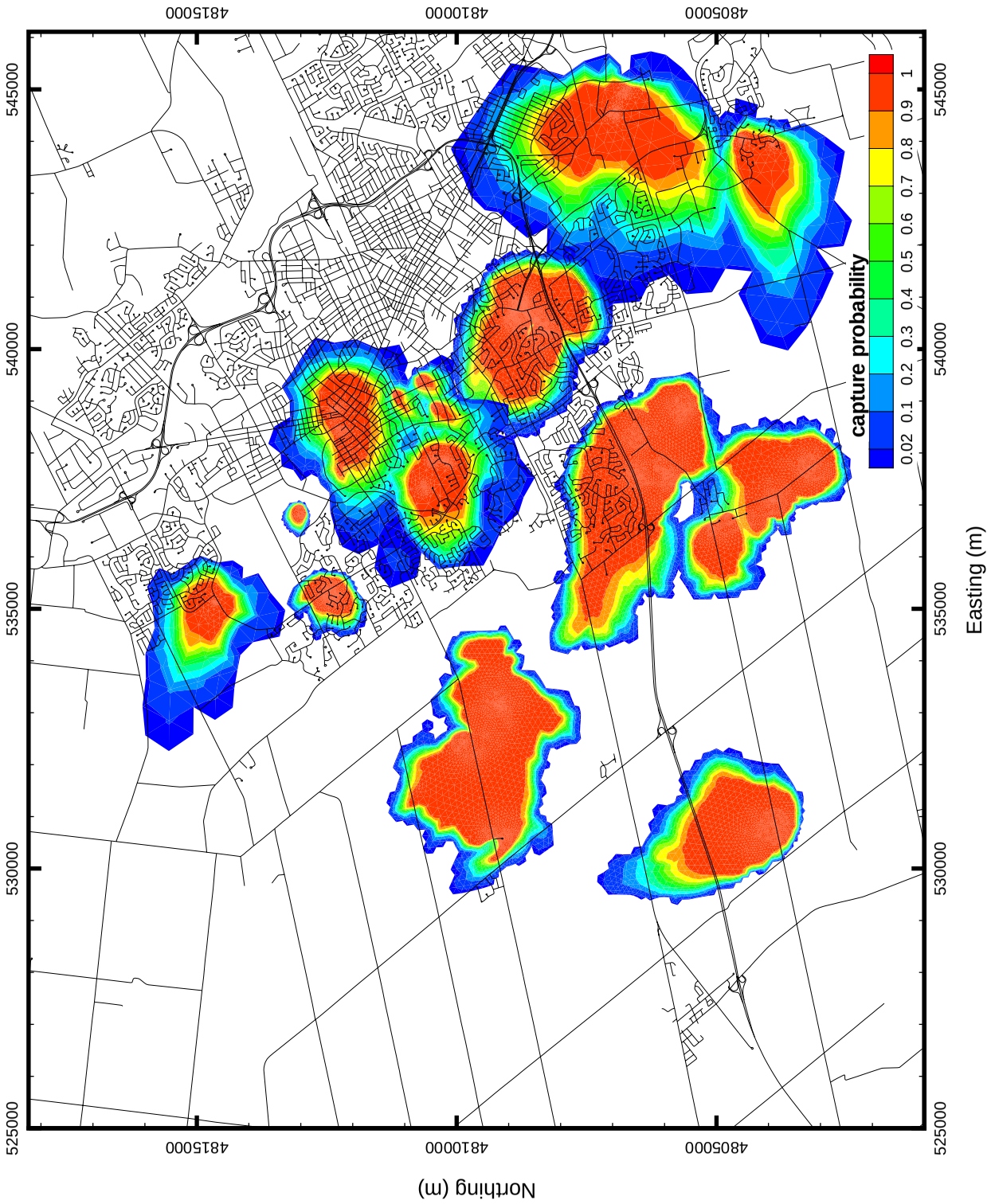

Figure A.4: All major well fields: 10-year peak capture probability.

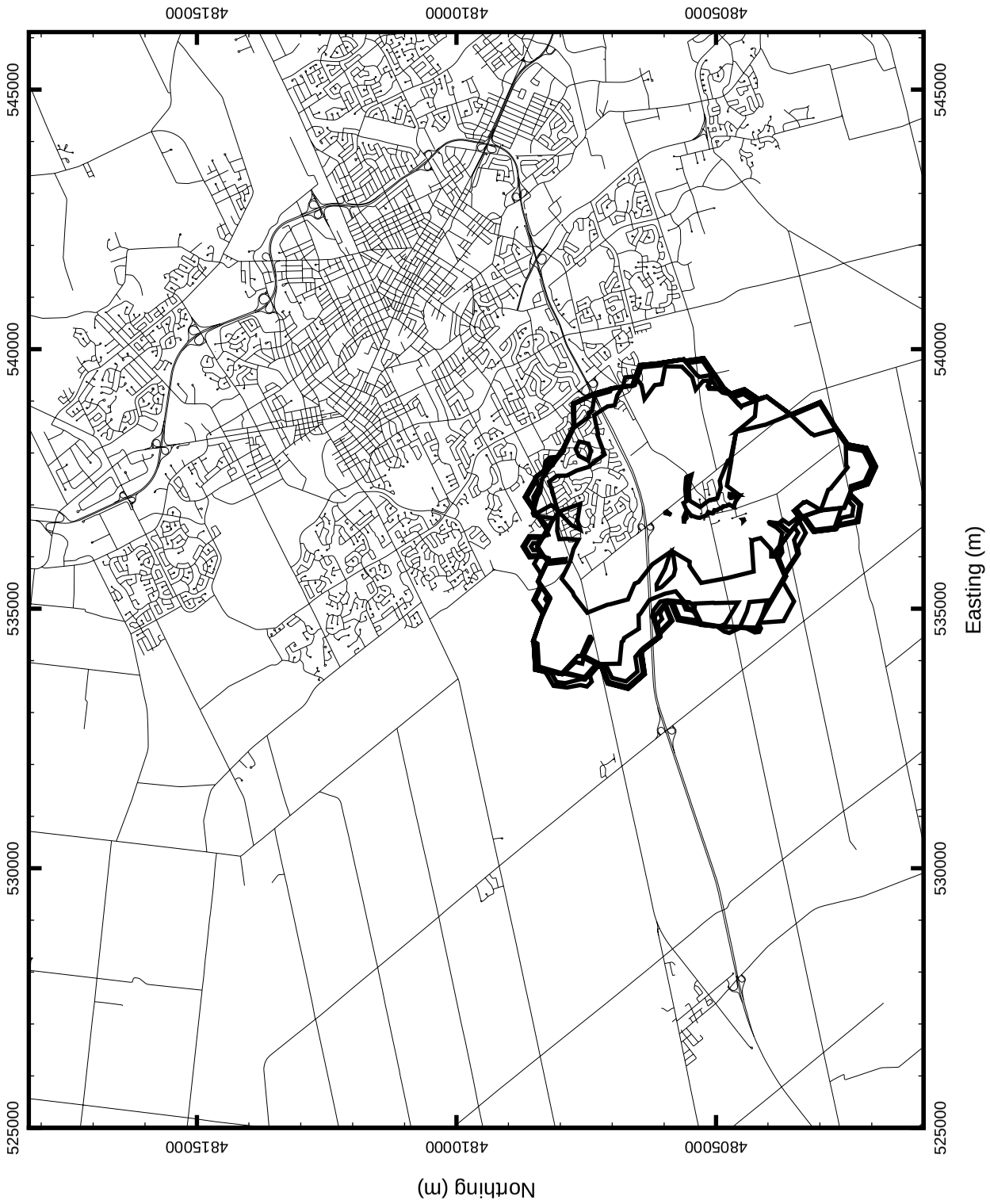

Figure A.5: Mannheim well field (coarse mesh): 0.02 peak capture probability contours; 2, 10, 20, 30, 40, & 60 years.

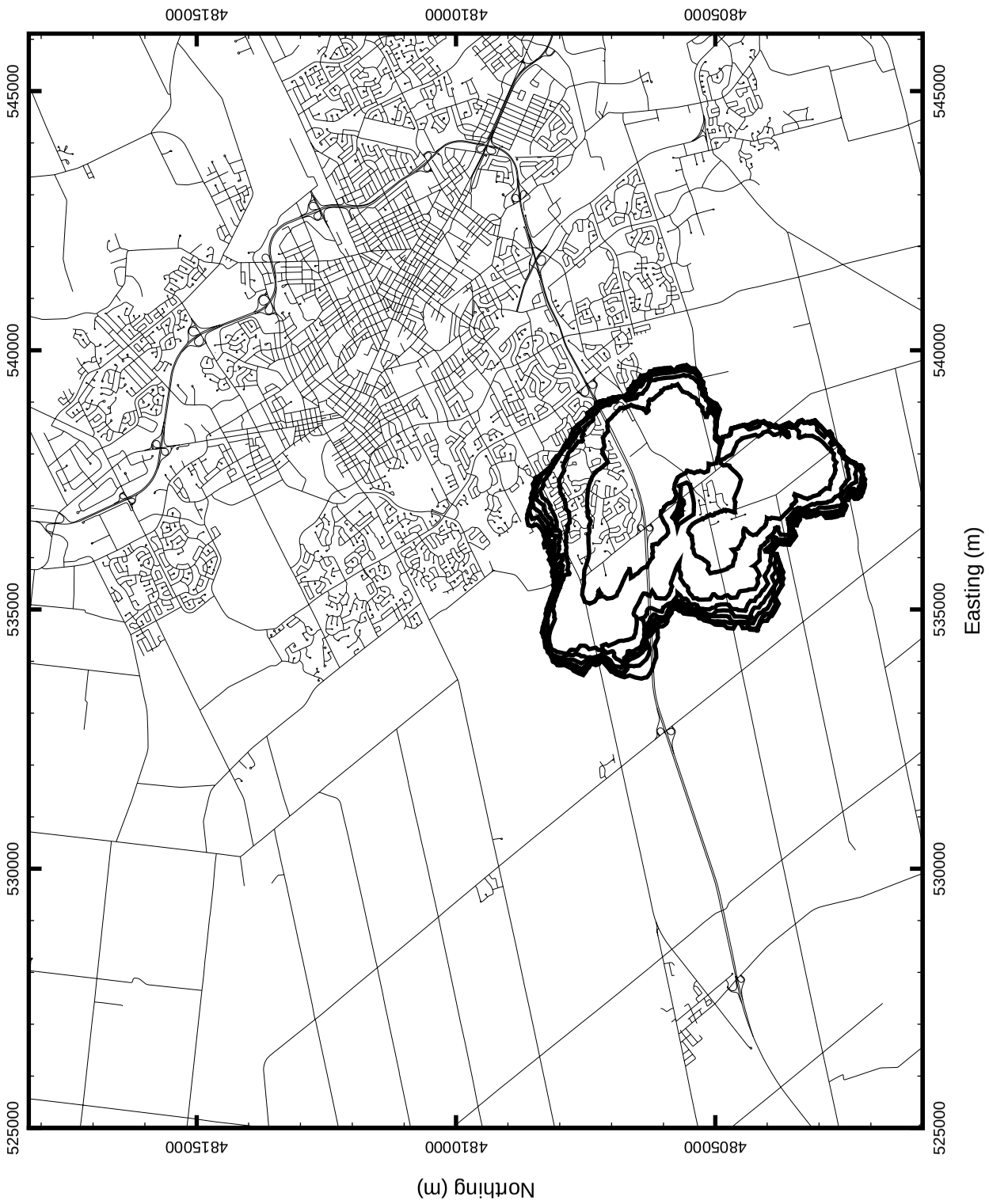

Figure A.6: Mannheim well field (fine mesh): 0.02 peak capture probability contours; 2, 10, 20, 30, 40, & 60 years.

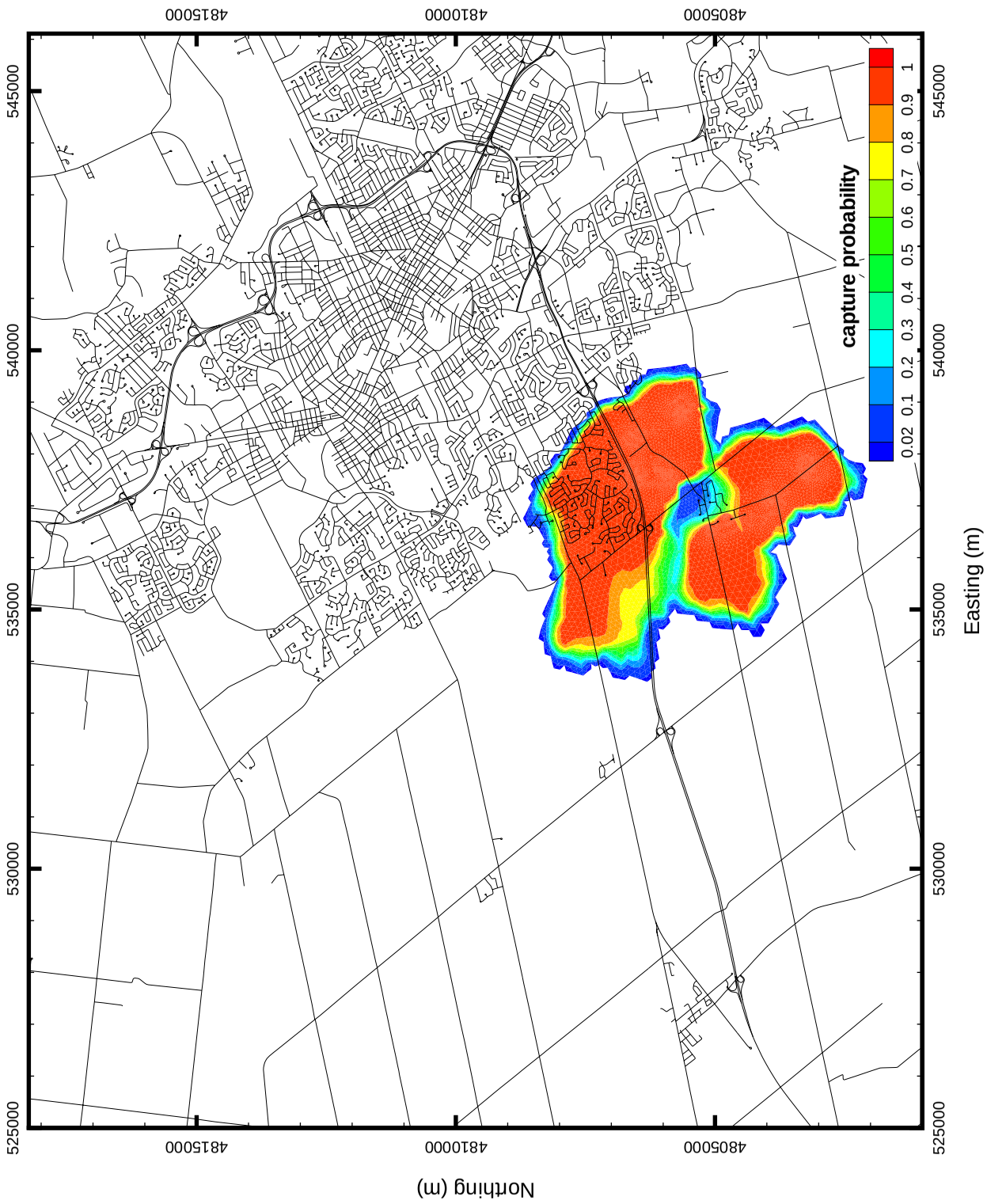

Figure A.7: Mannheim well field (fine mesh): 60-year peak capture probability.

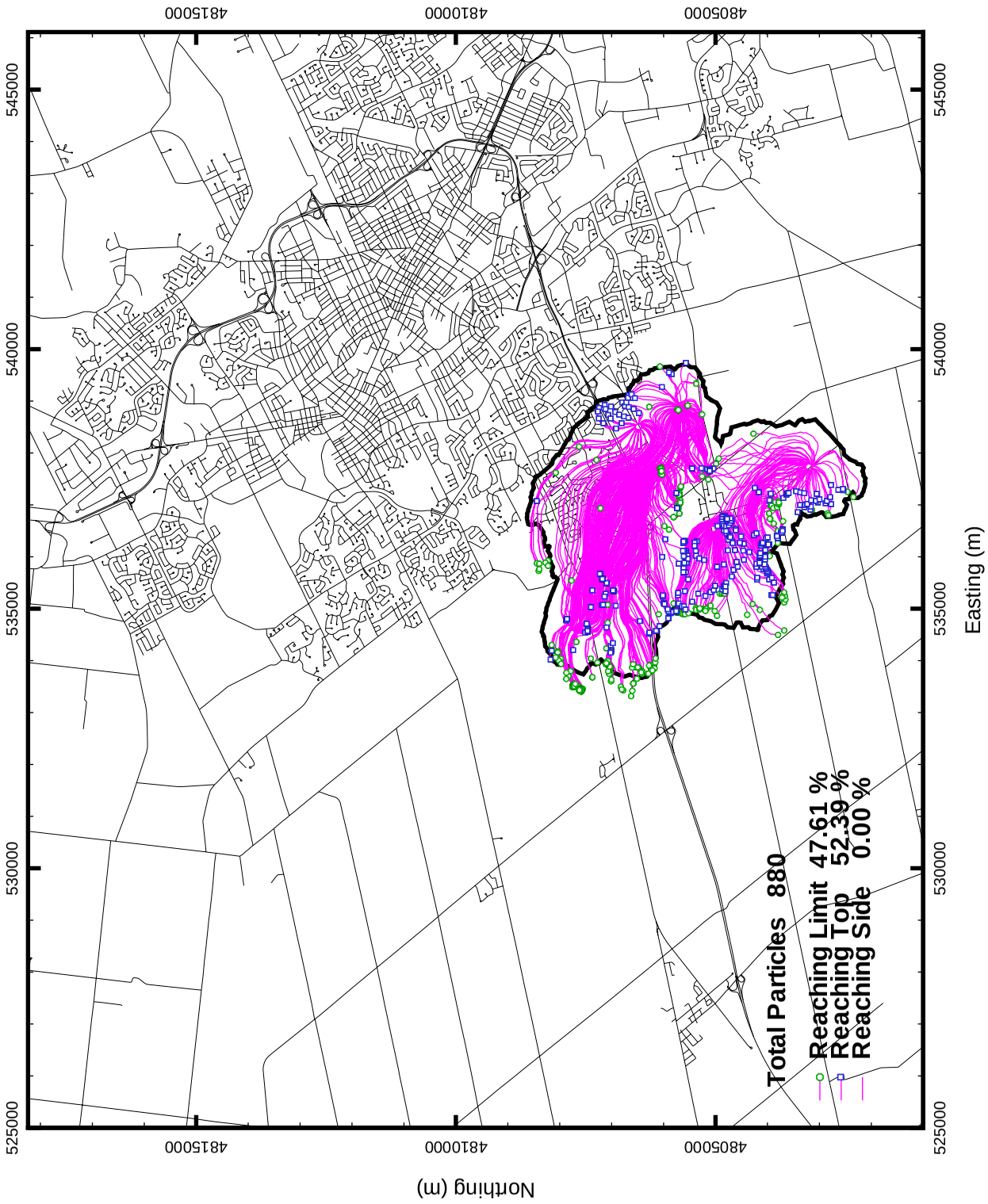

Figure A.8: Mannheim well field (fine mesh): 60-year particle tracks with outline of 0.02 peak capture probability.

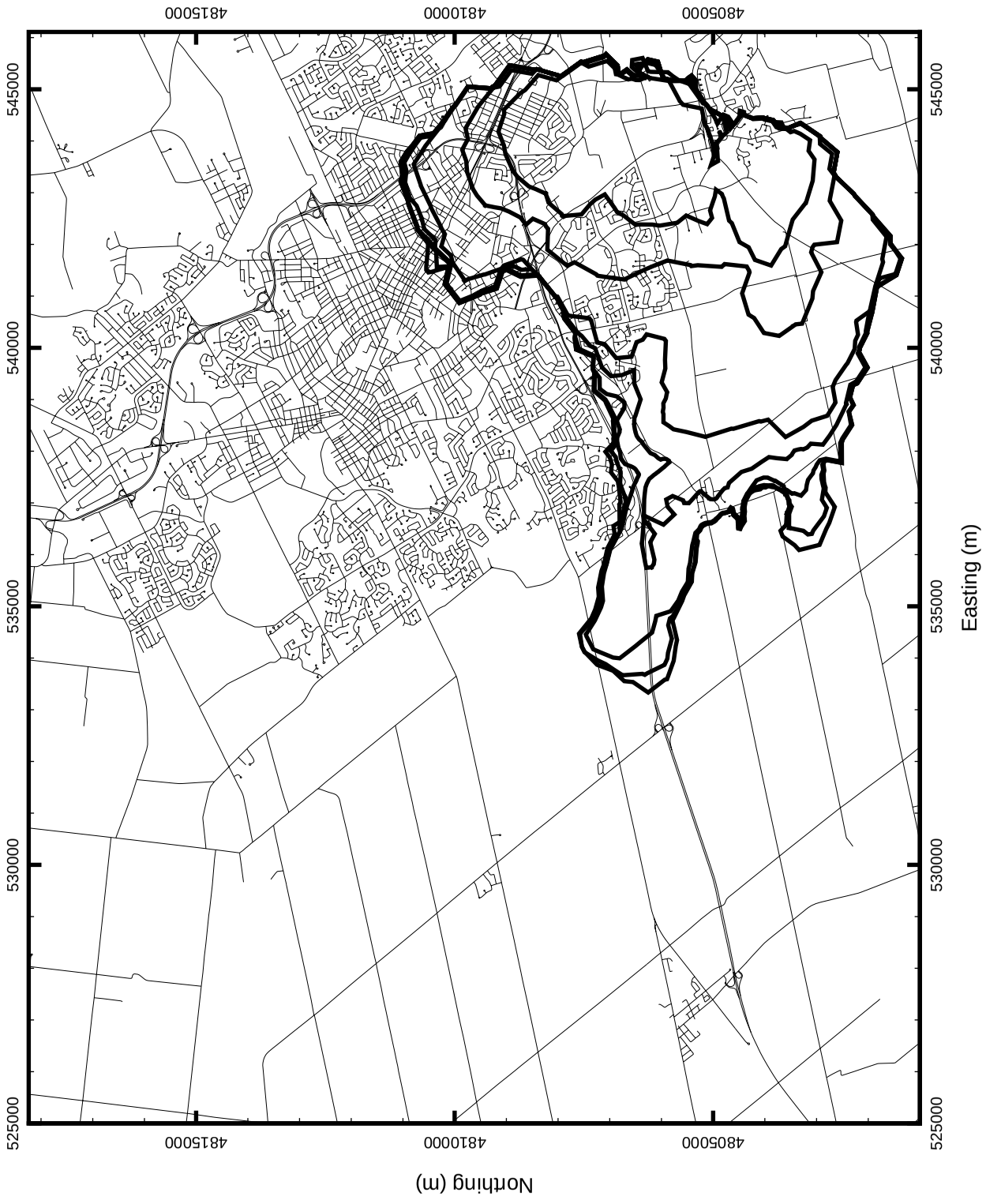

Figure A.9: Parkway well field (coarse mesh): 0.02 peak capture probability contours; 2, 10, 50, 100, 200, 300 & 360 years.

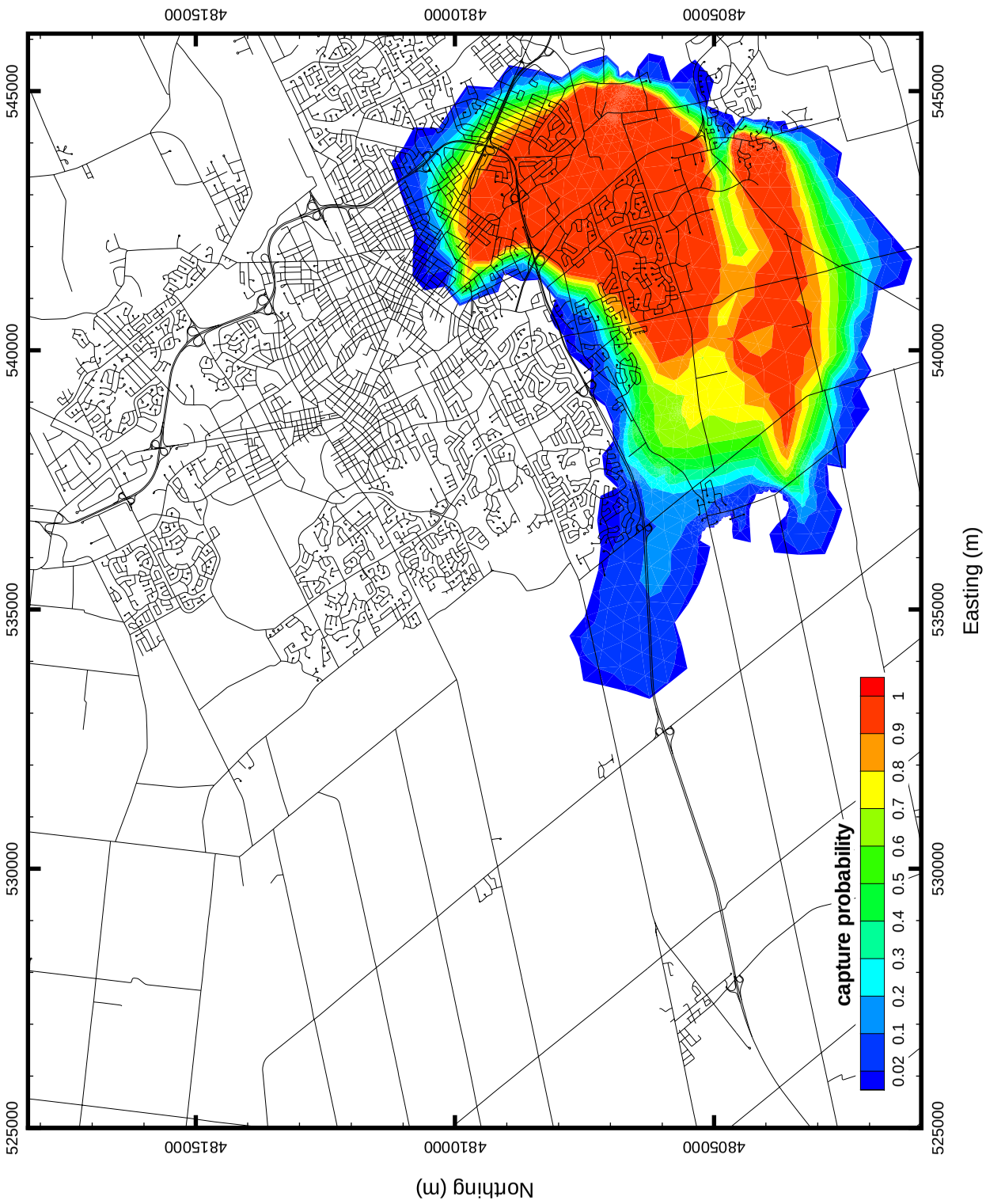

Figure A.10: Parkway well field (fine mesh): 360-year peak capture probability.

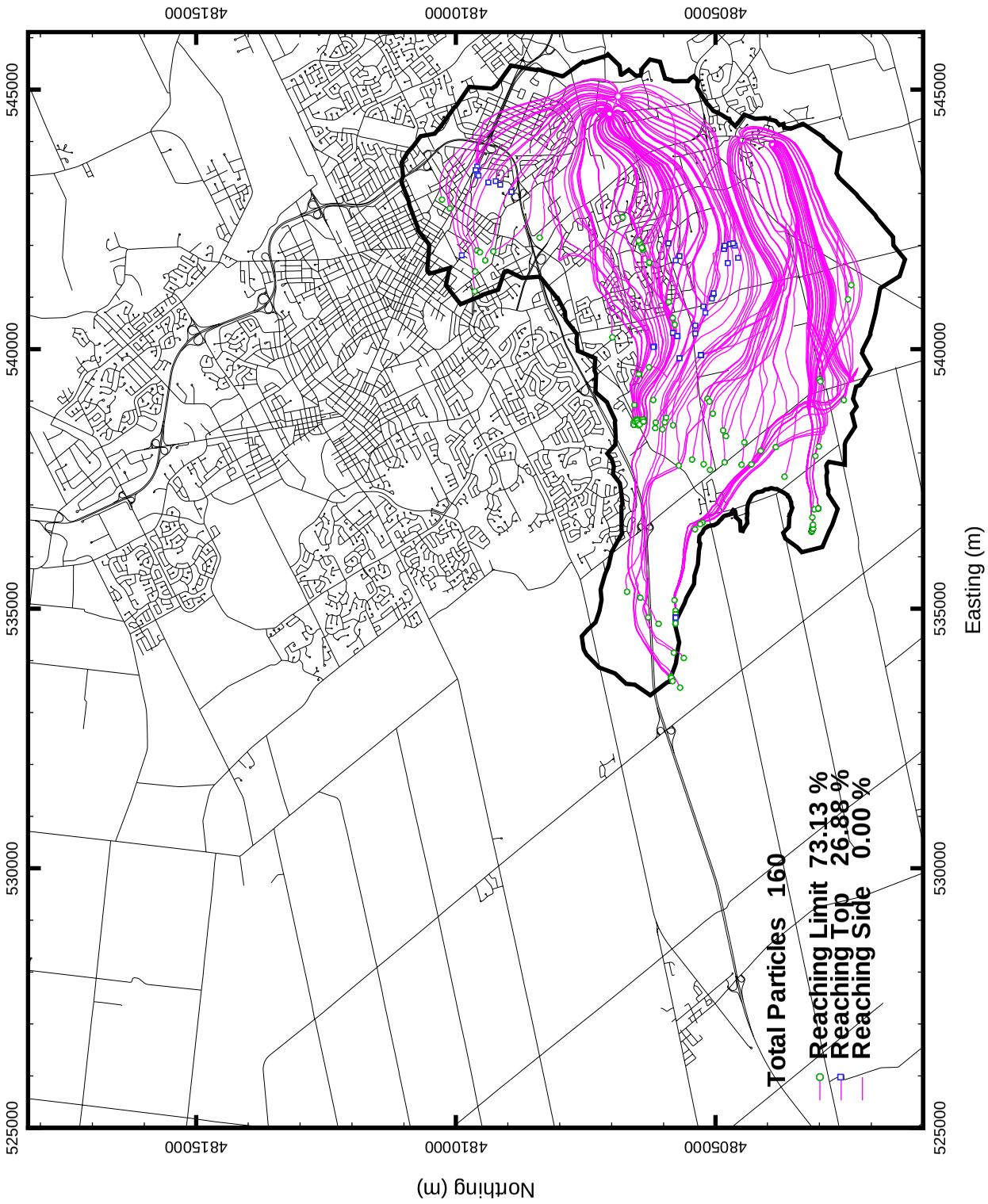

Figure A.11: Parkway well field (fine mesh): 360-year particle tracks with outline of 0.02 peak capture probability.

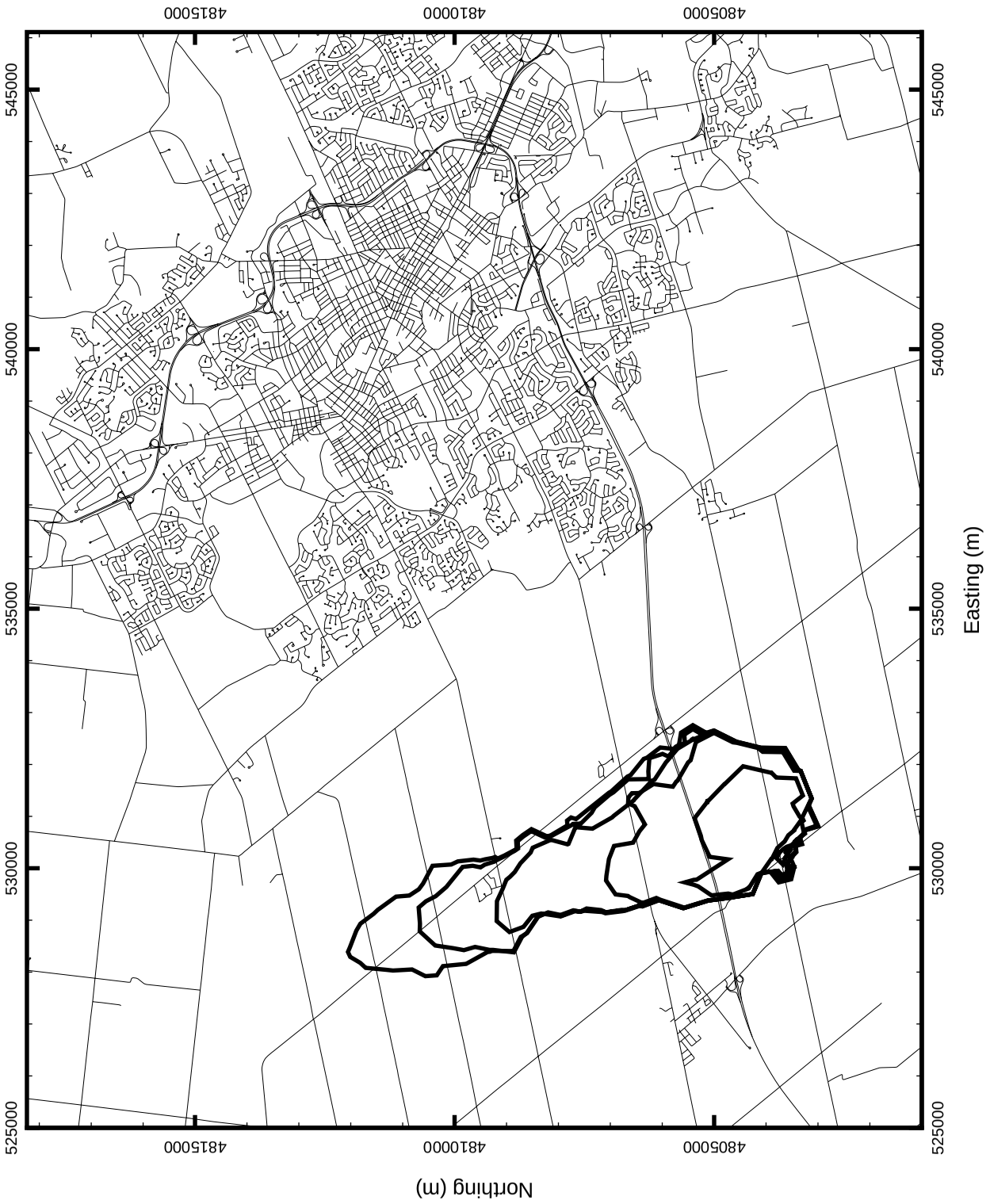

Figure A.12: Wilmot well field (coarse mesh): 0.02 peak capture probability contours; 2, 10, 20, 30, & 40 years.

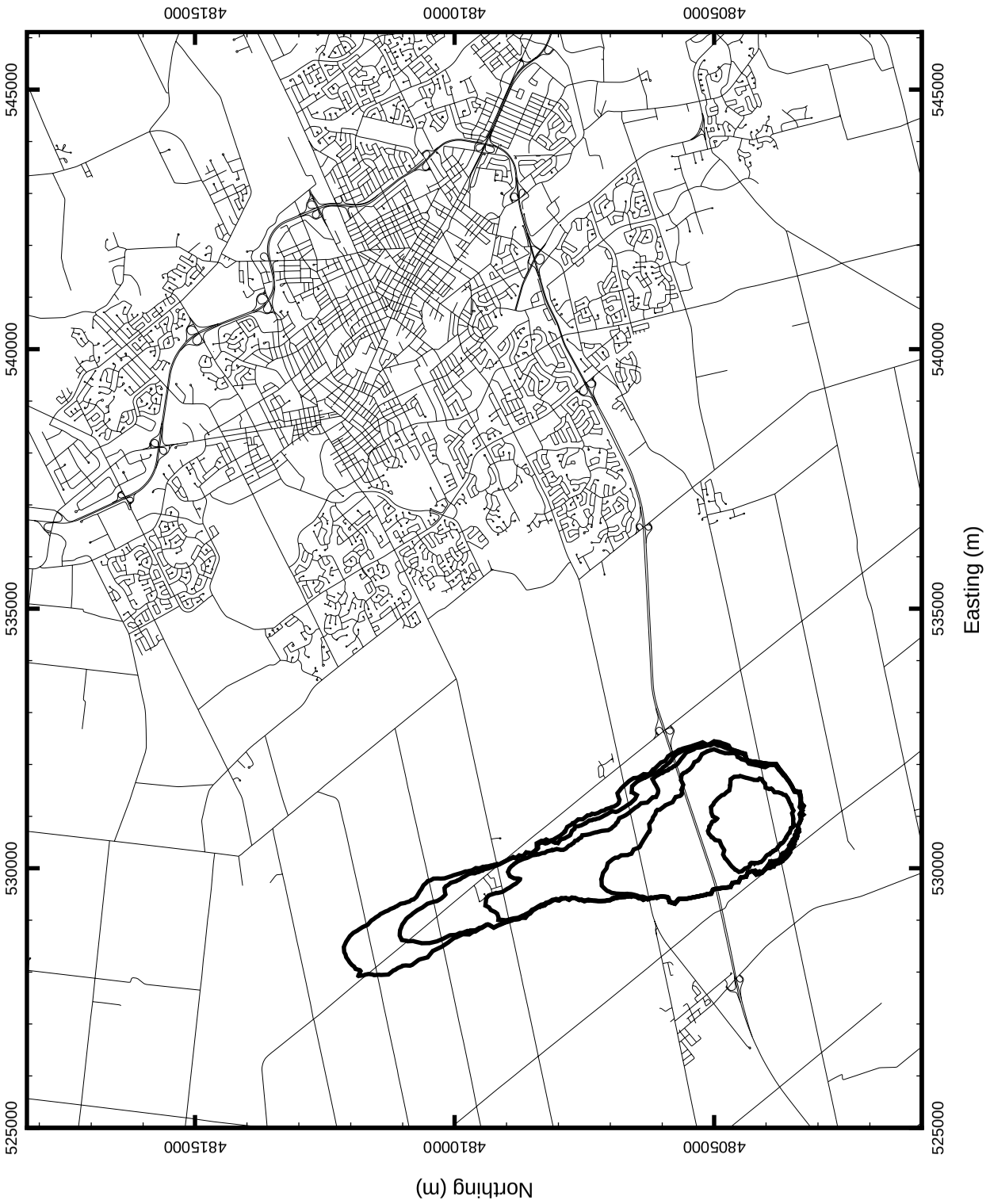

Figure A.13: Wilmot well field (fine mesh): 0.02 peak capture probability contours; 2, 10, 20, 30, & 40 years.

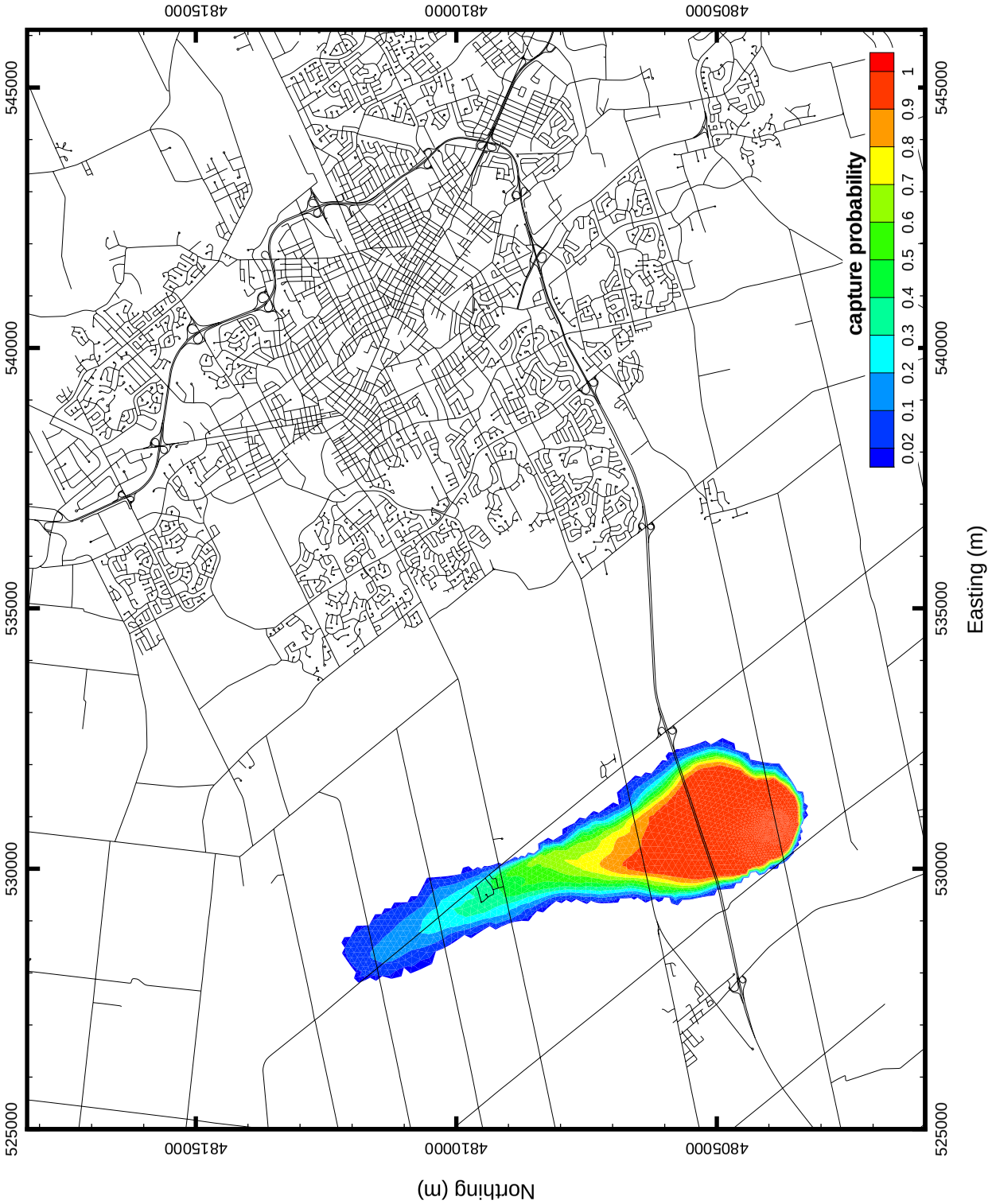

Figure A.14: Wilmot well field (fine mesh): 40-year peak capture probability.

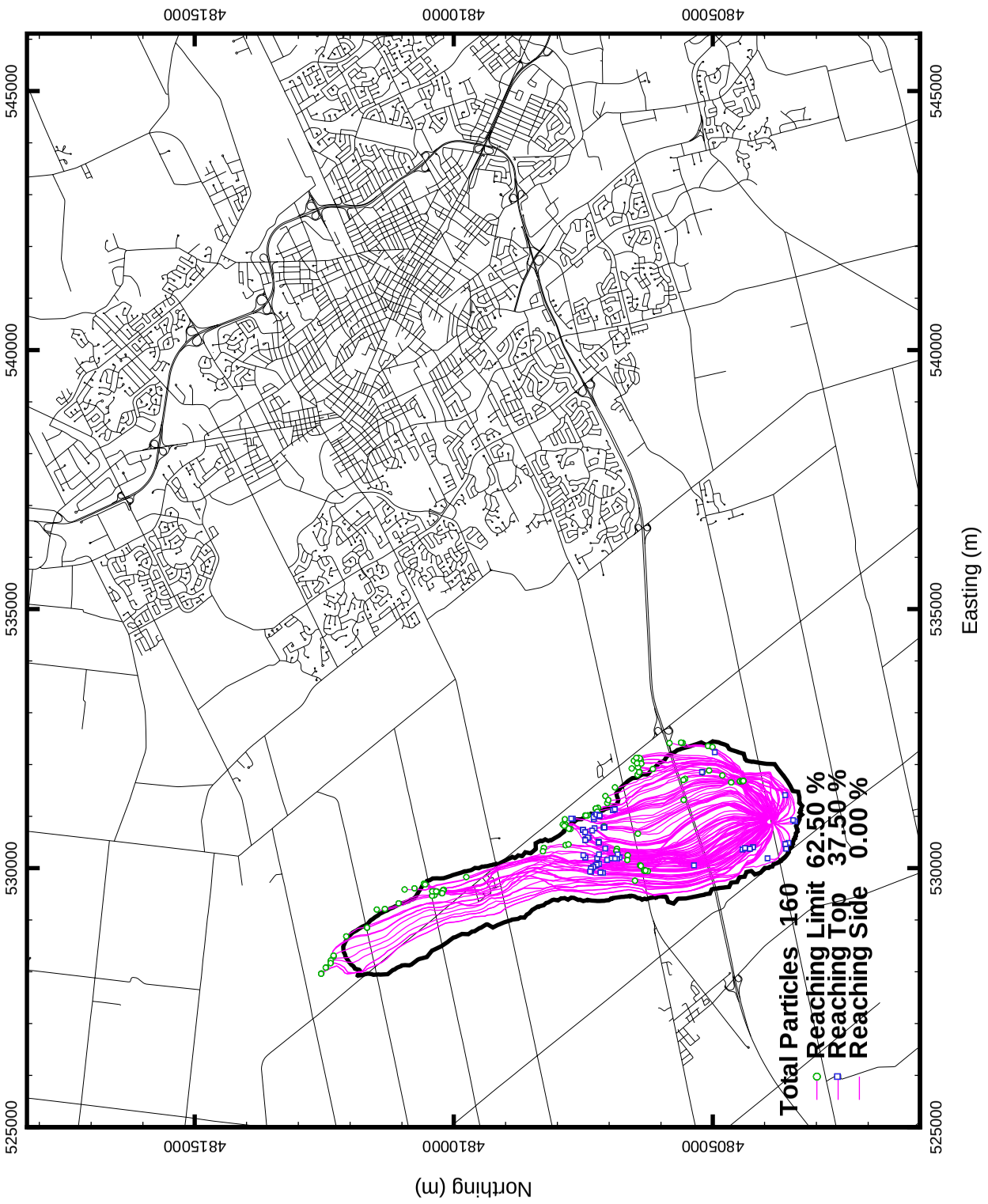

Figure A.15: Wilmot well field (fine mesh): 40-year particle tracks with outline of 0.02 peak capture probability.

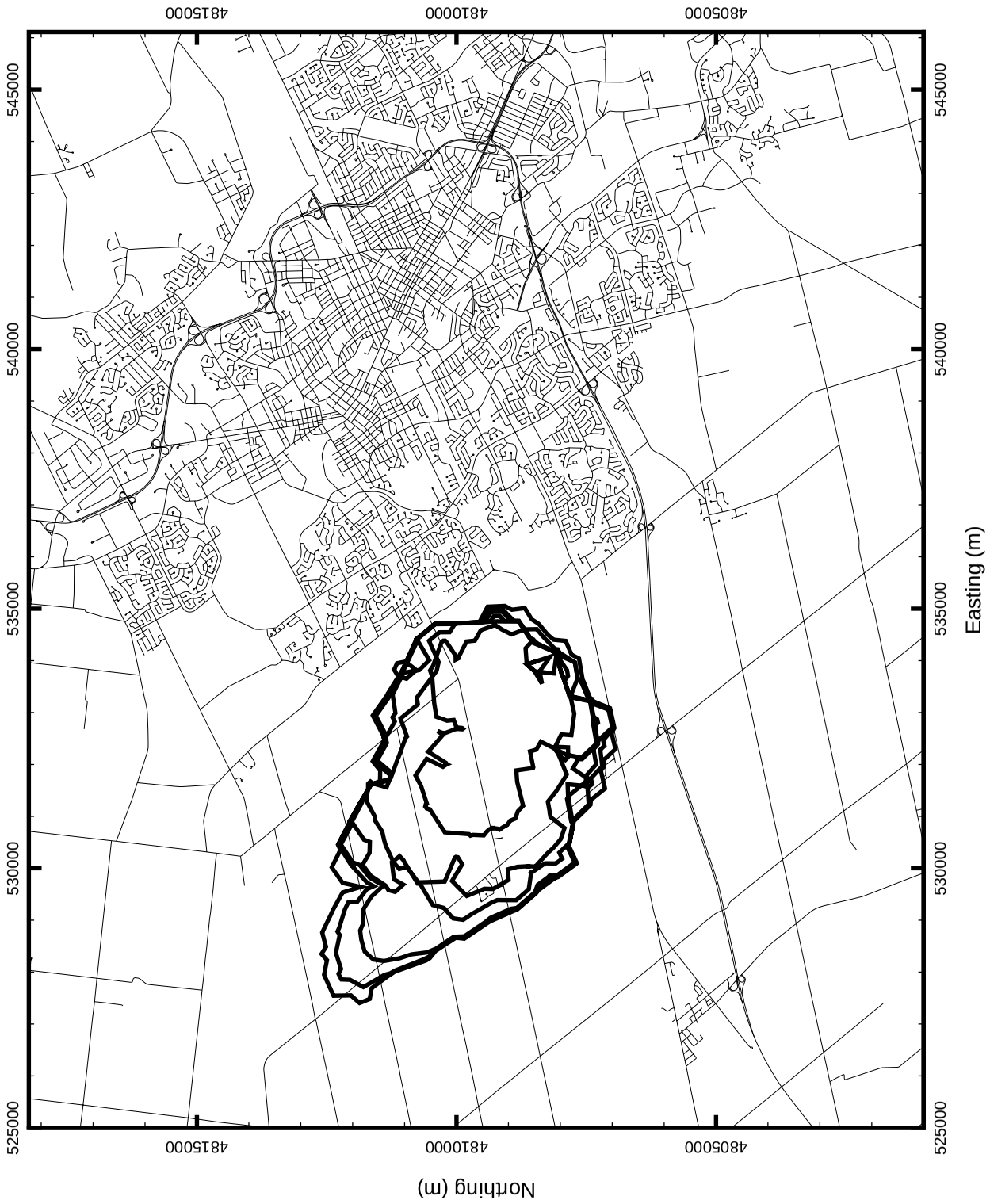

Figure A.16: Erb Street well field (coarse mesh): 0.02 peak capture probability contours; 2, 10, 20, 30, 40 & 55 years.

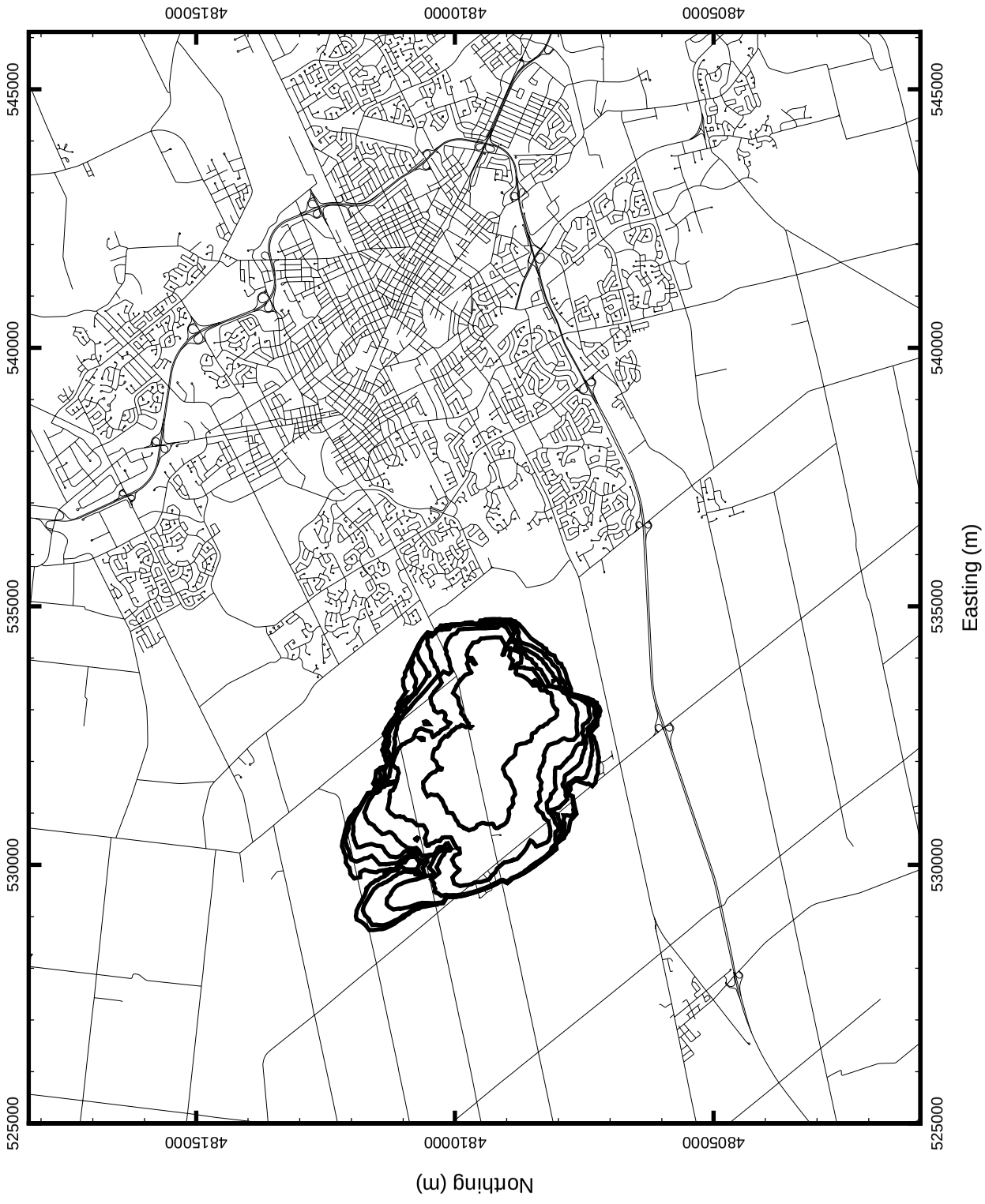

Figure A.17: Erb Street well field (fine mesh): 0.02 peak capture probability contours; 2, 10, 20, 30, 40 & 55 years.

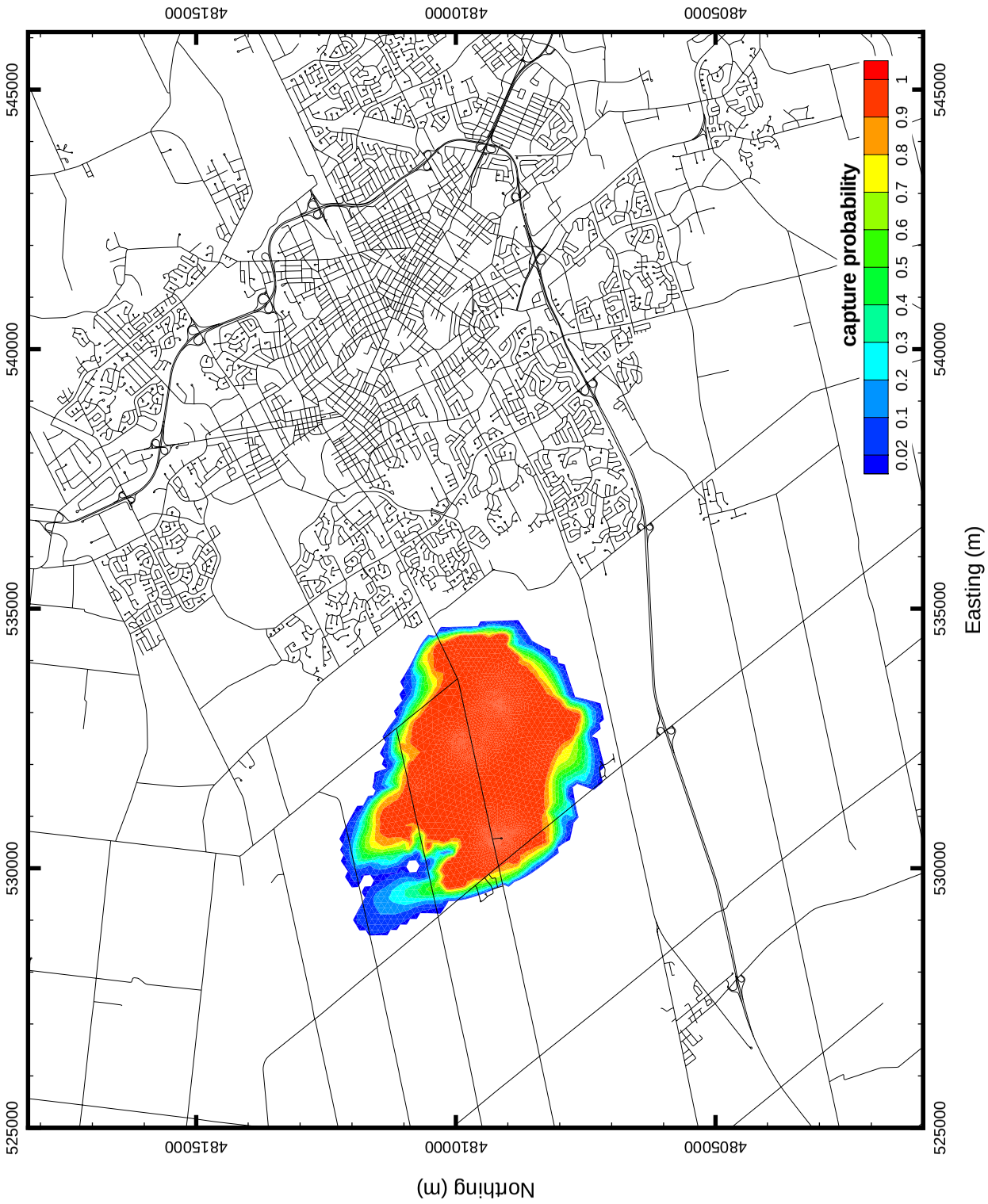

Figure A.18: Erb Street well field (fine mesh): 55-year peak capture probability.

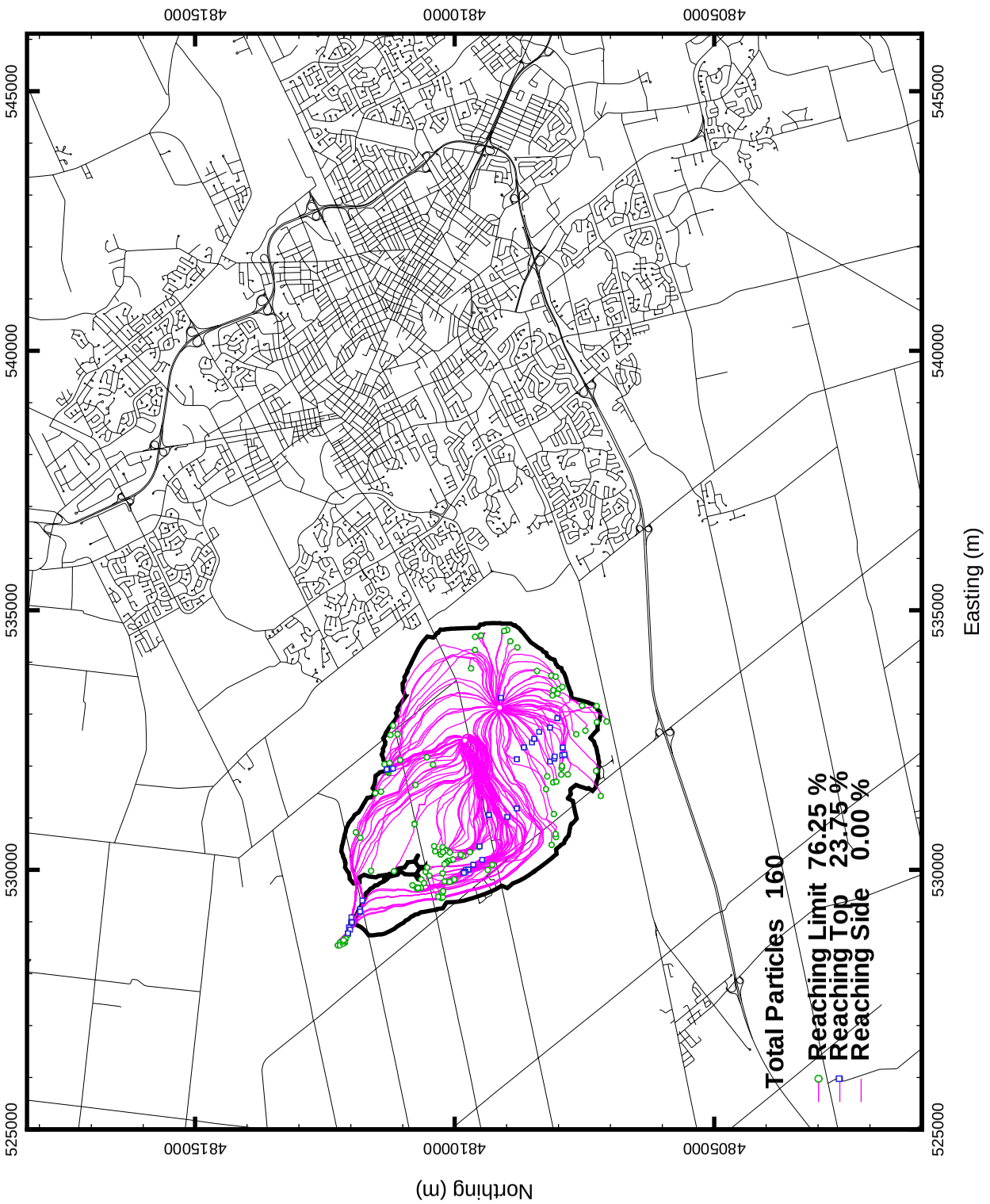

Figure A.19: Erb Street well field (fine mesh): 55-year particle tracks with outline of 0.02 peak capture probability.

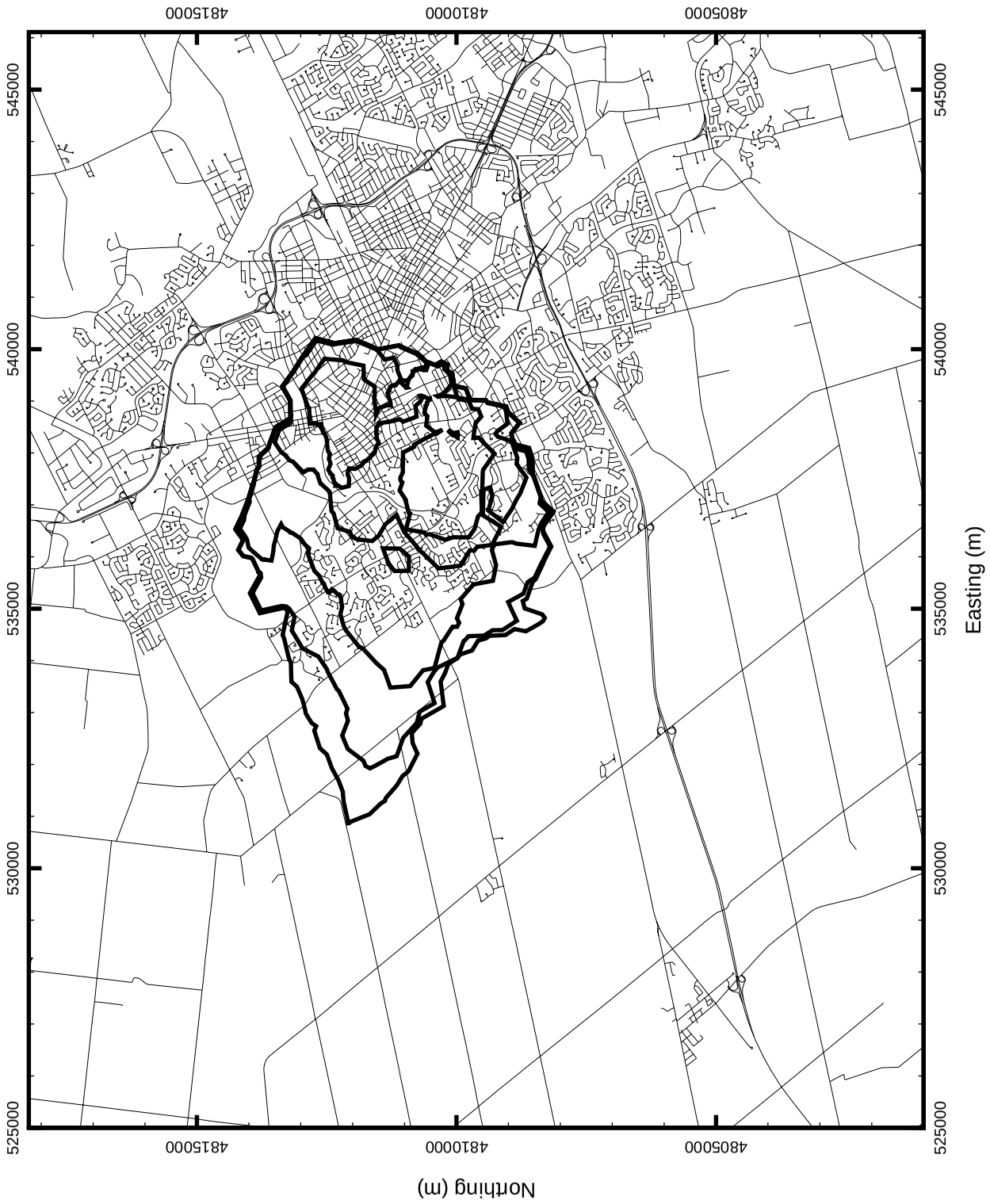

Figure A.20: William Street, Strange Street and Private wells (coarse mesh): 0.02 peak capture probability contours; 2, 10, 50, 100, & 140 years.

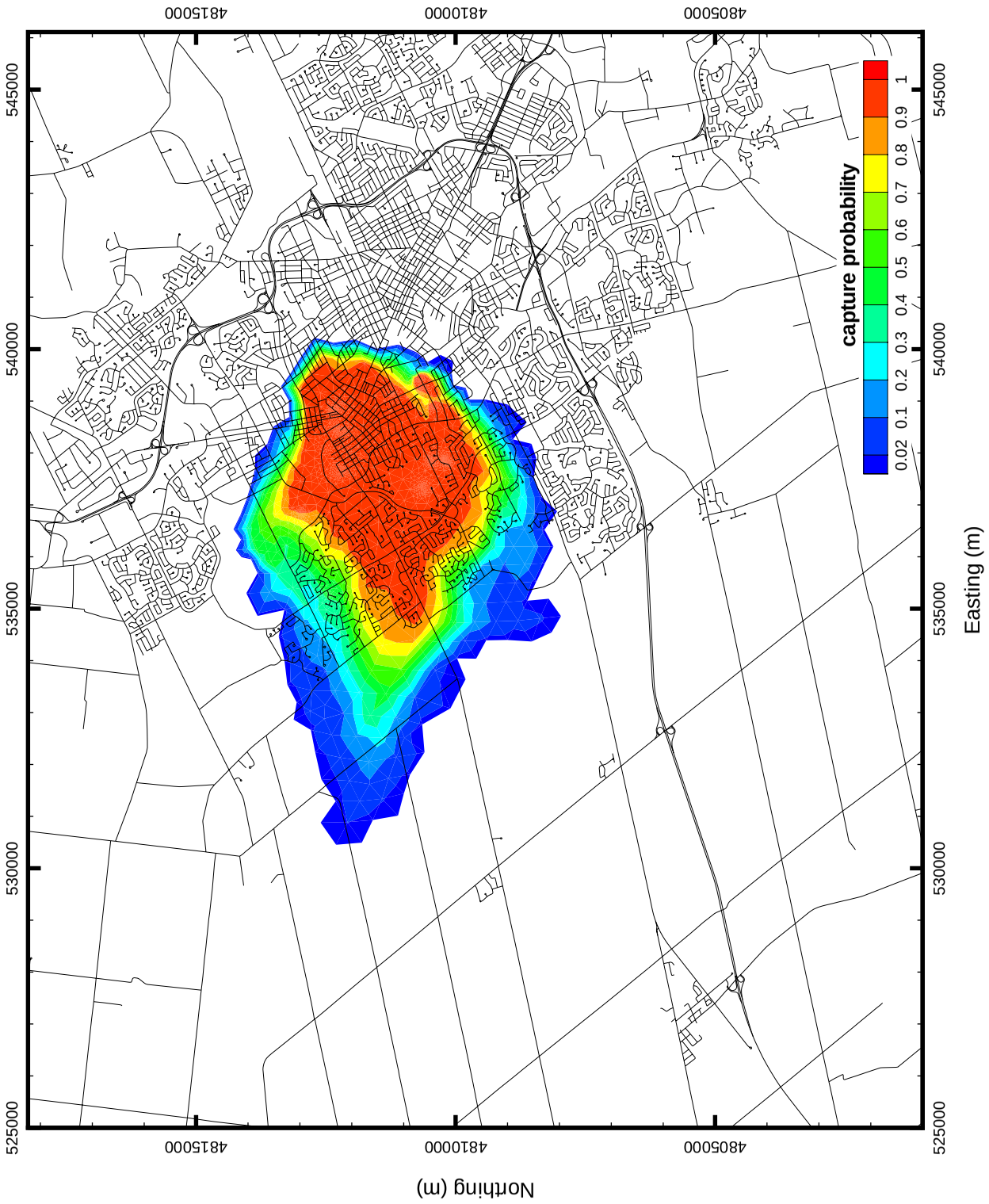

Figure A.21: William Street, Strange Street and Private wells (coarse mesh): 140-year peak capture probability.

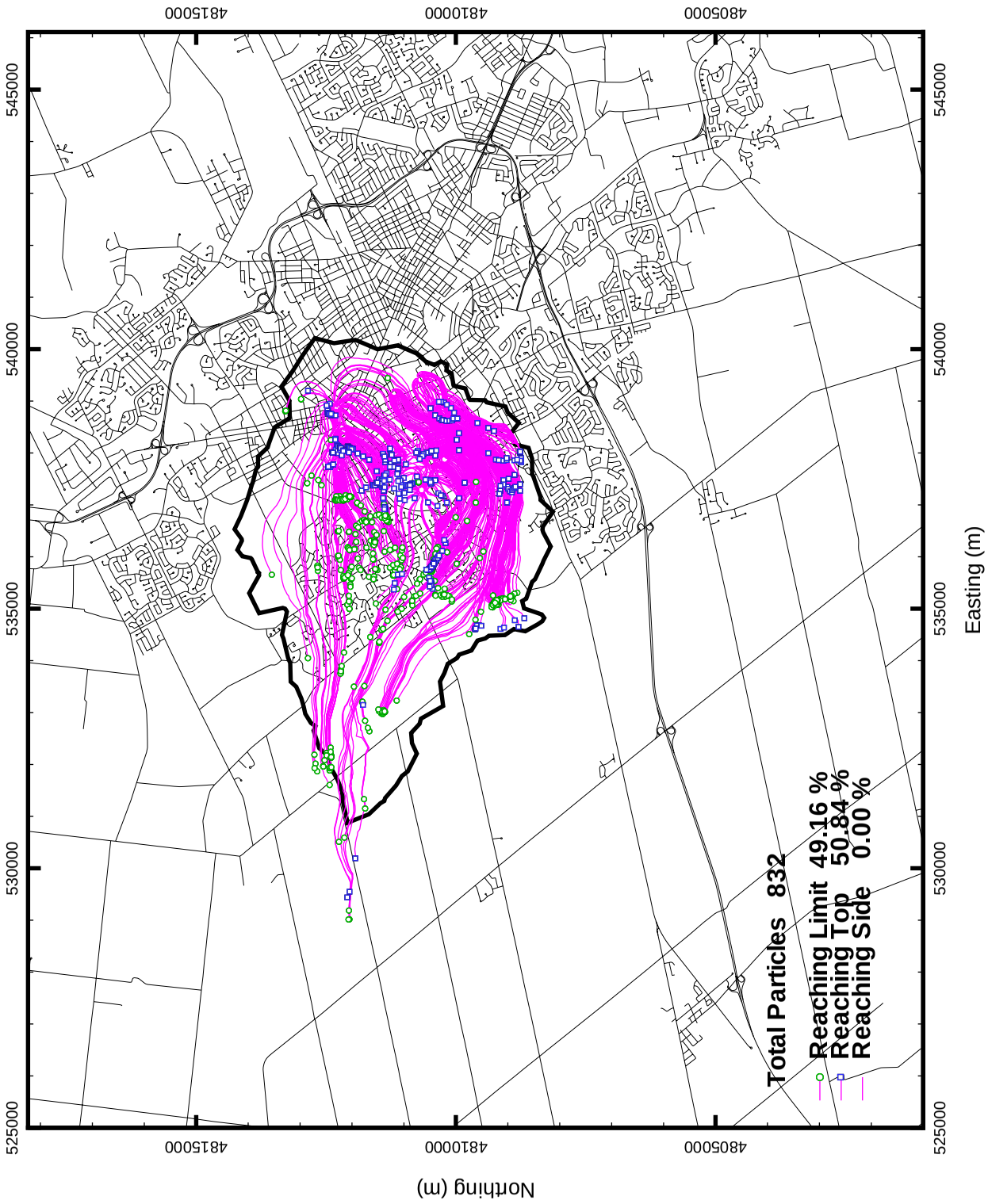

Figure A.22: William Street, Strange Street and Private wells (fine mesh): 140-year particle tracks with outline of 0.02 peak capture probability.

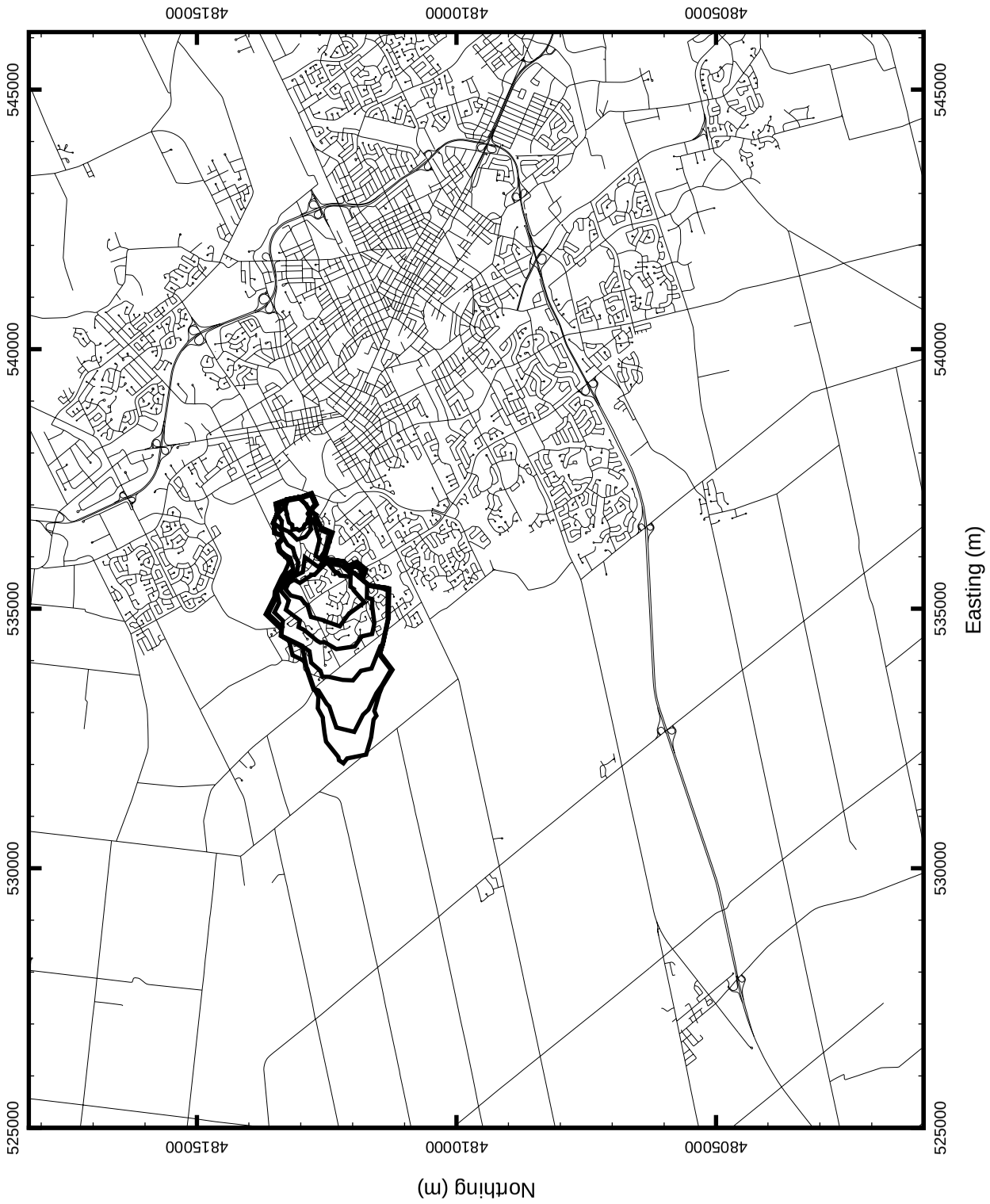

Figure A.23: W4 & W10; Waterloo North well field (coarse mesh): 0.02 peak capture probability contours; 2, 10, 25, 50, & 75 years.

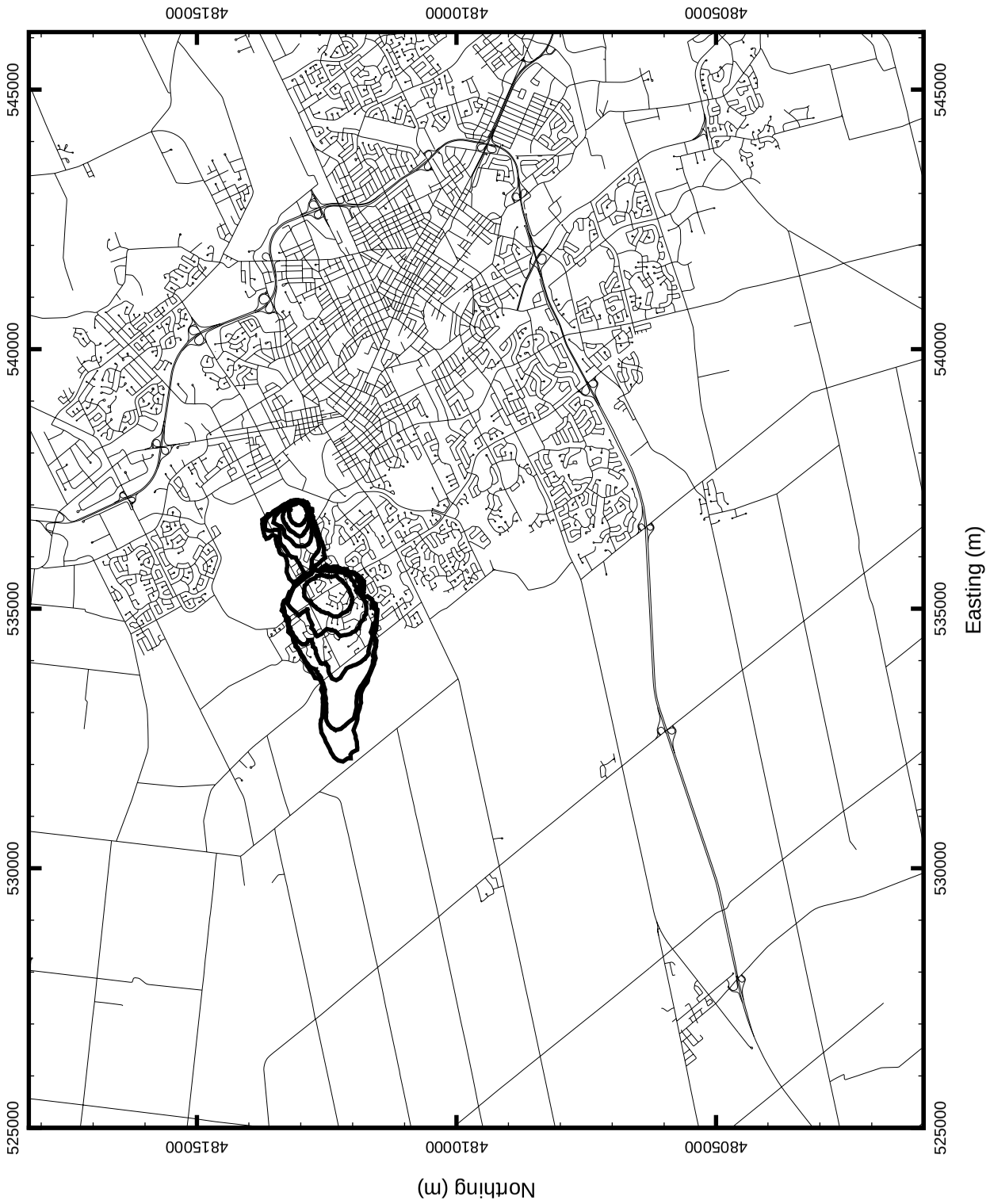

Figure A.24: W4 & W10; Waterloo North well field (fine mesh): 0.02 peak capture probability contours; 2, 10, 25, 50, & 75 years.

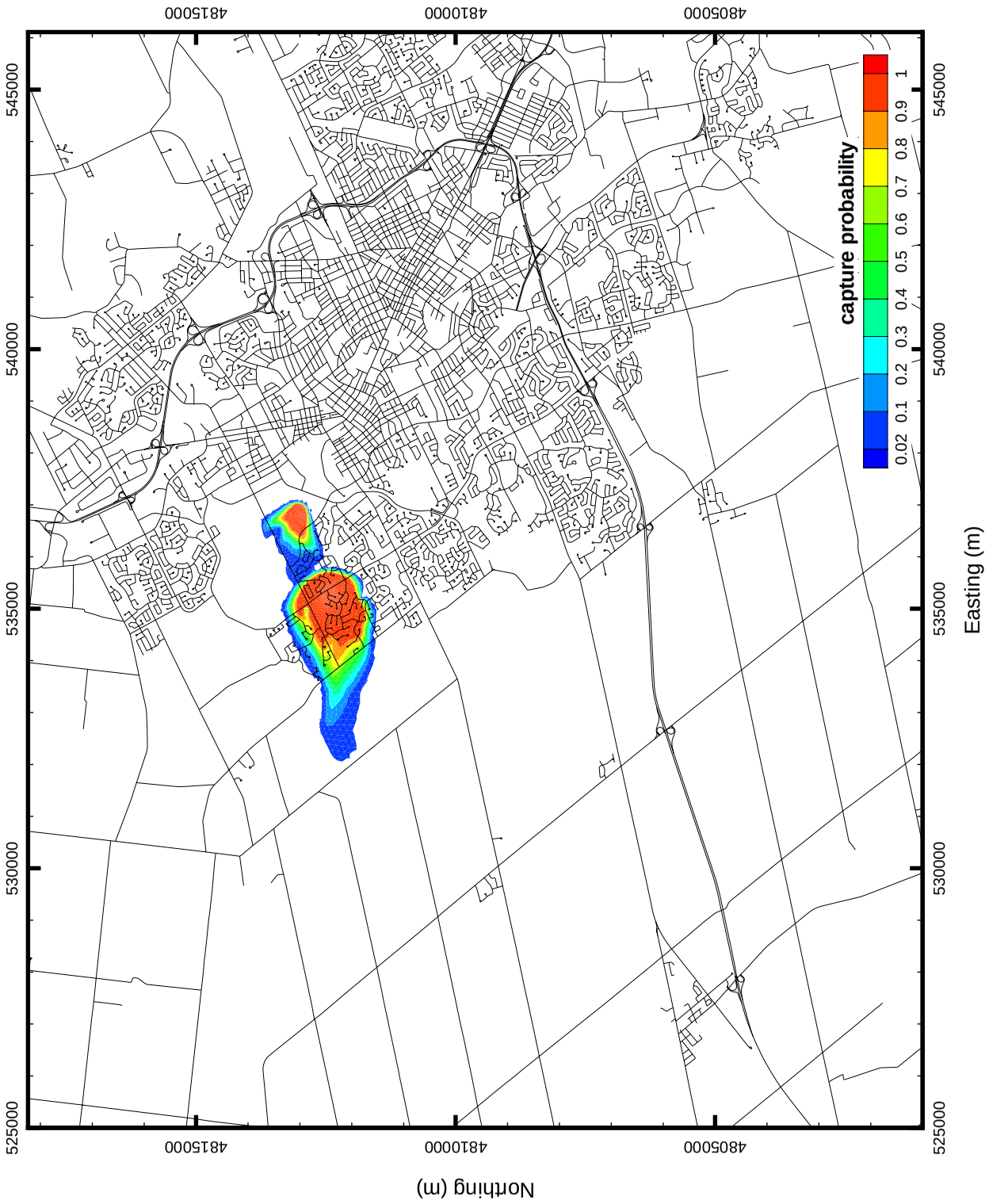

Figure A.25: W4 & W10; Waterloo North well field (fine mesh): 75-year peak capture probability.

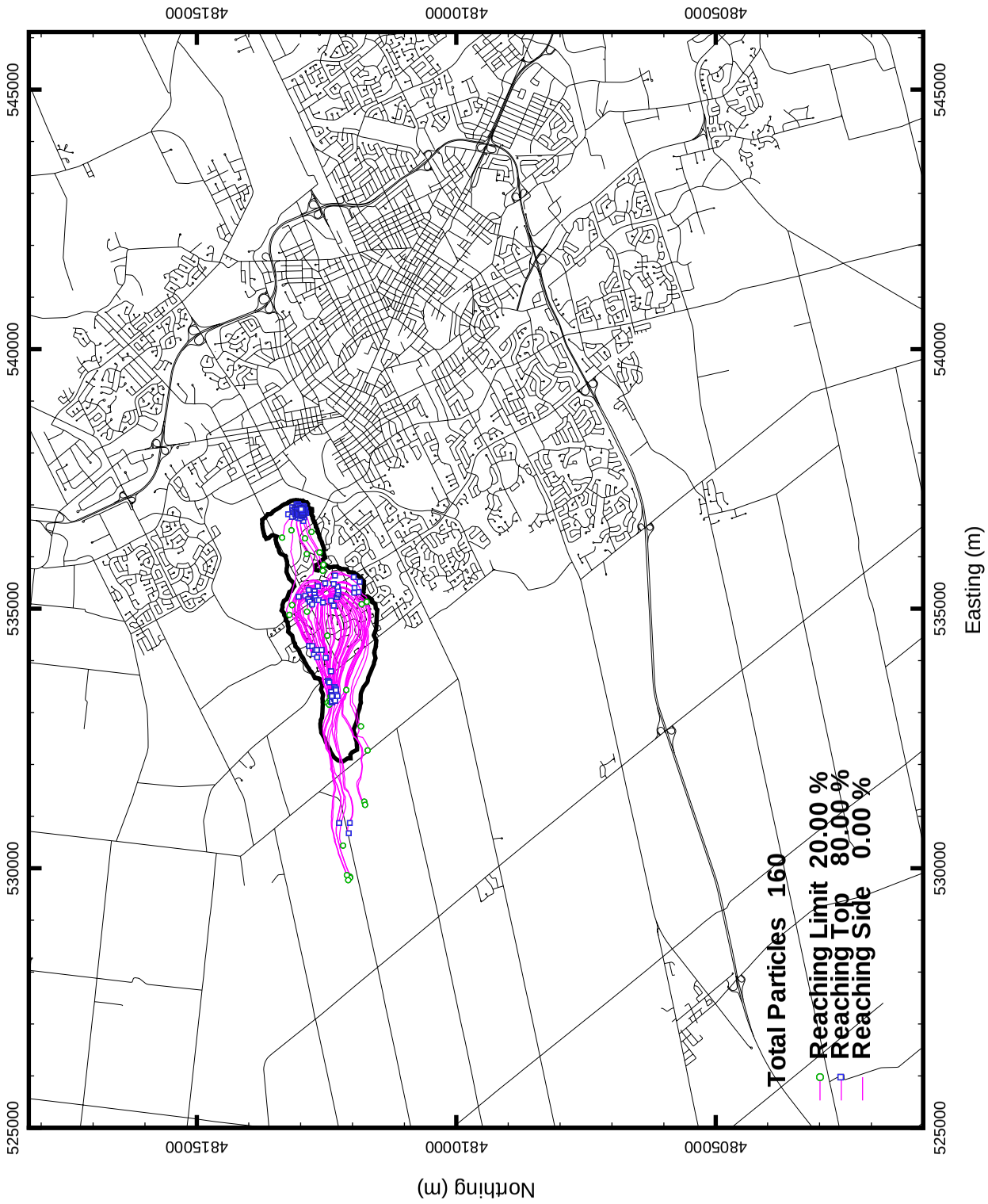

Figure A.26: W4 & W10; Waterloo North well field (fine mesh): 75-year particle tracks with outline of 0.02 peak capture probability.

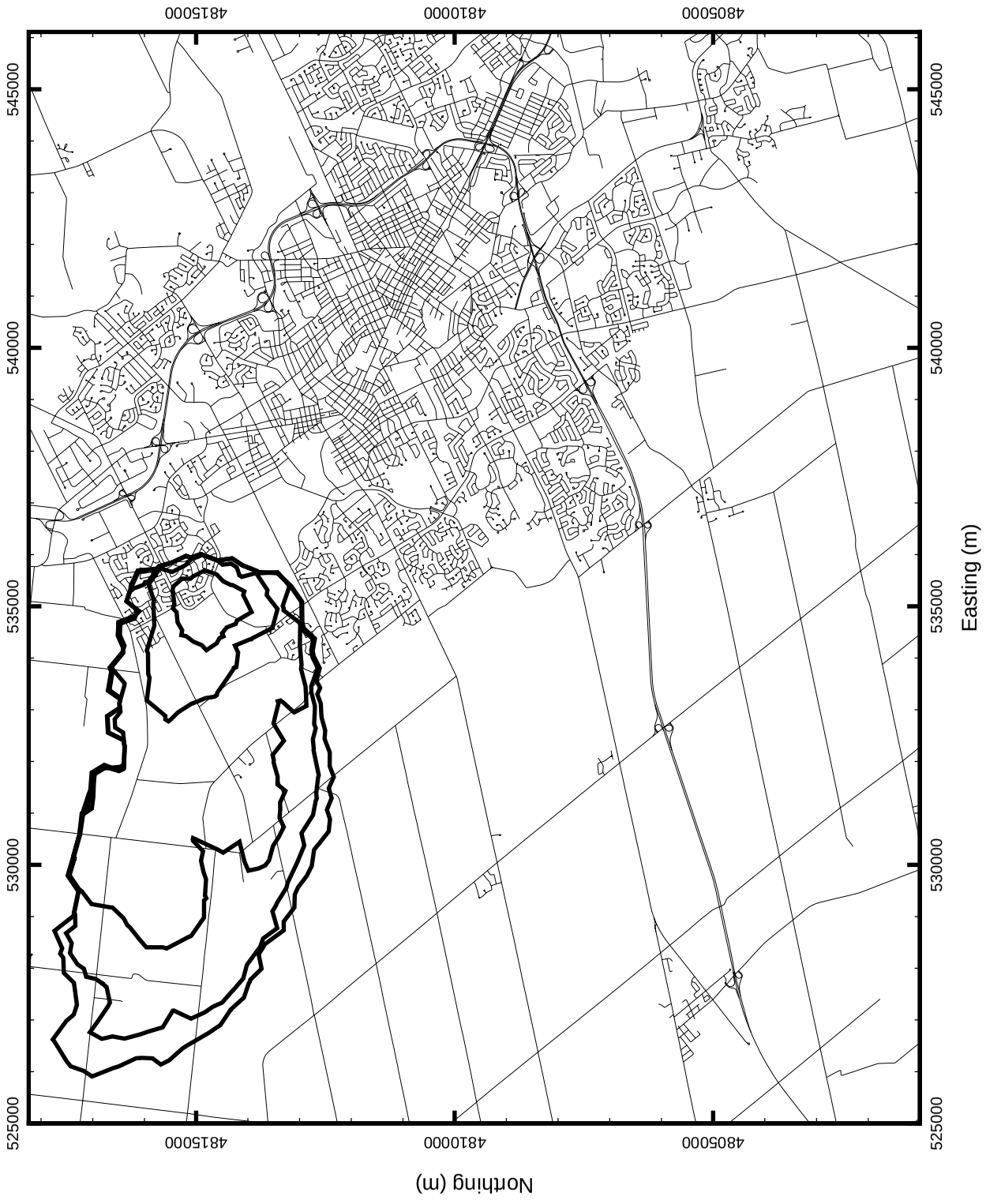

Figure A.27: W5; Waterloo North well field (coarse mesh): 0.02 peak capture probability contours; 2, 10, 50, 100, & 140 years.

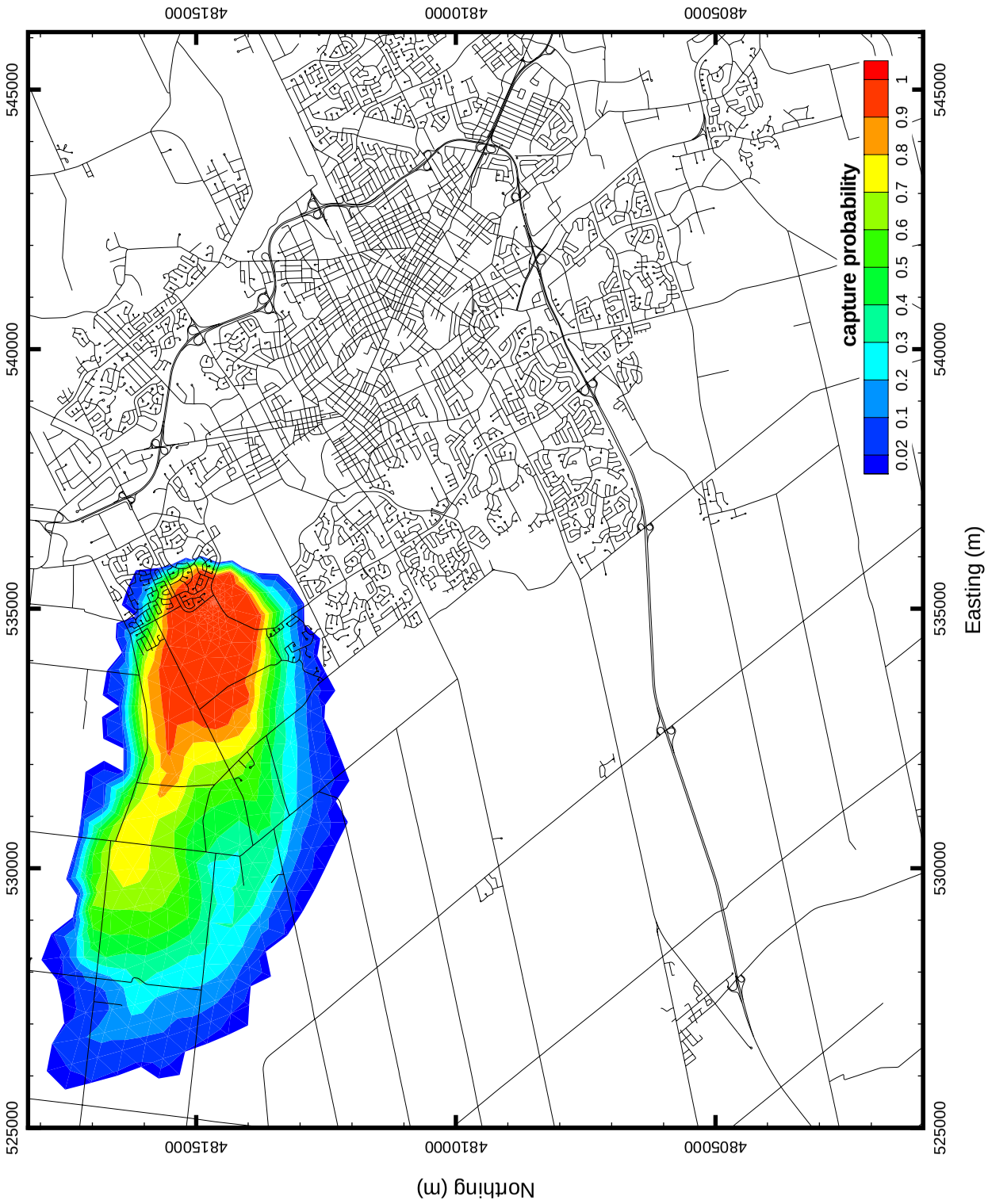

Figure A.28: W5; Waterloo North well field (coarse mesh): 140-year peak capture probability.

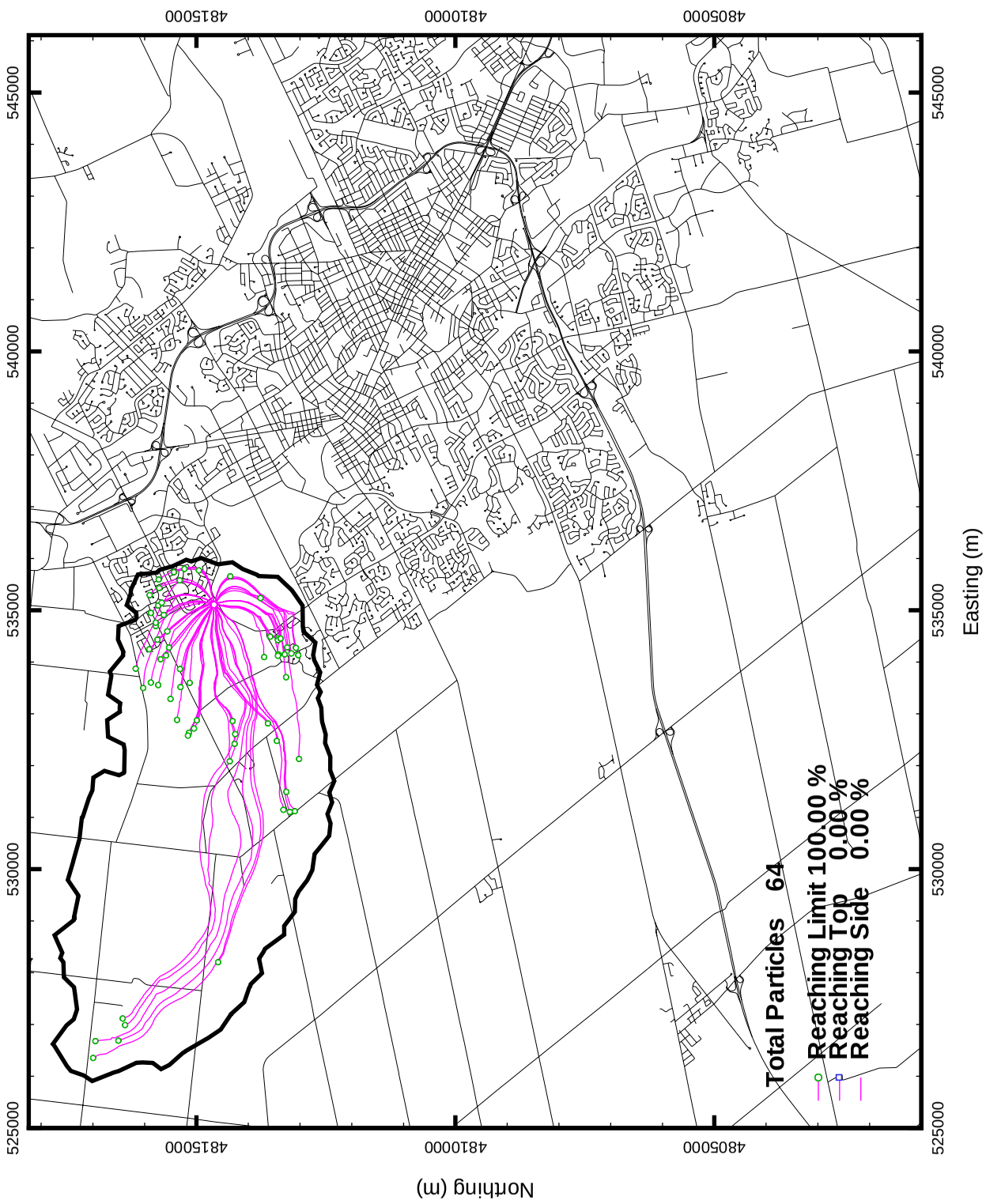

Figure A.29: W5; Waterloo North well field (fine mesh): 75-year particle tracks with outline of 0.02 peak capture probability.